8-19-2021 10:30 AM

Real-time Parkinsonian Tremor Signal Identifier Based on Internal Model Principle

Jian Dong, *The University of Western Ontario*

Supervisor: Lyndon J. Brown, *The University of Western Ontario*

A thesis submitted in partial fulfillment of the requirements for the Master of Engineering Science degree in Electrical and Computer Engineering

Abstract

Parkinsonian tremor is one of the clinical hallmarks of Parkinson's disease. Since the traditional medical treatments are not effective, many wearable devices are being developed to help suppress the tremor. In order to suppress the tremor, a well-designed tremor estimator is needed. Previous tremor estimators treat a 3-D tremor signal as three independent 1-D signals. Moreover, they did not consider the real-life characteristics of tremor signals. For instance, the tremor does not always exist in the postural tremor signal, and the patient's voluntary motion can be included in the kinetic tremor signal. This paper presents a real-time adaptive Parkinsonian tremor signal identifier based on the internal model principle and instantaneous Fourier decomposition, and tests on tremor signals collected by a special glove from 18 patients. The result showed that our proposed identifier could identify a 3-D tremor signal, and have the ability to recognize the presence of tremor and separate the voluntary motion from the tremor signal. We also showed that our proposed identifier could achieve 80 %+ in signal identification accuracy and 90 %+ in power estimation accuracy in different tremor signals. Finally, we achieved real-time tremor identification in a bench-top tremor simulator.

Keywords: Parkinsonian tremor, internal model principle, voluntary motion, real-time tremor identification

Lay Summary

Parkinson's disease (PD), also known as shaking palsy, is a neurodegenerative disease commonly developed in people older than 60. PD's signs and symptoms may include Parkinsonian tremor, slowness of movement and rigidity. Unfortunately, there are no medical therapies that can completely cure PD nowadays. Therefore, researchers are already looking to improve symptoms through external treatments like wearable devices.

Among all symptoms, the Parkinsonian tremor, or shaking, is the most prominent and troublesome symptom in patients' daily life. In recent years, many wearable devices are being invented to help suppress the tremor. In order to achieve good tremor suppression, it is necessary to achieve good tremor identification priorly. This research presents a Parkinsonian tremor signal identifier to achieve real-time tremor identification on the 3-D signals collected by a specially designed glove from 18 patients' hands. The simulation results showed that our proposed identifier could achieve expected accuracy in resting tremor signals, which were recorded when patients' hands were completely resting against gravity.

However, in real-life scenarios, the tremor may exhibit different characteristics. Moreover, it may become less noticeable or disappear entirely when patients try to control their hands to do voluntary movements. Hence, we improved the identifier and granted its ability to identify different types of tremors, recognize the tremors' presence and disappearance and separate voluntary motion from tremor signal. The simulation results showed that our proposed identifier could maintain high identification performance in postural and kinetic tremor signals, which were recorded when patients were asking to do different tasks with their hands. Finally, we achieved real-time tremor identification in an artificial tremor simulator.

Acknowlegements

Writing a master thesis is more challenging than I thought and more rewarding than I could have ever imagined. I would like to thank everyone who helped me in these two years. I couldn't go this far without your love, support and encouragement.

First of all, I would like to express my deepest appreciation to my supervisor Dr. Lyndon J. Brown. Thanks for providing me with the opportunity to go forward in my research and giving me constant support. His honest suggestions brought me the knowledge and space to progress. I'm extremely grateful to work with such a wise and kind professor like him.

I would also like to thank Dr. Yue Zhou. Dr. Yue put forward many valuable opinions for my thesis and provided great technical assistance for my experiment in the laboratory. I also want to send my thanks to Dr. Ana Luisa Trejos for giving me help and letting me conducting research in her laboratory. One more special thanks go to Western WearMe lab for providing the device and space for me to do my research.

Finally, I want to express my most sincere gratitude to my wife, Jiaqi Kan, for always being the person I can turn to during those grieved and stressful days. To my unborn daughter Queenie: for choosing me as your father and giving me the motivation. To my parents, Manyun Xu and Qinghua Dong: thank you for bringing me to this world and raising me. To my grandma Nayi Liu: thank you for sustaining me in ways that I never knew that I needed. And to everyone in my family and all my good friends. I'm so lucky to have you all in my life.

Contents

List of Figures

List of Tables

List of Appendices

Chapter 1

Introduction

1.1 Background

Parkinson's disease (PD) is a continuous neurological disorder caused by the death of dopaminergic neurons in the substantia nigra. Recent research shows that the prevalence of PD ranges from 100 to 797 per 100,000 among individuals aged above 45 years in Canada, the USA and China [31, 40, 34, 49]. The overall numbers are ever-growing and are expected to double in 2030 in developed and developing countries. Patients suffering from PD usually have many motor-related troubles in their daily life, including tremor, rigidity and bradykinesia [28]. Among all symptoms, tremor is often considered to be the symptom causing the most significant impact. Unfortunately, the cause of PD is unknown and regular treatments can only reduce the effects of symptoms but not stop the progress of PD. Given the lack of effectiveness of traditional medical treatments, externally wearable devices are developed to suppress the Parkinsonian tremor in the past few years [57, 58]. For the purpose of tremor suppression, it is necessary to understand the nature of tremor.

Although tremor is one of the clinical hallmarks of the disease, its pathophysiology remains unclear [26]. While some studies considered Parkinsonian tremor as a monoharmonic signal, other papers treated it as a multi-harmonic signal [29, 43, 48, 6]. Moreover, a tremor signal can be described as a quasi-periodic and nonstationary signal, but there is no uniform statement about the most suitable model for describing the tremor signal [6, 3]. In order to better understand the Parkinsonian tremor and achieve real-time estimation, our research studied an adaptive internal model principle-based algorithm [36, 11] and extended its function to identify different types of Parkinsonian tremors.

1.2 Motivation

Generally speaking, a Parkinsonian tremor can be described as a rhythmic, oscillatory and unintentional movement with time-varying frequency and amplitude. Also, it can be divided into three categories of tremor: resting, postural and kinetic tremor [26, 56, 18]. In control theory and signal processing, such kinds of signals are very common in real life. A tremor signal can be described as a quasi-periodic and nonstationary signal. The amplitude, frequency

and phase of the tremor are considered to be changing over time. In this thesis, we are using the harmonic model [4] to simulate Parkinsonian tremor signals. The harmonic model is also referred to as a Fourier series model. Every periodic signal can be presented by this model due to the properties of the Fourier series. Although the tremor signal is not defined as a typical periodic signal, its principal frequency only changes slowly. This feature allows for the use of the harmonic model as an approximation of the natural tremor signal. The mathematical model of a tremor signal is given below.

$$d(t) = \sum_{i=1}^{N} \sum_{j=1}^{N_i} a_{ij}(t) \sin(j \int_{t_0}^{t} \omega_i(t)dt + \theta_{ij}) \tag{1.1}$$

where N is the number of fundamental frequencies, N_i is the number of harmonics of each fundamental frequency, a is the time-varying Fourier coefficients, ω_i is the instantaneous tremor frequency of each fundamental frequency and θ is the relative phase.

Many algorithms have been proposed to identify these signals, including fast Fourier transform, wavelet analysis and Hilbert Huang Transform [20, 8, 13, 27, 15]. However, these traditional methods are not working well because of the complexity and randomness of the tremor signal. Considering the characteristics of Parkinsonian tremor, many new approaches are presented to identify and estimate tremor signals. For instance, Fourier linear combiner, weighted Fourier linear combiner and adaptive Kalman filter are three widely used tremor estimators [42, 52, 51, 1, 30, 53, 5]. Nevertheless, research on these methods is mainly conducted on pure simulated tremor signals. Besides, their identification effect on different types of tremors has not been verified. The contents mentioned above are discussed in the literature review.

The previous studies conducted on the Parkinsonian tremor treated the whole signal as a tremor signal. However, the Parkinsonian tremor that is necessary to be suppressed is only a part of the whole signal. In a real-life scenario, the Parkinsonian tremor and patient's voluntary movement may exist simultaneously, which means that the tremor signal may also contain a voluntary motion signal. Thus, the approach that considers the whole signal as a tremor signal may result in suppressing the patient's voluntary motion. Given that the common estimation algorithm cannot achieve real-time Parkinsonian tremor estimation and separate tremor from voluntary motion, a more complete and universal algorithm is needed. In 2017, Mohsen and Brown presented an adaptive internal model principle-based periodic signal identifier [36] to identify the signal with a similar model as equation (1.1). Although this signal identifier can track periodic signals with unknown frequencies and cancelling disturbances, it is fixed and lacks flexibility. Thus, this research focuses on designing a new adaptive estimator based on the original system to adapt to different Parkinsonian tremor signals, ensure stability and performance in varied situations and achieve estimation in real time.

1.3 Objectives

The overall objective of this thesis is to develop a controllable Parkinsonian tremor signal identifier capable of estimating different types of tremors with high accuracy in both simulation

and real-time experiments. The specific objectives are:

1) Design a new structure for the old signal identifier that allows the user to modify all changeable parameters. Enhance the flexibility of this internal model principle-based signal identifier.

2) Design a Parkinsonian tremor signal identifier based on the new structure and simulate actual data recorded by the tremor signal acquisition glove.

3) Improve the proposed tremor signal identifier to adapt to resting tremor, postural tremor and kinetic tremor signal.

4) Identify whether the single-fundamental or multiple-fundamental model is most appropriate for the Parkinsonian tremor signal.

5) Investigate the relationship between the frequencies of different axis and different joints.

6) Investigate the relationship between time and frequency of tremor *i.e.* does the frequency vary on a certain amount of time, or is it constant.

7) Transfer codes in MATLAB and Simulink to Python and achieve real-time Parkinsonian tremor estimation on a bench-top tremor simulator.

1.4 Thesis Outline

The structure of this thesis is as follow:

Chapter 2 Presents the previous internal model principle-based signal identifier, and the literature review of Parkinsonian tremor estimation algorithm.

Chapter 3 Describes the new flexible signal identifier,and the adaptive algorithm for Parkinsonian tremor signal identification.

Chapter 4 Gives the simulation results in synthesized tremor, resting tremor, postural tremor and kinetic tremor signal, and the analysis of different results.

Chapter 5 Presents the estimation results in real-time test, and the analysis of different results.

Chapter 6 Presents the conclusions of this research and advice for future work.

Chapter 2

Literature Review

2.1 Overview

This chapter is organized as follows: Section 2.2 reviews the previous work on identifying the signal with unknown frequency. Section 2.3 reviews an internal model principle-based adaptive signal identifier developed by Mohsen and Brown [36]. It is divided into five parts corresponding to different areas in that approach. Section 2.4 reviews several techniques which were used to estimate the Parkinsonian tremor previously. Section 2.5 reviews some technologies related to intermittent control.

2.2 Signal Processing Literature Review

A great number of approaches have been used to analyze signals and identify the frequency. One of the most common schemes is to decompose the signal into a sum of narrow-band components corresponding to one harmonic and generating a Fourier representation of the input signal. Fourier transform is one of the most efficient signal analysis techniques applied in signal processing and other varying applications. There are several algorithms of Fourier transform which are widely used, such as fast Fourier transform. It computes the discrete Fourier transform (DFT) of a signal with less complexity of computation, which decomposes signals into many sinusoidal components with different frequencies. Moreover, by dividing a long signal into several short signals with equal length and do the FFT in the continuous-time, the short-time Fourier transform (STFT) is obtained [44]. The STFT is described as following:

$$X(\tau, w) = \int_{-\infty}^{\infty} x(t)w(t-\tau)e^{-i\omega t}dt \tag{2.1}$$

where $x(t)$ is the signal to be transformed and $w(\tau)$ is the window function. However, the Fourier transform is not based on an adaptive basis. In other words, FFT and STFT are only applicable for linear and stationary data. Furthermore, the estimation of the frequency of this algorithm is sensitive to noise [20].

Another frequently used method is wavelet transform, which decomposes the signal into a sum of local linear, time-dilated and time-translated wavelet components. A wavelet is a small

picture of the wave, which has oscillation and amplitude. According to [8], our function $f(t)$ can be represented as a linear decomposition as

$$f(t) = \sum_{\ell} a_{\ell}\psi_{\ell}(t) = \sum_{k}\sum_{j} a_{j,k}, \psi_{j,k}(t) \tag{2.2}$$

where j and k are integer indices, and $\psi_{j,k}(t)$ is the wavelet expansion function. The set of expansion parameters $a_{j,k}$ are called the discrete wavelet transform of the signal $f(t)$, and the equation (2.2) is the inverse transform. The integral wavelet transform is defined as

$$X(a,b) = \frac{1}{\sqrt{a}}\int_{-\infty}^{\infty} \Psi(\frac{t-b}{a})x(t)dt \tag{2.3}$$

where a is the scaling factor and b is the translation factor. This algorithm is well proved for approximation data with sharp discontinuities. However, one of the main shortcomings is the difficulty of design the proper mother wavelet for a given application [13].

However, most of the data, either natural or artificial, are nonlinear, non-stationary and stochastic. Therefore, the Hilbert Huang Transform (HHT) based on the empirical mode decomposition (EMD) was developed by Huang to meet this requirement [27]. It has two main parts: the first is the EMD, the second is the Huang spectral analysis.

In the EMD part, the signal is decomposed into the sum of a finite number of different components named intrinsic mode function (IMF). The IMF can have a varying magnitude and frequency as a function of time instead of a fixed magnitude and frequency. The function can be decomposed following this procedure: identify the local extreme value, then use these local extreme values to produce the upper envelope. Repeat this procedure for the local minimum value to obtain the lower envelope. This procedure is called a sifting process [27] which is shown below

$$h_1 = X(t) - m_1 \tag{2.4}$$

where m_1 is the mean of the envelopes, $X(t)$ is the data, and h_1 is the first component (difference between the data and its mean). After the first round of the sifting process, a new upper and lower envelope of the function is created. The sifting process needs to be repeated until the final IMF is obtained.

Once the IMF components are obtained, the Hilbert transform is applied to the j^{th} IMF to produce the instantaneous amplitude $a_j(t)$ and frequency $\omega_i(t)$ of the signal. The original data are represented as the real part of the following equation

$$x(t) = \Re \sum_{j=1}^{n} a_j(t)e^{i\int \omega_j(t)dt} \tag{2.5}$$

where a_j and ω_j are different amplitudes and frequencies. Because the variability of a_j and ω_j, HHT has the capability for analyzing nonlinear, non-stationary and stochastic data. Hence the Hilbert transform of a narrow band signal can be approximated represented as

$$y(t) = \mathcal{H}\{x(t)\} \approx -\frac{1}{\omega}\dot{x}(t) \tag{2.6}$$

Nevertheless, the main limitation of the HHT approach during the sifting procedure is that the EMD can not separate components when their frequencies are adjacent, which is known as mode mixing [15]. Another restriction called the end effect is due to the lack of data before and after the data window. Moreover, further constructions of envelopes do not have a unique answer, so different implementations of the HHT can give different answers. Hence, this method still has limitations while tracking a signal with an unknown frequency.

2.3 Signal Identification Based on Internal Model Principle

This section mainly focuses on the system structure and algorithm of a real-time signal identifier based on the internal model principle presented by Brown and Mohsen [36].

2.3.1 Internal Model Principle Literature Review

The internal model principle is a feedback control principle that was first presented by Francis and Wonham in 1976[21]. It was a specific definition of the Conant and Ashby good regulator problem [17]. The objective of an internal model is to produce a replicate of an input disturbance or the plant input necessary for the output of the plant to equal the desired reference trajectory. In other words, it provides a set-point signal by providing close-loop transmission zeros that eliminate the critically stable poles of the periodic disturbance or set-point. However, the premise of this principle is that it requires prior knowledge of the frequency of the signal. To put it simply, the controller must know the exact frequency of disturbance and reference signal before tracking it. Hence, the performance of this approach is limited by this prerequisite. Moreover, many problems in the real world have an uncertain frequency. So, this is considered to be the main restriction of this approach in the application.

Since then, many extension schemes from the internal model principle were developed to achieve signal tracking and disturbance cancellation with uncertain frequency. In 1988, a method called the repetitive control system, which is based on the internal model principle, was presented by Hara, *et al.*[25]. It fulfilled the goal of tracking a periodic disturbance to reduce the error to a small number and reject the disturbances but suffered from a lack of system stability because of the positive feedback loop. Another different technique called adaptive feedforward cancellation that is based on the phase-locked loop was proposed by Bodson, *et al.* in 1994 [7]. Despite the fact that this approach has good system stability, it requires the gains to be calculated for all estimated frequencies, which is not reliable with a complicated plant.

In 2001, Brown and Zhang proposed an adaptive algorithm for cancelling periodic disturbances with uncertain frequencies and extended it to the identification of periodic signals with uncertain frequencies [9, 10]. These approaches are formed on state-space variables of an internal

model principle controller and used a PI controller in parallel. It showed high performance on identifying periodic signals and rejecting a periodic disturbance. However, the analysis was done in the absence of noise, and the algorithm needed a good knowledge of the plant gains at all potentially identified frequencies. Moreover, one of the main restrictions in these algorithms is that the frequency of periodic signal and disturbance cannot be identified when the fundamental frequencies of them are too low. Additionally, an adaptive internal model principle-based principle for frequency identification and disturbance cancellation was proposed by Brown and Zhang to ensure the system is exponentially stable [11]. Since the disturbance re-builder should add after the estimation frequency convergence in this method, this causes a rebuilding delay, which is considered the main limitation.

In recent years, several approaches were proposed in this particular area. A method of disturbance cancellation for linear systems by adaptive internal models was presented by Marino and Tomei in 2013 [33]. Besides, an internal model-based approach of adaptive disturbance compensation in delayed linear systems was proposed by Gerasimov, *et al.* in 2015 [24].

2.3.2 Adaptive Notch Filter

In the field of signal analysis, the adaptive notch filter (ANF) is one of the essential techniques that has many applications such as frequency estimation and noise cancellation [37, 38]. ANF has been commonly used in our daily life like cell phones and hearing aids. In this particular design, the second-order of infinite impulse response (IIR) form of the adaptive filter is considered as following

$$G(z^{-1}, \Omega, \rho) = \frac{1 - z\cos\Omega z^{-1} + z^{-2}}{1 - 2\rho\cos\Omega z^{-1} + \rho^2 z^{-2}} \tag{2.7}$$

where the parameter ρ ($0 \leq \rho < 1$) is known as the pole contraction factor, and Ω is uncertain notch frequency. Equivalently, the analog adaptive notch filter can be expressed as

$$H(s) = \frac{s^2 + \omega_n^2}{s^2 + 2\epsilon_n\omega_n s + \omega_n^2} \tag{2.8}$$

where s is Laplace operator, ω_n is the notch frequency and ϵ_n ($0 < \epsilon_n \leq 1$) is the damping ratio. Note that the notch frequency ω_n is controlled by means of an adaptive algorithm that includes stochastic gradient approach such as least mean square error (LMS) and normalized least mean square (NLMS), or least square estimation such as recursive least squares filter (RLS). Hence, this filter can reject or attenuate signals with specific frequency ω_n. By incorporating this filter into the control system, the algorithm's noise rejection ability is improved.

2.3.3 Instantaneous Fourier Decomposition

The instantaneous Fourier decomposition (IFD) algorithm is adapted from the basic internal model principle. This method was first presented by Malhorta in 2005 [32], developed by Sun and implemented in continuous time and for offline estimation in 2006 [46]. Its crucial function is to identify or cancel a sinusoidal disturbance. The structure of the IFD block diagram is

shown in Fig. 2.1, where $G(s)$ is a tuning function. Assume the input mixed-signal $d(t)$ contains m signals with different fundamental frequencies, and each individual signal has n harmonics. The signal is decomposed into narrow-band signals based on the orthogonal state variables combined with internal models(IM_{ij}). The state-space equation for internal model IM_{ij} is given as

$$\dot{X}_{ij} = \begin{bmatrix} 0 & j\hat{\omega}_i \\ -j\hat{\omega}_i & 0 \end{bmatrix} X_{ij} + \begin{bmatrix} 0 \\ 1 \end{bmatrix} e \tag{2.9}$$

$$u_{ij} = \begin{bmatrix} K_{1ij} & K_{2ij} \end{bmatrix} X_{ij} \tag{2.10}$$

where $i = 1, 2, \cdots, m$ and $j = 1, 2, \cdots, n$, $j \neq \sqrt{-1}$ and

$$X_{ij} = \begin{bmatrix} x_{1ij} & x_{2ij} \end{bmatrix}^T \tag{2.11}$$

The gains K_{1ij}, K_{2ij} are in the input vector from the output vector so that adjustments in their value do not directly change u. Each transfer function IM_{ij} is an internal model for a sinusoidal of frequency $j * \hat{\omega}$ and behaves as a notch filter. Thus, the desired system behaves as a band-pass filter with multiple notch filters. This specific structure guarantees that the closed-loop system is stable for all choices of n, m and ω_i. However, the performance of this system can vary largely with different ω_i.

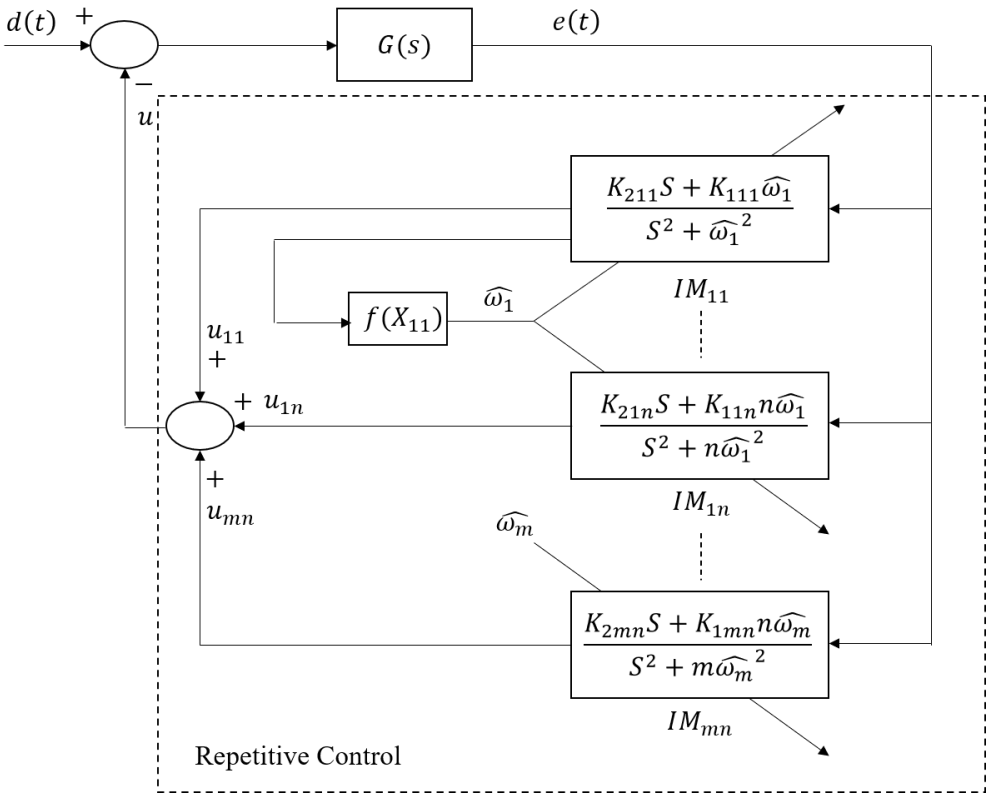

Figure 2.1: instantaneous Fourier decomposition block diagram

From Fig. 2.1, the transfer function from error $e(s)$ to the state variable $x_{2ij}(s)$ is $(k_{2ij}s + k_{1ij}j\hat{\omega}_i)/(s^2 + (j\hat{\omega}_i)^2)$ and the response at $x_{1ij}(t)$ and $x_{2ij}(t)$ in steady state are

$$x_{1ij}(t) = \bar{A_{ij}} \sin j\omega t + \theta_{ij} \tag{2.12}$$

$$x_{2ij}(t) = \bar{A_{ij}} \cos j\omega t + \theta_{ij} \tag{2.13}$$

where $\bar{A_{ij}}$ and θ_{ij} are uncertain magnitude and relative phases respectively. Consequently, we have

$$A_{ij} = \sqrt{K_{1ij}^2 x_{1ij}^2(t) + K_{2ij}^2 x_{2ij}^2(t)} \tag{2.14}$$

$$\theta_{ij} = \arctan(\frac{x_{2i1}(t)}{x_{1i1}(t)}) - j\omega_i(t) \tag{2.15}$$

Note if there is a DC component in the signal $e(t)$, the phase plot of the system will still be a circle but no longer centered about the origin. If the circle still contains the origin, only the average of the derivative over each rotation will equal ω_i, rather than at every point in time. Furthermore, if the DC component is sufficiently large, the phase plot will no longer encircle the origin and equation (2.16) will be completely invalid. In this case, the algorithm will fail miserably. Three approaches can be used to ensure $e(t)$ has no DC component. First, design the system so that there is a zero at the origin in the nominal transfer function between $d(t)$ and $e(t)$. Second, explicitly model the DC component of $d(t)$ by including an integrator as one of the internal models. Third, have a $d(t)$ with no DC component. The first method is presented above by incorporating the band-pass filter in the transfer function. The second and third will be presented in chapter 3 using the second-order low-pass filter and first-order low-pass filter.

2.3.4 Frequency and Magnitude Estimation

Since the state variables x_{1i1} and x_{2i1} are orthogonal to each other, a phase plot of them forms a circle with the state rotating at frequency ω_i. It can be shown that when $\hat{\omega}_i = \omega_i$ in the steady-state, without noise, we have

$$\omega_i = \frac{d}{dt}\angle(x_{2i1} + jx_{1i1}) \tag{2.16}$$

Accordingly, the difference $\Delta\omega$ between fundamental frequency ω_i and estimated frequency $\hat{\omega}_i$ can be presented as

$$\Delta\omega = \omega_i - \hat{\omega}_i \approx \frac{e(K_{2i1}x_{1i1} - K_{1i1}x_{2i1})}{x_{1i1}^2 + x_{2i1}^2} \tag{2.17}$$

We can use a simple integral controller to control the speed of frequency estimation convergence

$$\frac{d\omega}{dt} = K_a \Delta\omega \approx K_a \frac{e(K_{2i1}x_{1i1} - K_{1i1}x_{2i1})}{x_{1i1}^2 + x_{2i1}^2} \tag{2.18}$$

where K_a are the adaptation gains that control the frequency updating speed. Presumably, if the tuning function $G(s)$ was designed properly and the feedback gains $\{K_{111}K_{211}, ..., K_{1nm_n}K_{2nm_n}\}$ for each internal model were calculated, a quasi-periodic signal can be decomposed into a sum of narrow-band signals u_{ij} in terms of the state variables corresponding to each internal model. Here $u_{ij} = x_{2ij}$ since the second state is the sinusoidal component of the original signal and the first state is its quadrature. and a real-time Fourier representation of the reference signal can be obtained. The signal $u_{ij}(t)$ is the estimation from the internal model IM_{ij} representing the j^{th} harmonic of the i^{th} fundamental frequency. The total signal estimation $u(t)$ is represented as

$$u(t) = \sum_{i=1}^{n}\sum_{j=1}^{m_i} u_{ij}(t) = \sum_{i=1}^{n}\sum_{j=1}^{m_i} x_{2ij}(t) \tag{2.19}$$

$$\bar{A_{ij}} = \sqrt{x_{1ij}^2(t) + x_{2ij}^2(t)} \tag{2.20}$$

As the estimated frequency $\hat{\omega}_i$ and the actual frequency ω_i are getting closer, the error e that started high can be driven to a relatively small number. In addition, the steady-state solution becomes as

$$u_{ij} = x_{2ij} = \bar{A_{ij}} \cos j\omega t + \theta_{ij} \tag{2.21}$$

In [10], it is established for sufficiently small K_a that the algorithm is locally exponentially stable when $G(s)$ and the K_{1ij}, K_{2ij} are chosen so that the feedback loop in Fig. 2.1 is stable at each point in time. Choosing these controller parameters is a challenging problem as it is assumed that there is limited knowledge about the ω_i. Furthermore, there can be a significant difference between ω_i and $\hat{\omega}_i$ during the transient time.

2.3.5 Tuning Parameters Selection

As mentioned in [41], the above stability assumption is satisfied by designing the closed-loop system to incorporate a band-pass filter with notch filters. Let a second-order desirable band-pass filter be given by

$$T_{bp}(s) = \frac{d_1 s^2}{s^4 + c_1 s^3 + c_2 s^2 + c_3 s + c_4} \tag{2.22}$$

After incorporating the notch filters into equation (2.22), the transfer function of the desired system from d to e becomes as

$$T_{de} = \frac{d_1 s^2}{s^4 + c_1 s^3 + c_2 s^2 + c_3 s + c_4} \times \prod \frac{s^2 + (j\hat{\omega}_i)^2}{s^2 + 2\epsilon_{ij} j\hat{\omega}_i s + (j\hat{\omega}_i)^2} \tag{2.23}$$

where ϵ_{ij} are small real numbers, and $j * \hat{\omega}_i$ are the notches frequencies. Note that those notches frequencies are chosen to be in the pass-band of the band-pass filter. Therefore, only those signal components whose frequencies are on the notches frequencies will be captured by the desired system.

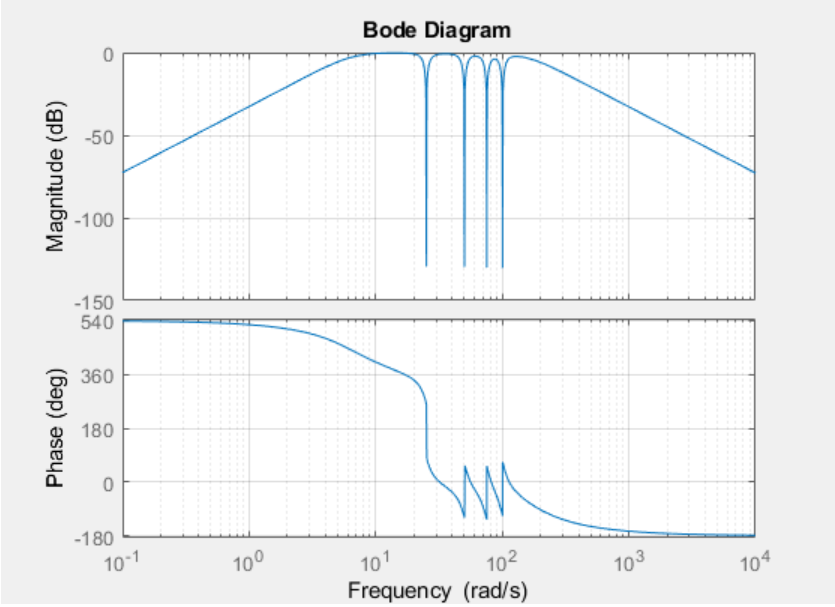

Figure 2.2: T_{de} bode plot diagram

Fig. 2.2 shows the theoretical bode plot of the desired band-pass filter with multiple notches filters. The pass-band is from 1 Hz to 25 Hz and 4 notches (located at 4 Hz, 8 Hz, 12 Hz and 16 Hz) are incorporated in it.

The analysis of Figure 2.1 gives

$$\begin{aligned} T_{de} &= \frac{G(s)}{1 + G(s) \sum_{i=1}^{n} \sum_{j=1}^{m_i} (\frac{K_{2ij} s + K_{1ij} j\hat{\omega}_i}{s^2 + (j\hat{\omega}_i)^2})} \\ &= \frac{b_1 s^2 \prod (s^2 + (j\hat{\omega}_i)^2)}{a(s) \prod (s^2 + (j\hat{\omega}_i)^2) + b_1 s^2 \sum (K_{2kl} s + K_{1kl} l\hat{\omega}_k) \gamma_{kl}(s)} \end{aligned} \tag{2.24}$$

where

$$G(s) = \frac{b_1 s^2}{s^4 + a_1 s^3 + a_2 s^2 + a_3 s + a_4} = \frac{b_1 s^2}{a(s)} \tag{2.25}$$

$$\gamma_{kl} = \prod_{i=1}^{n} \prod_{j=1}^{m_i} (s^2 + (j\hat{\omega}_i)^2) \qquad \{j \neq l \text{ if } i = k\} \tag{2.26}$$

Note in equation (2.24) $\prod$ represents $\prod_{i=1}^{n}\prod_{j=1}^{m_i}$ and $\sum$ represents $\sum_{k=1}^{n}\sum_{j=1}^{m_k}$. The terms γ_{kl} are the product of all terms $(s^2 + (j\hat{\omega}_i)^2)$ except the $i = k, j = l$ term. Now all the controller parameters can be calculated by matching the coefficients of numerator and denominators in equations. From the numerator we get $b_1 = d_1$. Unfortunately, we get a set of $2n_t + 4$ coupled equations with $2n_t + 4$ unknowns where $n_t = \sum_{i=1}^{n} m_i$, which is possible to solve off-line but not possible to achieve it in real time. In order to solve this crucial problem and make the system online, we assume that $s = \pm\sqrt{-1}l\hat{\omega}_k$. It can be seen that all of the terms in the denominator except the term containing γ_{kl} will be zero if $s = \pm\sqrt{-1}l\hat{\omega}_k$. Thus we have

$$\begin{aligned} & b_1 s^2 \sum (K_{2kl}s + K_{1kl}l\hat{\omega}_k)\gamma_{kl}(s) \\ & = (s^4 + c_1 s^3 + c_2 s^2 + c_3 s + c_4)\prod\prod s^2 + 2\epsilon_{ij}j\hat{\omega}_i s + (j\hat{\omega}_i)^2 \end{aligned} \tag{2.27}$$

This generates two complex and complementary conjugate equations with two unknown variables *i.e.* the real part of either equation gives K_{1ij} and the imaginary part gives K_{2ij}. The values of the control feedback gain parameters K_{1ij}, K_{2ij} for each internal model IM_{ij} can be obtained by solving these two linear decoupled equations. Those four a_i parameters in $a(s)$ can be explicitly solved by equating the coefficients of terms with the same degree in the denominator. In [35], J. Chen found out that these coefficients can be calculated by utilizing the relationships between the coefficients of a polynomial and the roots of a polynomial. Hence we have

$$\begin{aligned} \prod_{i=1}^{n_t}(s^2 + 2\epsilon_i w_i + w_i^2) = s^{2n_t} + \sum 2\epsilon_i w_i s^{2n_t-1} \\ (\sum w_i^2 + \sum_i \sum_{j>1} 4\epsilon_j w_j \epsilon_i w_i) s^{2n_t-2} \\ + \cdots + \prod w_i^2 \end{aligned} \tag{2.28}$$

Let $\{w_i\} = \{j\omega_i\}$, we get

$$\begin{aligned} a_1 &= c_1 + \sum 2\epsilon_i\omega_i \\ a_2 &= \sum_{i=1}^{n_t}\sum_{j>1} 4\epsilon_j\omega_j\epsilon_i\omega_i + c_1\sum_{i=1}^{n_t} 2\epsilon_i\omega_i + c_2 \\ a_3 &= c_3 + c_4\sum_{i=1}^{n_t}\frac{2\epsilon_i}{\omega_i} \\ a_4 &= c_4 \end{aligned} \tag{2.29}$$

Therefore, the computation complexity can be reduced, and it is possible to solve it online. Theoretically, this algorithm can identify signals with any number of fundamentals and harmonics without prior information. Other than continuous time, all previous work has been

replicated in the discrete-time domain by Chen [14]. However, the Z domain has serious stability issues, and a continuous implementation with low order numerical integration routines works better. Thus, the continuous-time algorithm is used in this thesis.

2.4 Parkinsonian Tremor Estimation

Parkinson's disease is a common long-term degenerative disease that mainly affects the motor system. One of the most apparent symptoms is tremor which is known as Parkinsonian tremor. Because it is an incurable disease, the estimation and suppression of the Parkinsonian tremor play an essential role in improving the life quality of patients with Parkinson's disease.

2.4.1 Parkinsonian Tremor

Parkinsonian tremor can be divided into three categories of movement disorder: resting, postural and kinetic tremor [19]. Resting tremor appears when muscles are relaxed, and its frequency range in hand is 3 to 6 Hz. Typical scenarios include when patients are lying on the bed or when their hands are resting on a table. Postural tremor can be found when muscles are contracted, and the frequency range is 5 to 12 Hz. Common scenarios include when patients are maintaining a part of the body at a fixed position against gravity or when they are holding their arms outstretched. Moreover, Parkinsonian tremor is typically unilateral, which will occur at rest, and become less prominent with voluntary motions. The amplitude of tremor varies from person to person.

2.4.2 Fourier Linear Combiner

In order to study the nature of the Parkinsonian tremor, it is important to estimate and extract the tremor from a combined signal. Filters are commonly used in this process. However, the time delay introduced by the filter is a drawback for tremor control because an actuator cannot generate an estimated tremor with zero-phase delay to oppose the vibrations.

The drawback of the typical filter prevents its use for tremor suppression. However, adaptive filtering is well suited for tremor estimation as it is constantly adapting its parameters to the input signal based on a learning algorithm. A Fourier linear combiner (FLC) was proposed by Vaz, *et al.*[50] based on the assumption that tremor can be simplified to a roughly periodic signal. It used an adaptive algorithm called the least mean square (LMS) algorithm. This algorithm attempts to estimate a possibly time-varying linear system whose weight or parameter vector $\underline{w}_k^0$ obeys

$$y_k = \underline{x}_k^{*\prime} \underline{w}_k^0 + v_k \tag{2.30}$$

$$x_k = [e^{j\omega_0 Nk}\ e^{j\omega_0 (N-1)k} \cdots e^{j\omega_0 k}\ e^{-j\omega_0 k} \cdots e^{-j\omega_0 Nk}]^T \tag{2.31}$$

$$\underline{w}^0 = [w_{-N}^0\ w_{-N-1}^0 \cdots w_{-1}^0\ w_1^0 \cdots w_N^0] \tag{2.32}$$

where the prime denotes transposition and the asterisk denotes complex conjugation, N is the number of harmonics and v_k is the inherent noise in the system. It aims to minimize the square of the error

$$e_k = y_k - \underline{x}_k^{*\prime} \underline{w}_k \tag{2.33}$$

by means of the recursion

$$\underline{w}_{k+1} = \underline{w}_k + \mu \underline{x}_k e_k \tag{2.34}$$

where μ is the step size that determines the tuning speed of each iteration. In [50], it shows that a periodic signal s_k with a period of T sampling intervals can be represented by a Fourier series shown below

$$s_k = \sum_{n=\pm 1}^{\pm N} w_n^0 e^{j\omega_0 nk} = x_k^{*\prime} \underline{w}^0, \qquad \omega_0 = 2\pi/T \tag{2.35}$$

Presumably, the signal s_k can be described by no more than N harmonics. Then by combining (2.31) and (2.34), we have

$$e_k = x_k^{*\prime} \underline{w}^0 + v_k - x_k^{*\prime} \underline{w}_k \tag{2.36}$$

which yields adaptive estimates of the Fourier series $\underline{w}^0$. However, this algorithm is based on a known frequency and assumes that the noise v_k is independent of the signal s_k. Moreover, because Parkinsonian tremor is not an ultimately periodic signal, the estimation accuracy will be flawed when the tremor is not obvious or changing.

2.4.3 Weighted-Fourier Linear Combiner

Soon after the FLC was proposed, Riviere *et al.* came up with a new tremor estimator based on FLC, called the weighted-frequency Fourier linear combiner (WFLC) [42]. It replaced the fixed reference frequency ω_0 in FLC with an adaptive frequency ω_{0_k}, (2.36) becomes

$$e_k = s_k - \sum_{r=1}^{N} [w_{r_k} \sin(r\omega_{0_k} k) + w_{N+r_k} \cos(r\omega_{0_k} k)] \tag{2.37}$$

where w_{r_k} and w_{N+r_k} are the adaptive filter weights, and N is the number of harmonics. An adaptive recursion for ω_{0_k} can then be constructed using the simplified approach underlying the LMS algorithm. The frequency components are given as follows:

$$x_{r_k} = \begin{cases} \sin(r\omega_{0_k} k) & 1 \le r \le N \\ \cos[(r-N)\omega_{0_k} k] & N+1 \le r \le 2N \end{cases} \tag{2.38}$$

Finally, ω_{0_k} is provided with its own adaptive gain μ_0. This generates the frequency recursion of the WFLC

$$\omega_{0_{k+1}} = \omega_{0_k} + 2\mu_0 e_k \sum_{r=1}^{N} r(w_{r_k} x_{N+r_k} - w_{N+r_k} x_{r_k}) \tag{2.39}$$

This gives WFLC the ability to adapt both the frequency and amplitude parameters of the Fourier series to the input signal. The implementation of the adaptive weighted frequency estimation greatly improves the performance of the tremor estimator. However, it is insufficient to represent natural tremors by applying a pure sinusoidal estimation of tremor motion. In recent years, several techniques were proposed based on WFLC. In 2007, Veluvolu, *et al.* presented a band-limited multiple Fourier linear combiner which comprised of several Fourier linear combiners [52]. It can track multiple frequency components in a signal tremor. Not long after it, a double adaptive band-limited multiple Fourier linear combiner was proposed by Veluvolu, *et al.* [51], which can tune itself to an optimum band, thereby decreasing the number of weights in [52]. Nevertheless, the experiment was done in modulated synthesized tremor signal, which was less complicated than the real tremor signal. In 2016, Adhikari, *et al.* presented a quaternion weighted Fourier linear combiner [1]. It modeled the tremor in 4-D (x, y, z and f) and yielded a more accurate model of tremor.

2.4.4 High-order Weighted-frequency Fourier Linear Combiner-based Kalman Filter

In addition to FLC and WFLC, the Kalman filter and its derivative algorithms have also been used as tremor estimator [30, 53, 5]. A great effort has been made to designing new Kalman filter derivatives. However, the descriptions of tremors are not unified, and the assessment of applying different tremor models has not been well studied, limiting the versatility and adaptability of these algorithms when they face different kinds of Parkinsonian tremors.

In 2016, a high-order weighted-frequency Fourier Linear combiner-based Kalman filter (HWFLC-KF) is proposed by Y. Zhou, *et al.*[55]. This method combined the WFLC and the Kalman filter to enhance the accuracy of tremor estimation. It divided the Parkinsonian tremor signal into two parts: the first harmonic and the combination of other higher harmonics and used two high-order WFLCs to estimate them separately. Assume that a tremor signal can be described as

$$\begin{aligned} S_t(k) &= S_{t1}(k) + S_{t2}(k) \\ S_{t1}(k) &= A_{n1}(k)\sin(2\pi f_{t1} k T_s) + b_{n1}(k)\cos(2\pi f_{t1} k T_s) \\ S_{t2}(k) &= A_{n2}(k)\sin(4\pi f_{t2} k T_s) + b_{n2}(k)\cos(4\pi f_{t2} k T_s) \end{aligned} \tag{2.40}$$

where S_{t1} and S_{t2} are the first and second harmonics, respectively. a_{n1}, a_{n2}, b_{n1} and b_{n2} are the Fourier coefficients, f_{t1} and f_{t2} are the estimated frequencies of the first and second harmonics from two high-order WFLCs, T_s is the sampling time. Then a Kalman filter is used to increase the accuracy of tremor amplitude estimation by minimizing the covariance of a posteriori estimation error. This approach significantly improves the performance of WFLC in both

frequency and amplitude estimation. However, the computation time is higher than the WFLC because of the Kalman filter.

Not long after that, an extension work based on HWFLC-KF is presented in 2018[54]. Rather than only considered the second harmonic, this enhanced HWFLC-KF also considered the third harmonic. The evaluation result on real Parkinsonian tremor signals indicates that the enhanced HWFLC-KF has high accuracy and lower computation time than HWFLC-KF. However, its performance on different types of tremors has not been verified.

2.4.5 Other Tremor Estimators

Other than the tremor estimators presented above, several other tremor estimation algorithms have been proposed and adopted as well [39, 45, 47]. In [39], a tremor estimation algorithm based on WFLC was presented to track tremor within a band of frequencies. However, similar to the WFLC, applying a pure sinusoidal estimation of tremor is inadequate to represent natural tremor. [47] designed an adaptive control system for tremor estimation and suppression. This system treated tremor as an unknown harmonic disturbance. Although the author claimed that the tremor's peak amplitude reduction is substantial, the use of a sinusoidal function as the simulated tremor is still questionable. In [45], a new framework called WAKE is developed based on wavelet decomposition and Kalman filtering to first estimate the voluntary motion in a myopic fashion and then use this information to extract involuntary movement (tremor). However, the experiment was done using the tremor data recording from a smartphone mounted on the patient's hand. The information of Parkinsonian tremor is not fully collected while the tremor is passing from arm and hand to the smartphone.

With the rapid development of neural networks, many papers use this technique to recognize and identify the tremor signal. In 2010, Cole, *et al.* applied the dynamic neural network approach to detect time-varying tremor [16]. It was able to detect Parkinsonian tremors from wearable sensor data in a high level of sensitivity. Unfortunately, it could not provide detailed information like the amplitude or frequency of the tremor signal. In addition, Eduard, *et al.* proposed an algorithm to identify Parkinsonian tremor with multiple local field potential feature classification [2]. This method used a trained classifier based on a neural network to identify the presence of tremor without the necessity of parameter-tuning. However, it was required to divide patients into certain groups and do the training separately, and the accuracy depended on the quality and quantity of collected data.

2.5 Intermittent Control

Since our ultimate goal is to achieve real-time Parkinsonian tremor suppression, some situations that may happen in reality need to be considered. For instance, the tremor signal does not always exist. While the patient is trying to do a voluntary movement or keeping arm still against gravity, the Parkinsonian tremor is likely to decrease or even disappear. In continuous-time signal tracking, these human movements will have an inestimable impact on our system. Thus, a real-time tremor suppression device requires the ability to determine whether there is

a tremor signal or a voluntary motion and respond accordingly. It can be described as doing intermittent actions in continuous observation. A technique called intermittent control can be adequately used to solve this problem.

In control theory, intermittent control is used when the control signal consists of a sequence of parameterized trajectories whose parameters are adjusted intermittently. Moreover, it can be used in psychological control system control such as the human motor system. In recent years, several papers are published in this specific area. In 1999, Brown, *et al.* proposed an intermittent cancellation control method which aimed to improve the performance of the closed-loop system by only applying the integral action intermittently in PI controller [12]. This implementation can make the proportional controller more aggressive while maintaining the stability margins and control actions at similar levels. The idea of designing to separate control laws for different disturbances is also easy to achieve and gives more robustness. However, it is restricted to plants that have infrequent changes or outstanding models of disturbance.

Further, Gawthrop, *et al.* resented an event-driven controller which recast the previously fixed sampling interval intermittent control [23] to provide an explanation for some human control systems in 2009. Rather than dividing the signal into equal intervals, it used feedforward events to detect known signals and feedback events to detect disturbance. Different control method was activated due to different event, which solved the problem of asynchronization between signal and disturbance. To extend the previous work, a computational theory of human control based on event-driven intermittent control was proposed in 2011 [22]. It provided a structure to explain the behaviour of the human operator under a broader range of conditions than continuous control. However, these articles were only in theory and had not actually been applied in real time.

Chapter 3

Algorithm Development and System Design

3.1 Overview

In this chapter, a flexible system was developed based on [36] to obtain the ability to choose a proper filter to identify signals with any number of fundamentals and harmonics. Furthermore, a new adaptive algorithm based on the new flexible system was presented to identify the Parkinsonian tremor signal.

3.2 Flexible System Design

An identifier of the signal given in equation (1.1) based on the internal model principle was proposed in Chapter 2. In [36], it is shown that the proposed system behaves as a band-pass filter with notch filters. Its main advantage is to estimate the frequency and magnitude of an unknown periodic signal. However, the Matlab / Simulink implementation is fixed and hard to modify if a signal with a different number of fundamentals or harmonics needs to be identified. Moreover, the performance of the system is only verified using a synthesized signal. Therefore, the system needs to be reprogrammed to be more flexible and easier to use, as well as the ability to estimate signals in real life.

3.2.1 Alternative Filter Selection

Second-order Low-pass Filter

As discussed in [36], although the old system does not lose stability or accuracy by allowing the difference between d and u to have a substantial DC content, the performance of this controller system can be improved by adding an additional internal model to estimate the low-frequency component and replacing the band-pass filter with a second-order low-pass filter. Notice that the low-frequency component includes all signal components below the fundamental frequency. The block diagram of this alternate system is given in Fig. 3.1. More precisely, it is necessary to remove the low-frequency component from the input to the internal models for

correcting frequency estimation. The faster poles of the low-pass filter result in a faster system and better performance. A second-order low-pass filter T_{slp} can be given by

$$T_{slp}(s) = \frac{b}{s^2 + ds + c} \tag{3.1}$$

After the controller parameters of the system have been calculated, the transfer function of the second-order low-pass filter with notch filters becomes as

$$T_{slpn} = \frac{b}{s^2 + ds + c} \times \prod \frac{s^2 + (j\hat{\omega}_i)^2}{s^2 + 2\epsilon_{ij} j\hat{\omega}_i s + (j\hat{\omega}_i)^2} \tag{3.2}$$

The tuning function $G(s)$ is reduced from five unknown coefficients to two

$$G(s) = \frac{\bar{b}}{s + a} \tag{3.3}$$

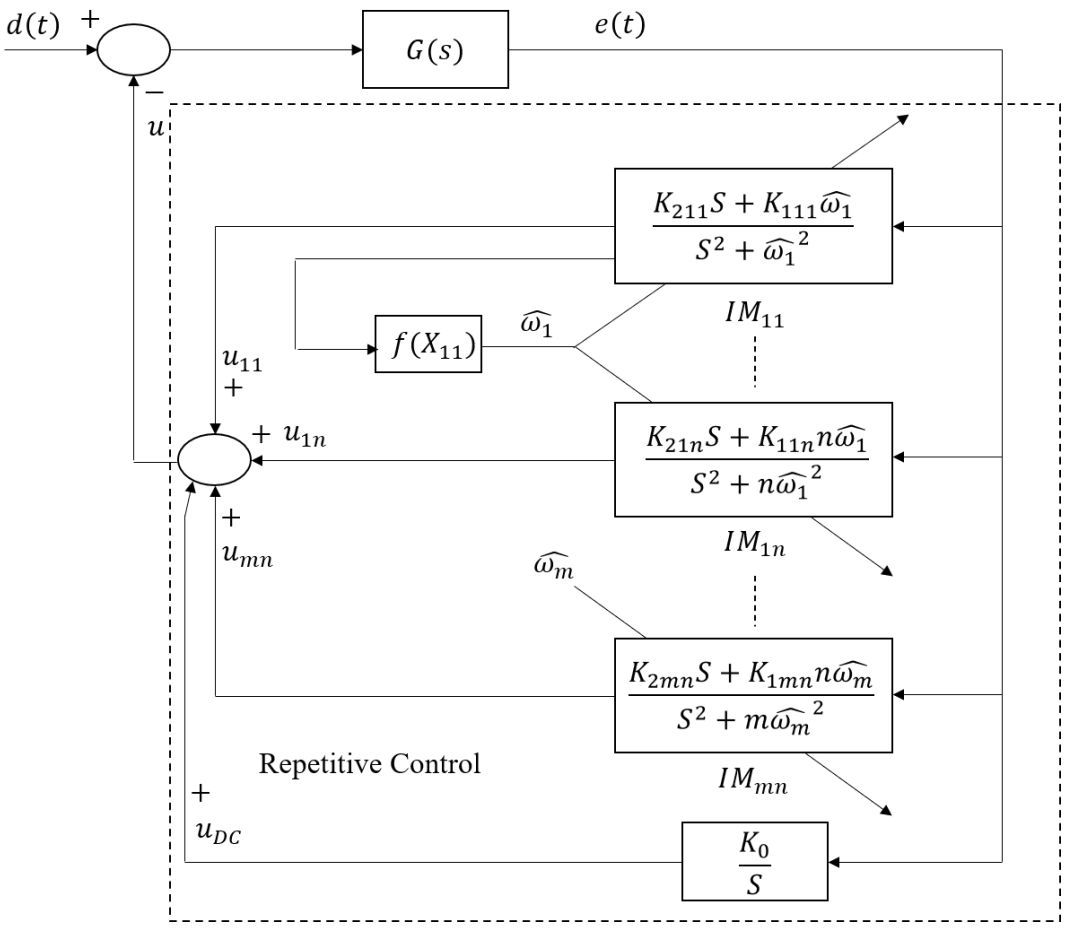

Figure 3.1: Alternative instantaneous Fourier decomposition block diagram

The transfer function of the closed-loop feedback system in Fig. 3.1 can be represented as

$$\begin{aligned} T_{de} &= \frac{G(s)}{1 + G(s)\sum_{i=1}^{n}\sum_{j=1}^{m_i}(\frac{K_{2ij}s + K_{1ij}j\hat{\omega}_i}{s^2 + (j\hat{\omega}_i)^2} + \frac{K_0}{s})} \\ &= \frac{\bar{b}\prod(s^2 + (j\hat{\omega}_i)^2)}{(s+a)\prod(s^2 + (j\hat{\omega}_i)^2) + \bar{b}\sum(K_{2kl}s + K_{1kl}l\hat{\omega}_k)\gamma_{kl}(s) + \bar{b}K_0\prod(s^2 + (j\hat{\omega}_i)^2)} \end{aligned} \tag{3.4}$$

After repeating the feedback control system gains calculation procedure in Chapter 2 for each internal model and match the numerators and denominators' coefficients in equations (3.2) and (3.4), we have $\bar{b} = b$, and when $s = \pm\sqrt{-1}l\hat{\omega}_k$

$$\begin{aligned} &\bar{b}s\sum(K_{2kl}s + K_{1kl}l\hat{\omega}_k)\gamma_{kl}(s) \\ &= (s^2 + ds + c)\prod\prod\prod s^2 + 2\epsilon_{ij}j\hat{\omega}_i s + (j\hat{\omega}_i)^2 \end{aligned} \tag{3.5}$$

Similarly when $s = 0$, $K_0 = b/c$. Besides, the a coefficient for the tuning function $G(s)$ can be calculated by equating the coefficients of the second-highest degree term of the denominator. Thus, this generates a linear equation that can be solved by back substitution.

$$a = d + \sum_{i=1}^{n_i} 2\epsilon_i w_i \tag{3.6}$$

First-order Low-pass Filter

However, some sensor families cannot produce a DC component or very low-frequency signals inherently. In those cases, neither the high-pass portion of the band-pass filter nor the integrator is needed. Particularly, the sensors being used for Parkinsonian tremor acquisition have that characteristic. Therefore, we can continue dropping the order of the low-pass filter from two to one and reducing the number of unknown parameters from two to one. More precisely, we can remove the additional internal model from the IFD block diagram. Thus, the lower order of the low-pass filter results in a more straightforward calculation and faster system.

Our goal here is to improve the performance and speed of the proposed algorithm by omitting the low-frequency component when we do not need to consider it. Hence, the IFD block diagram is the same as the system with a band-pass filter in Fig. 2.1. Accordingly, a first-order low-pass filter can be shown as

$$T_{flp}(s) = \frac{b}{s + d} \tag{3.7}$$

The transfer function of a low-pass filter with notches become as

$$T_{flpn} = \frac{b}{s+d} \times \prod \frac{s^2 + (j\hat{\omega}_i)^2}{s^2 + 2\epsilon j\hat{\omega}_i s + (j\hat{\omega}_i)^2} \tag{3.8}$$

The tuning function $G(s)$ is given by

$$G(s) = \frac{\bar{b}}{s+a} \tag{3.9}$$

and the transfer function of the closed-loop feedback system can be presented as

$$\begin{aligned} T_{de} &= \frac{G(s)}{1 + G(s)\sum_{i=1}^{n}(\frac{K_{2ij}s + K_{1ij}j\hat{\omega}_i}{s^2 + (j\hat{\omega}_i)^2})} \\ &= \frac{\bar{b}\prod(s^2 + (j\hat{\omega}_i)^2)}{(s+a)\prod(s^2 + (j\hat{\omega}_i)^2) + \bar{b}\sum(K_{2kl}s + K_{1kl}l\hat{\omega}_k)\gamma_{kl}(s)} \end{aligned} \tag{3.10}$$

Equating the numerators gives $\bar{b} = b$, and when $s = \pm\sqrt{-1}l\hat{\omega}_k$,

$$\bar{b}\sum(K_{2kl}s + K_{1kl}l\hat{\omega}_k)\gamma_{kl}(s) = (s+d)\prod_{i=1}^{n}(s^2 + 2\epsilon j\hat{\omega}_i s + (j\hat{\omega}_i)^2) \tag{3.11}$$

The a coefficient can be calculated by equating the coefficients of the degree $2n$ term of the denominator, which is also the second-highest degree term. Finally, we have

$$a = d + \sum_{i=1}^{n} 2\epsilon_i w_i \tag{3.12}$$

3.2.2 Enhancement on System Flexibility and the Solution for Common Frequencies

As mentioned at the beginning of this section, the old system is fixed and hard to modify. Because of the structure of the Simulink model, it has to be rewired and reprogrammed once a signal with a different number of fundamentals or harmonics is needed to be identified. Theoretically, this algorithm should be capable of identifying a quasi-periodic signal with any number of fundamentals or harmonics. It can be used to identify a complicated signal with many fundamentals and extract the specific signal or track a long-term signal and withdraw the characteristics of the signal. In other words, this algorithm can have many applications in the field of signal processing, automation or control. In order to extend the functionality of this system, a new flexible model is developed to let the user choose all the setting and tuning parameters to identify different kinds of periodic signals that can be described by the equation (1.1).

Basically, there are four setting parameters and five tuning parameters that influence the performance of the algorithm. In the setting part, m refers to the number of fundamentals, n refers to the number of harmonics. T_i is the system initialization time *i.e.* the system will not start to identify the signal at the first T_i seconds, which is used to omit the starting part of the signal if it does not contain any valid signal. F_{type} is the type of filter *i.e.* band-pass filter, second-order low-pass filter and first-order low-pass filter. In the tuning part, K_a represents the adaptation gains which control the speed of frequency convergence, I_0 is the initial frequency vector *i.e.* the starting frequency for each fundamental. ϵ refers to the notch width of the notch filters, ω_n is the cut-off frequency of the desired filter.

By replacing the blocks in the old model with the S-function block and reprogramming the system, the structure and function of this signal identifier can be modified by inputting parameters instead of creating a new and different program. Consequently, the system's flexibility is enhanced, and the ability to identify the signal collected from the real world is attained.

However, when a signal with two or more fundamentals is identified, some of their harmonics may share the same frequencies. The set of equations that must be solved to calculate the free parameters K_{1ij}, K_{2ij} become dependent if two or more internal models have the same frequency. This is intuitively obvious because the set of internal models become redundant when two frequencies are the same. More accurately, each internal model must represent a harmonic with a unique frequency to prevent the system from being numerically unstable. Thus, the extra internal models need to be dropped to one when two or more internal models have common or near common frequencies, and the feedback gains of the corresponding internal models are divided by the number of internal models with similar frequencies. A periodic signal after instantaneous Fourier decomposition can be represented by the sum of fundamentals and their harmonics, thus we have estimated frequencies $\{\omega_{11}, \omega_{12}, \cdots, \omega_{1n}, \omega_{21}, \cdots, \omega_{mn}\}$ for each internal models, where ω_{mn} is the n-th harmonic of the fundamental ω_{m1}, which is integer n times ω_{m1}. Once the system detected similar frequencies in different internal models *e.g.* $\omega_{12} \approx \omega_{23} \approx \omega_{34}$, equation (2.19) becomes

$$\begin{aligned} u(t) = u_{11}(t) + u_{12}(t) + \cdots + u_{22}(t) + u_{24}(t) \\ + \cdots + u_{33}(t) + u_{35}(t) + \cdots + u_{mn}(t) \end{aligned} \tag{3.13}$$

Therefore, the feedback gains for each internal model become
$\{K_{111}, K_{211}, K_{112}/3, K_{212}/3, \cdots, K_{122}, K_{222}, K_{112}/3, K_{212}/3, \cdots, K_{133}, K_{233}, K_{112}/3, K_{212}/3, \cdots\}$,
which equally divides and distributes the gain of the internal model with this particular frequency to other internal models with similar frequencies. This method prevented the confliction of internal models with the same frequencies and guaranteed the stability of the system.

3.3 Improvements for Parkinsonian Tremor Signal

In order to apply our new flexible system to the Parkinsonian tremor signal, it is essential to make improvements based on the characteristic of the data we want to identify. Approval for this research was obtained from the University of Western Ontario's Human Research Ethics Board prior to the start of the experiments. The data used in this thesis are collected from 18 patients with Parkinson's disease. The tremor signal is acquired by a special glove which has one IMU (inertial measurement unit) on each side of the index finger metacarpophalangeal joint, thumb metacarpophalangeal joint and wrist joint to record the angular velocity of three axes (pitch, roll and yaw) of each joint. The unit of angular velocity is degree per second (DPS). Hence, we have nine sets of signals to represent the tremor on a single hand simultaneously. Considering the characteristic of the tremor signal, the modifications that are needed to be developed based on the new proposed signal identifier are listing below.

1) The signals recorded from IMU contain no DC component. We need to choose a proper filter for the new system for good performance.

2) The tremor signal of each joint is a 3-D signal. The new system needs to identify this 3-D signal, not identify three 1-d signals separately.

3) The Parkinsonian tremor does not exist all the time. The new system needs to recognize the presence of tremors and find a solution for periods without tremors because the new proposed signal identifier is only guaranteed to be stable if the signal obeys equation (1.1) with at least one non-zero amplitude and frequency.

4) The patient was doing voluntary movements in some tasks. The new system needs to separate voluntary motion components from tremor signals and only suppress Parkinsonian tremors.

5) The recorded data included measurement noise with large and completely spurious values. These unexpected noises need to be omitted or eliminated, or the algorithm will be severely degraded.

3.3.1 Signal Classification

During the experimental phase, these patients were asked to do six groups of experiments with different actions. While the patient is performing different actions, the signals collected by the glove will also contain different types of tremors. The resting tremor occurred when the patient's hand was completely resting against gravity and the arm was supporting by the table. The postural tremor occurred when the patient was maintaining a position against gravity in the air, and kinetic tremor occurred during voluntary movement. The category of these actions and type of tremor within is shown in the Table. 3.1. Fig. 3.2 displayed the experiment scene when the patient was doing tasks 1B.

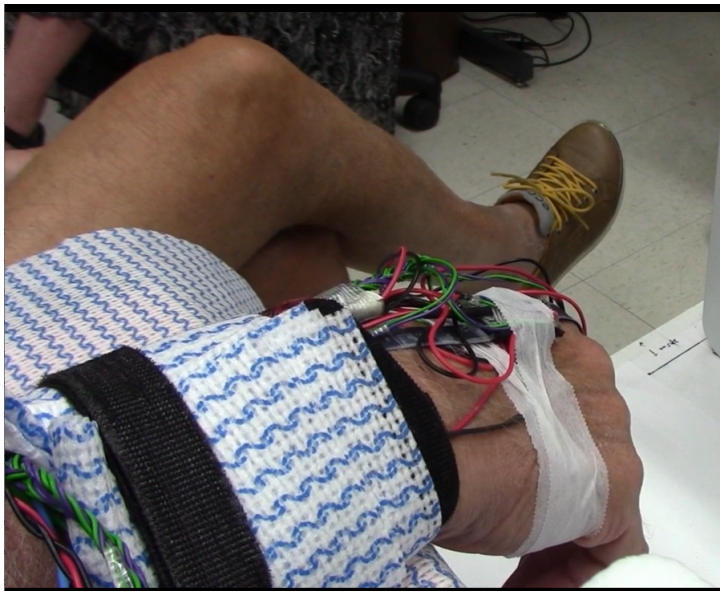

Figure 3.2: Experiment scene

Data No.	Action	Type of tremor
1A	The patient's arm keeps still on the table (thumb up)	Resting tremor
1B	The patient's arm keeps still on the table (palm down)	Resting tremor
2	The patient's palm keeps still at 45 degree angle (palm down)	Postural tremor
3	The patient moves wrist and finger joints to hold a pencil	Kinetic tremor / Voluntary motion
4	The patient moves wrist and finger joints to move pencil up and down	Kinetic tremor / Voluntary motion
5	The patient uses a pen to draw spiral circles	Kinetic tremor / Voluntary motion

Table 3.1: Category of different actions and types of tremor in these actions

An example of different types of tremors are shown in Fig. 3.3. Generally speaking, resting tremors in Task 1A and 1B are the most common type of tremor and can be easily identified because of the strong intensity of the tremor. Once the patient tried to control the hand because of the gravity in Task 2, the magnitude of the tremor would decrease accordingly. Hence, compared with resting tremors, the magnitude of postural tremors may be lower sometimes. Moreover, the tremor signal might be inconsistent since the patients were trying to maintain the position actively in Task 3,4 and 5. Because the kinetic tremor did not appear every time when a voluntary motion is conducted, and the magnitude of the kinematic tremor is much smaller than the other two kinds of tremor. Besides, the voluntary motion will also affect the identification results since it cannot be predicted.

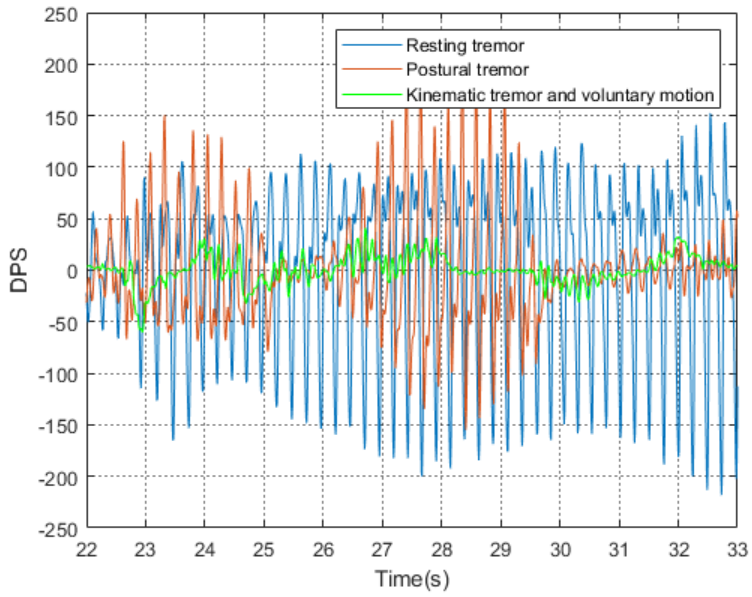

Figure 3.3: Different types of tremor (pitch signal of the index finger signal from same patient in different tasks)

3.3.2 Adaptive Frequency and Magnitude Estimation

In most of the previous Parkinsonian tremor estimation algorithms, the identified signals are all 1-D signals. However, the human hand has freedom of three dimensions. Collecting and identifying data in only one direction may result in incomplete tremor information collected. Especially when the tremor is not obvious or when the patient's hands are moving horizontally or vertically.

In order to apply the new purposed signal identifier on collected 3-D tremor data, some setting parameters have to be adjusted to adapt the Parkinsonian tremor. The first question that must be asked is how many harmonics exist in a 1-D tremor signal. Fig. 3.4 shows the short-time Fourier transform (STFT) and fast Fourier transform (FFT) of a resting tremor signal data in Task 1A. The window size and overlapped window size of STFT are 256 and 128. The sampling rates in STFT and FFT are both 100 Hz. The colour in STFT indicates the magnitude of the tremor signal, where the value of the yellow part is greater than the green part and blue part. Obviously, harmonics above the fourth order are too weak so that they can be ignored. This test is repeated in other 53 1-D signals in Task 1A, and it is observed that the obvious harmonics are usually below the fourth harmonics (the fundamental is considered to be the first harmonic). The next question is whether the tremor signal is a single fundamental signal *i.e.* only has one fundamental frequency. After setting the number of fundamentals m in signal identifier to one, Fig. 3.5 gives the square of the estimated fundamental amplitude of the pitch, roll and yaw signal from the index finger in Task 1A. It can be seen that the result does not vary periodically. If there are multiple fundamentals, the result will appear periodic because the identifier will alternately track different fundamental frequencies. Thus, we conclude that the Parkinsonian tremor signal only has one fundamental frequency. Therefore, signals from

three directions on a single joint are inputted simultaneously and treated as a signal with one fundamental and up to the fourth harmonic initially.

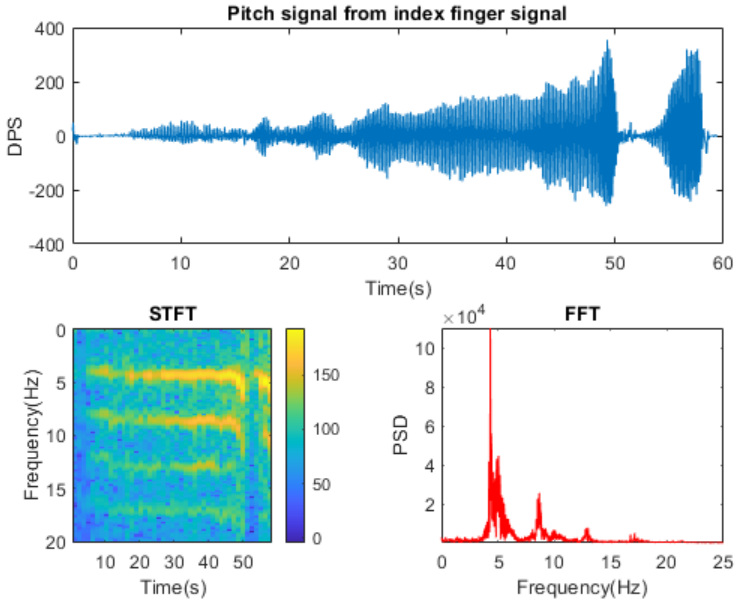

Figure 3.4: Top: Pith signal from index finger signal in Task 1A. Bottom left: STFT of the signal at top. Bottom right: FFT of the signal at top.

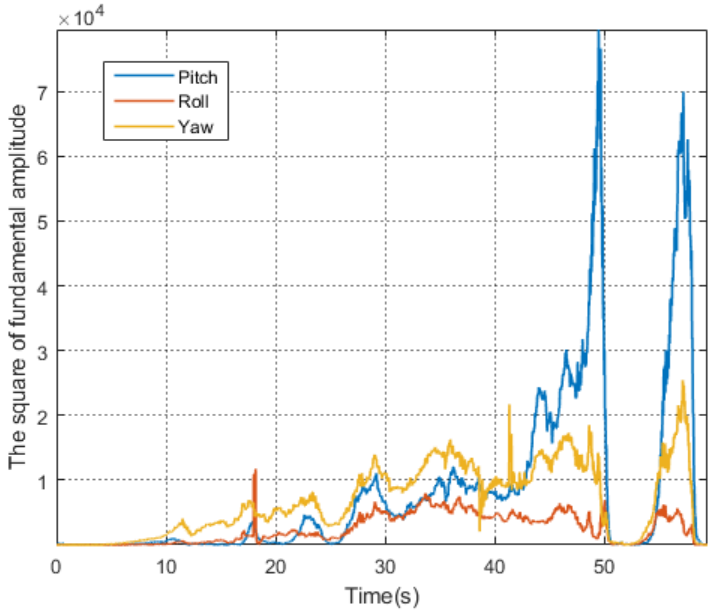

Figure 3.5: The square of the estimated fundamental amplitude of pitch, roll and yaw signals from index finger

The third question is whether the frequencies of the pitch, roll and yaw signals from the same joint are the same. Presumably, tremor signals of three directions should share the same frequency because they are coming from the same joint simultaneously. Fig. 3.6 shows the frequency estimation result when treating tremor signals of three directions from the same joint as three separate 1-D signals. It can be seen that frequencies of the three directions are similar and have the same trend. We repeated this test on the other 17 resting tremor signals in Task 1A, and the results were similar. Hence, we consider the frequencies of signals of three directions from the same joint are identical.

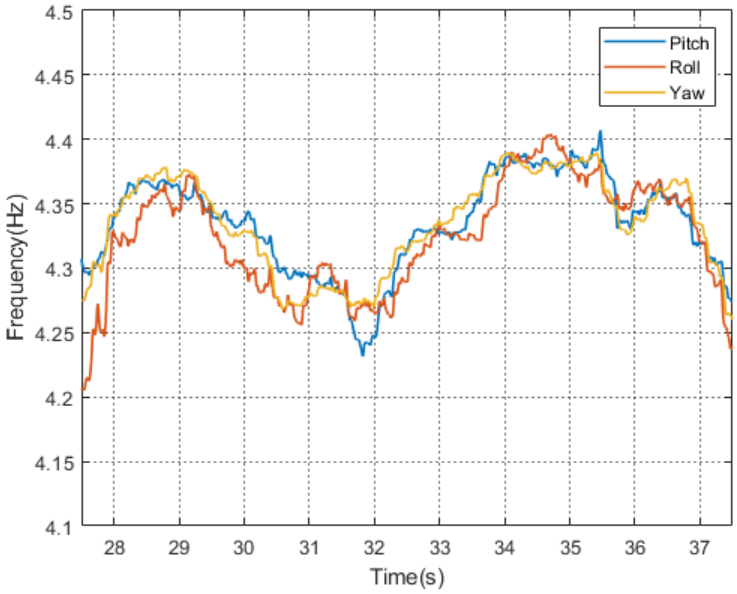

Figure 3.6: Frequency estimation of pitch, roll and yaw signals from index finger signal in Task 1A

Let a tremor signal on one joint is given by

$$d(t) = d_X(t)\hat{x} + d_Y(t)\hat{y} + d_Z(t)\hat{z} \tag{3.14}$$

where $\hat{x}$, $\hat{y}$ and $\hat{z}$ are the unit vectors pointing in the pitch, roll and yaw directions, respectively. The frequency estimation for all three directions becomes

$$\begin{aligned}\hat{\omega}_i &= \frac{1}{3}(\hat{\omega}_X\hat{x} + \hat{\omega}_Y\hat{y} + \hat{\omega}_Z\hat{z}) \\ &= \frac{1}{3}\int (Ka_X\frac{e(K_{2i}x_{X1i} - K_{1i}x_{X2i})}{x_{X1i}^2 + x_{X2i}^2} + Ka_Y\frac{e(K_{2i}x_{Y1i} - K_{1i}x_{Y2i})}{x_{Y1i}^2 + x_{Y2i}^2} + Ka_Z\frac{e(K_{2i}x_{Z1i} - K_{1i}x_{Z2i})}{x_{Z1i}^2 + x_{Z2i}^2})dt\end{aligned} \tag{3.15}$$

Note in equation (3.15) the feedback gains $\{K_{1i}, K_{21i}\}$ are the same to all three directions since their internal models are using an equivalent frequency.

Fig. 3.7 shows the IFD block diagram for Parkinsonian tremor signal identification. Instead of identifying the signal of each direction with its own frequency $\{\hat{\omega}_X, \hat{\omega}_Y, \hat{\omega}_Z\}$, our proposed system used the average of the frequencies of three directions ($\hat{\omega}_i$) to identify signals of three directions. Furthermore, the estimated signals $\{u_{Xj}, u_{Yj}, u_{Zj}\}$ of each internal model $\{IM_{Xj}, IM_{Yj}, IM_{Zj}\}$ are also calculated with average frequency $\hat{\omega}_i$ and its integer multiples. Unlike other previous studies that only analyze 1-D signals, analyzing signals in three directions simultaneously can improve the integrity and accuracy of signal identification. When the patient's hand moves vertically or horizontally in real-life situations, there may be no tremor signal in a particular direction. Only analyzing the signal in a single direction may lead to incorrect results. Moreover, the influence of a significant sensor disturbance and noise interference on a single direction can be reduced by averaging the estimated frequencies of three directions.

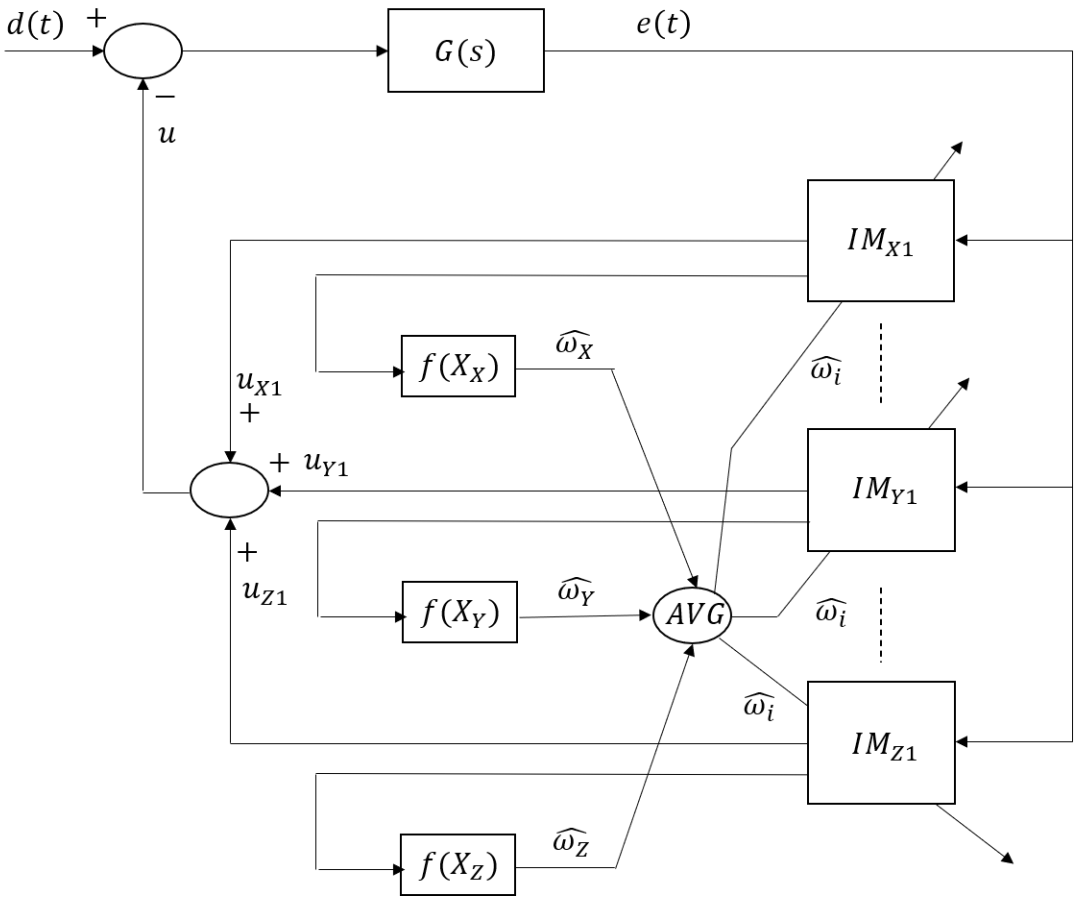

Figure 3.7: Instantaneous Fourier decomposition block diagram of signals of three directions from one joint

The magnitude of three signals are estimated separately, which is represented as

$$u(t) = \sum_{j=1}^{4} u_{Xj}\hat{x} + \sum_{j=1}^{4} u_{Yj}\hat{y} + \sum_{j=1}^{4} u_{Zj}\hat{z} \tag{3.16}$$

The final question is whether the frequencies of three joints on one hand are the same. This is a more complicated question and will be addressed later in Chapter 4. Because of the different sensor positions on each joint, the quality of the collected data may deviate. Here we use weighted factors to adjust the proportion of different joint's signals. The frequency estimation of tremor signal on a single hand can be presented as

$$\omega = A\hat{\omega}_{IF} + B\hat{\omega}_{T} + C\hat{\omega}_{W} \tag{3.17}$$

where A, B and C are weighted coefficients to be calculated and $A + B + C = 1$. The subscript IF, T and W are referring to the index finger, thumb and wrist.

3.3.3 Distinguish Between Tremor, Noise and Voluntary Motion

We showed how our new purposed signal identifier was modified to adapt to the 3-D Parkinsonian tremor signal. However, there are several different manifestations of the Parkinsonian tremor. As mentioned early in this chapter, a kinematic tremor may occur when patients are making a voluntary motion. A voluntary motion can be varied, such as when a patient is fetching a glass of water or when a patient is writing with a pen. Hence, a Parkinsonian tremor signal may contain three components: a predictable tremor, an unpredictable noise and a semi-predictable voluntary motion. The tremor is predictable because we know the frequency range and have an actual model to describe it. The noise is unpredictable because it exists all the time and cannot be identified. The voluntary motion is semi-predictable because although its external performance is varied and unforeseeable, it always appears as a low-frequency component in the signal. Identifying noise and voluntary motion will not increase our tremor estimation accuracy but pull down the system performance. Thus, rather than estimating the whole tremor signal, we aim to recognize and only estimate the tremor. Therefore, the system needs to have the ability to distinguish between tremor, noise and voluntary motion. Thus, a proper value of fundamental amplitude can be used as a threshold to distinguish between tremor, noise and voluntary motion. The amplitude of each harmonic in the tremor signal is given by

$$A_i = \sqrt{x_{1i}^2(t) + x_{2i}^2(t)} \tag{3.18}$$

where i is the order of the harmonic. Generally speaking, the fundamental (first harmonic) of the signal carries most of the information of a signal, which results in higher amplitude than other harmonics. Moreover, the fundamental amplitude A_1 of the tremor signal is much higher than the fundamental amplitude of the noise or voluntary motion signal because the tremor can be described as a quasi-periodic signal.

An analysis of the square of fundamental amplitude $(A_1)^2$ between noise and tremor in pitch

signal in Task 1B is presented in Fig. 3.8, where the blue part is the tremor, and the red part is noise. Here we use $(A_1)^2$ instead of A_1 because the value difference is more significant and easier to find a suitable threshold. Apparently, $(A_1)^2$ rises quickly once the tremor signal appears. Fig. 3.9 shows the difference of $(A_1)^2$ between voluntary motion and tremor. This signal is collected when the patient moves the wrist and finger joints to move a pencil. Similar to Fig 3.8, $(A_1)^2$ drops rapidly when the tremor signal disappears, and it does not increase when the voluntary motion arises. Moreover, $(A_1)^2$ had a small peak at around 16 seconds during the voluntary motion period as the signal that time was showing a weak pattern of tremor. Note that only the square of the fundamental amplitude of the signal in one direction is shown in Fig. 3.8 and Fig. 3.9 for a clear illustration. Hence, a proper threshold A_{max} for $(A_i)^2$ can be set during the signal estimation to recognize tremor. Unfortunately, the distinction between voluntary motion and noise cannot be achieved since their $(A_i)^2$ values are similar at most times.

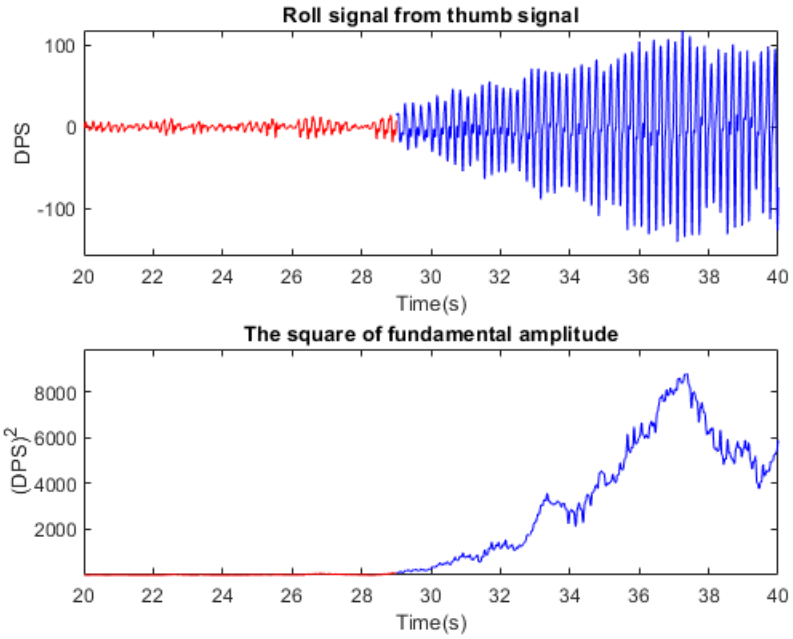

Figure 3.8: $(A_1)^2$ estimation result of tremor (blue) and noise (red) in roll signal from thumb signal in Task 1B

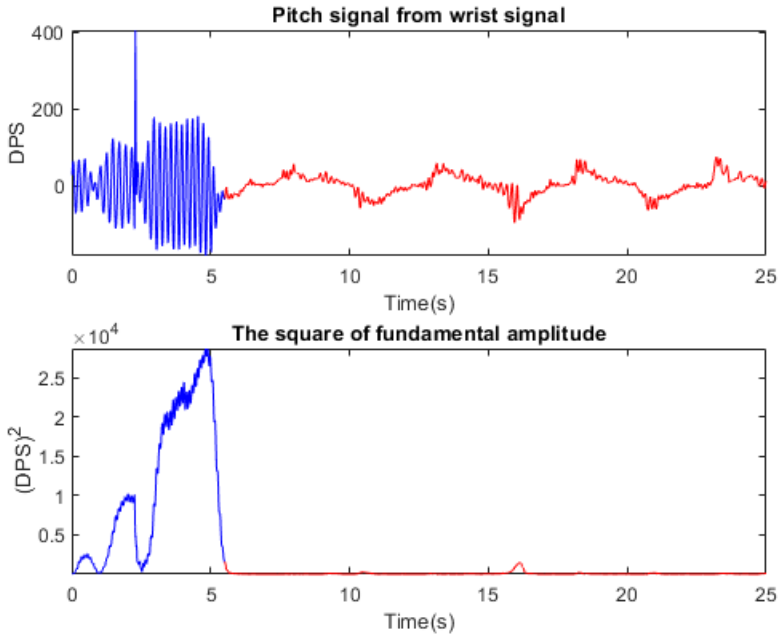

Figure 3.9: $(A_1)^2$ **estimation result of tremor (blue) and voluntary motion (red) in pitch signal from wrist signal in Task 4**

However, the system will still attempt to identify the noise or voluntary motion even if no tremor signal is included since it is a continuous-time system. As mentioned in Chapter 2, the system will become unstable if the input signal does not follow the harmonic model, which will cause the frequency estimation to drop to zero and the system stoppage. Therefore, the system also requires the ability to activate signal estimation when the tremor appears and deactivate signal estimation when only noise exists to prevent the system from collapsing *i.e.* intermittent control, which was discussed in Chapter 2 previously. Here we introduce a new parameter called substitute frequency $\bar{\omega}$ to achieve intermittent control. The structure of intermittent control is shown in Fig. 3.10 below. Assume the square of estimated fundamental amplitude, estimated frequency, substitute frequency and input signal at time t are $(A_{iT})^2$, ω_{iT}, $\bar{\omega}_{iT}$ and $d(iT)$ respectively. T is the sampling period and $iT = t$. First of all, the system calculates the square of fundamental amplitude of $d(iT)$ in 3 directions, the values are $\{(A_{1iT})^2\hat{x}, (A_{1iT})^2\hat{y}, (A_{1iT})^2\hat{z}\}$. If at least two of these three values are higher than the threshold A_{max}, signal at this time is considered as a tremor signal. Otherwise, the signal at this time is considered a non-tremor signal. The following steps can be divided into four cases based on the judgment conditions.

1) If $d((i-1)T)$ and $d(iT)$ are both tremors, the system will continue updating ω_{iT}, while the substitute frequency maintains the same.

2) If $d(iT)$ is not tremor and $d((i-1)T)$ is tremor, the system knows that the tremor just disappeared. The adaptation gains K_a will be reduced to lower frequency updating speed *i.e.* slow down the speed of system collapsing. Thus $\bar{\omega}_{(i-1)T}$ will be set equal to $\omega_{(i-1)T}$ and used to update $\bar{\omega}_{iT}$, while the estimated frequency maintains the same.

3) If neither $d((i-1)T)$ nor $d(iT)$ are tremors, the system will continue updating $\bar{\omega}_{iT}$, while the estimated frequency remains the same.

4) If $d((i-1)T)$ is not tremor and $d(iT)$ is tremor, the system knows that the tremor just appeared. Hence K_a will be restored to preset value to increase the speed of frequency updating. The latest estimated frequency will be used to update ω_{iT} since it maintained the same when there was no tremor.

Finally, the estimated magnitude of signals in three directions will be calculated separately depending on the frequency we choose. Note that the value of $\bar{\omega}$ is meaningless since its only function is to ensure the system will not fall quickly during the non-tremor period. Moreover, the substitute frequency will be reset to the latest estimated frequency if the tremor does not appear for a long period. This prevents the $\bar{\omega}$ from going to zero or infinite while it is trying to identify non-tremor signals continuously for a long time.

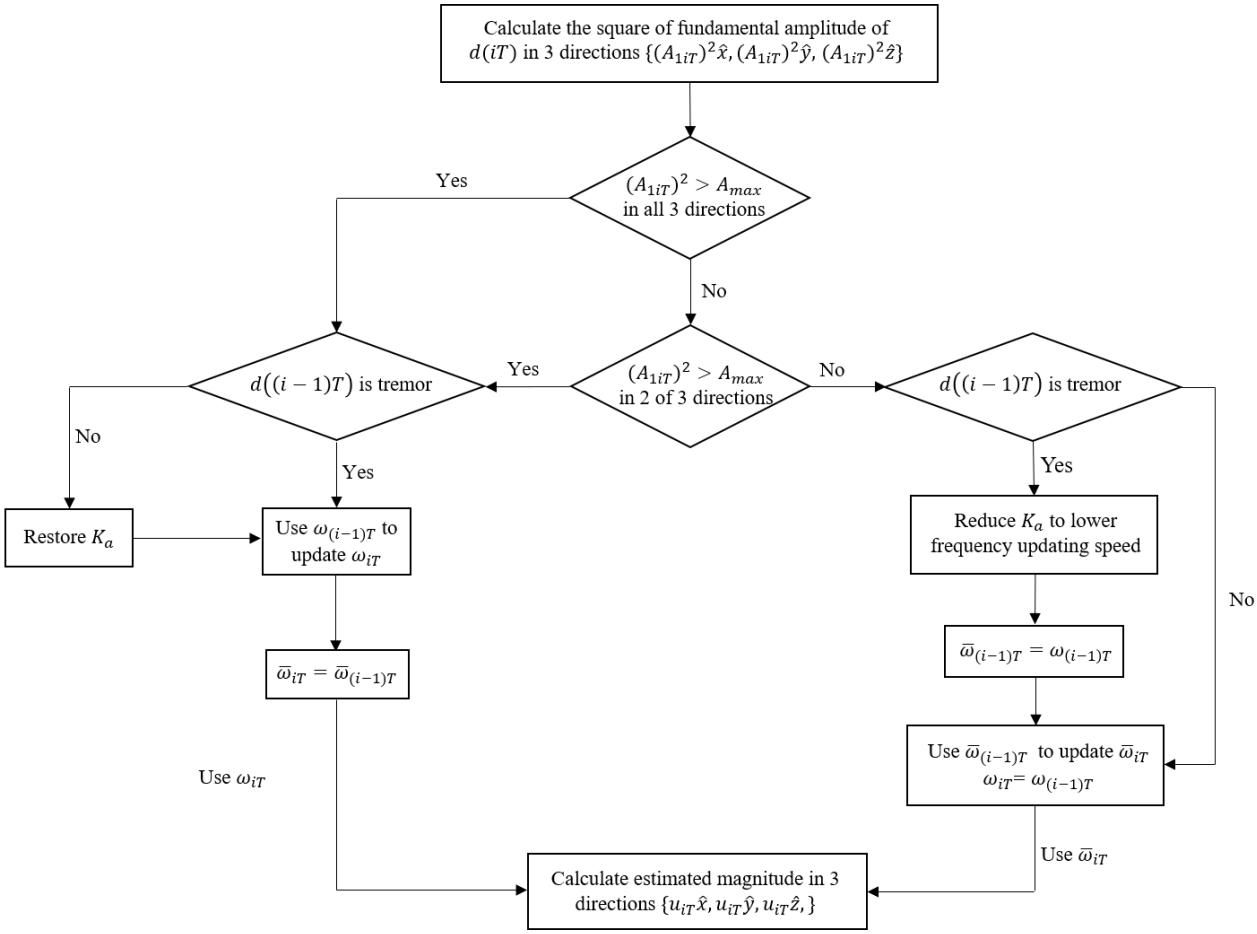

Figure 3.10: Flow chart of intermittent control with substitute frequency

3.3.4 Suppress Measurement Artifact

In general, the signal collected by the IMU sensor on the glove is accurate and stable, yet sometimes there may be offset and drift. One main measurement artifact is that the values of some sample points are large and completely arbitrary. Since our system is a continuous-time signal tracker, even a tiny error in the signal may lead to deviations in subsequent identifications and even system instability. Hence, a state transition method is presented to suppress measurement artifacts and enhance the system's robustness. The state transition diagram is shown in Fig. 3.11, where $(A_1)^2$ is the square of the fundamental amplitude, A_{max} is the threshold, and T is the sampling period in previous sections. Only when the tremor signal or non-tremor signal continues to appear for a period of time, the system will confirm the state transition and start or stop frequency updating. t_1 is normally longer than t_2 since the measurement artifact will have a more significant impact on the identification results when there are no tremor signals *i.e.* the system needs a longer time to confirm the presence of tremors than the disappearance of tremors.

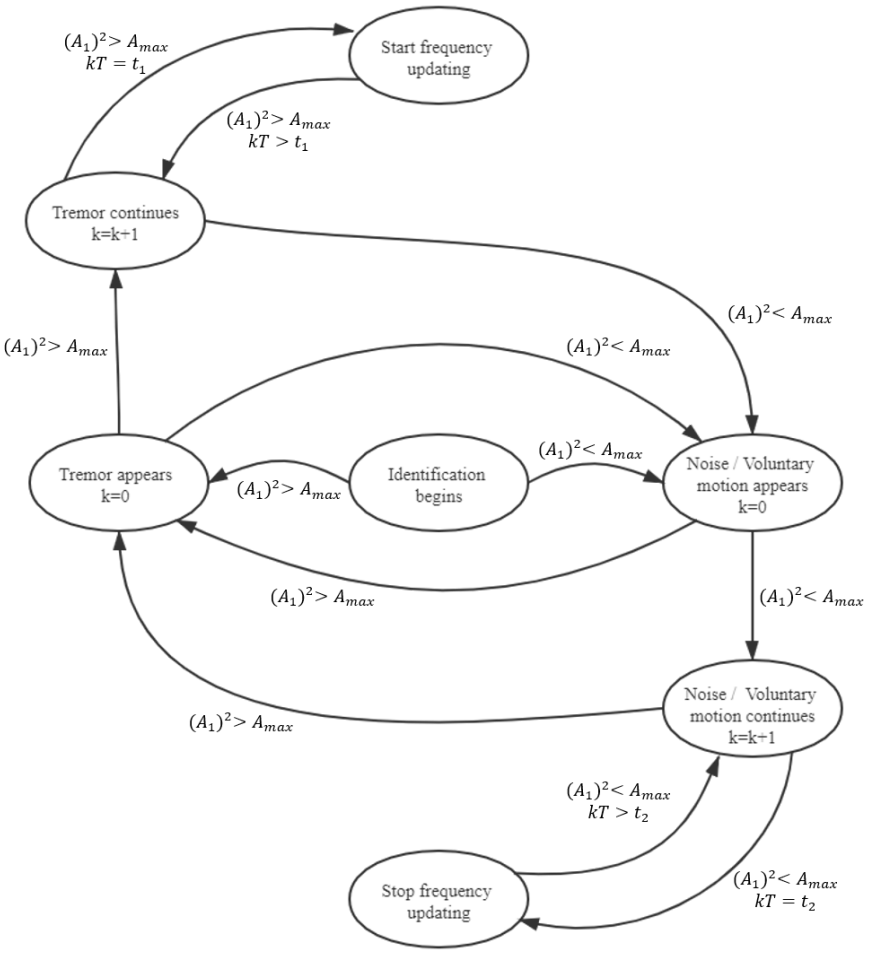

Figure 3.11: State transition diagram of system status decision process

Fig. 3.12 shows the simulation results of the system in both cases where measurement artifact suppression is not used, and measurement artifact suppression is used. This signal is composed of signals in all tasks from one patient. It can be seen that most of the signals from 200 seconds to 340 seconds are noise or voluntary motion. However, some enormous arbitrary spikes can be observed. Although those spikes are clear for us to recognize as unexpected noise, the system will consider them tremors because of the large absolute value. Without applying the state transition method, the system may mistakenly treat some measurement artifacts as tremor signals to identify. After incorporating our measurement artifact suppression method in the system, it is now able to omit those unexpected spikes or fluctuations and guarantee the robustness and stability of the system for a long period of time.

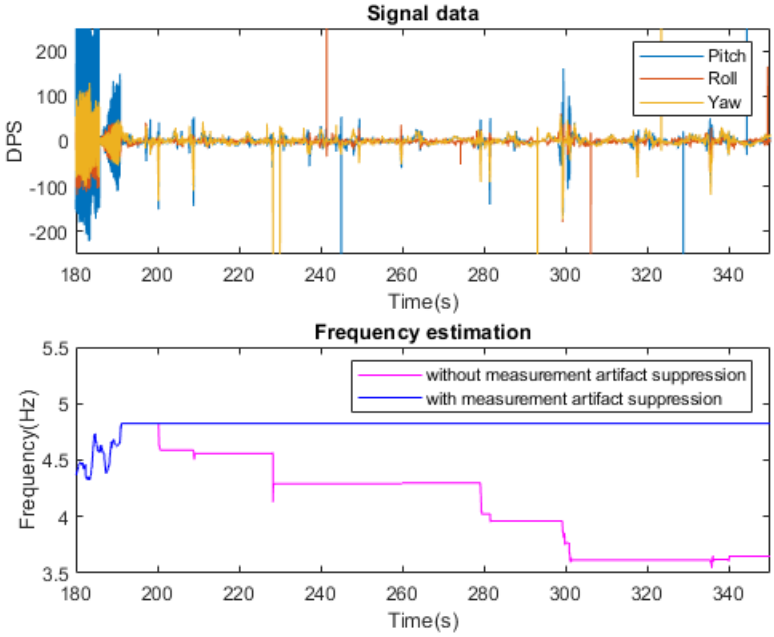

Figure 3.12: Frequency estimation with or without measurement artifact suppression in a long period of signal

Chapter 4

Simulation and Results and Comparison

4.1 Overview

In this chapter, we will show the effectiveness of the proposed Parkinsonian tremor signal identifier on different types of tremor signals. Moreover, the comparison of the first-order low-pass filter and second-order low-pass filter is shown in section 4.2. Section 4.3 shows the simulation results and comparison on synthesized Parkinsonian tremor signals. The simulation results and comparison of actual patient data are shown in section 4.4. We determined that the tremor has only one fundamental frequency and up to the fourth harmonic previously in Chapter 3. Hence, all simulation results in this chapter are based on this premise.

4.2 Comparison of first-order low-pass filter and second-order low-pass filter

4.2.1 Computing Tuning Function

In this section, the comparison of different incorporated filters is given. In [36], the comparison of a band-pass filter and a second-order low-pass filter was already presented. Thus, we will compare the second-order low-pass filter system with an integrator internal model and the first-order low-pass filter system without an integrator internal model. In addition, we need to compare the results to choose the most suitable filter for the Parkinsonian tremor identifier. We first test the performance of these two systems on synthesized signals. The signal to be identified was produced by the model shown in Fig. 4.1. The feedback loop containing the pure delay e^{-sT} is called a repetitive controller and is capable of producing any periodic disturbances with period T. The initial condition for the fundamental frequency ω is chosen to be 25.1327 rad/s (4 Hz). The disturbance input to the repetitive controller causes the amplitudes and relative phases to vary slowly with time as well. Additionally, measurement noise was added to the signal, which was band-limited to 50 Hz and had a variance of 0.1. The low-pass filter had a cut-off frequency of 157.0796 rad/s (25 Hz) to concentrate the energy in the harmonics to below the fourth harmonic. All data processing and analysis were performed offline using MATLAB (R2020a) and Simulink. The model configuration parameters used with the Matlab

environment are as follows: Solver ode5 (Dormand-prince) selection with fundamental sample time 0.1s.

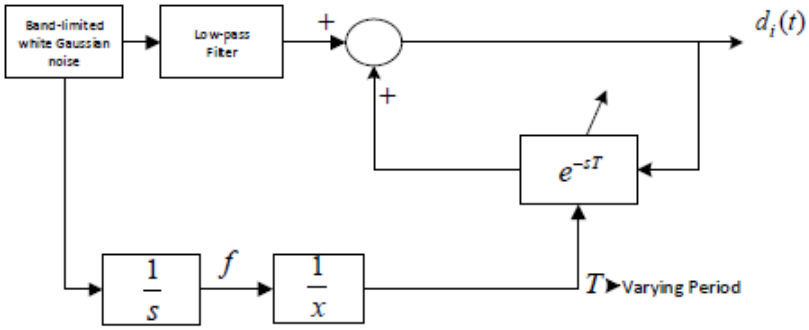

Figure 4.1: Block diagram of periodic signals generator

As mentioned in Chapter 3, the Parkinsonian tremor signals collected by IMU contained no DC component. Hence, to simulate the real situation, our signal to be identified was processed to subtract the DC component as much as possible. For the controller parameters, the frequency adaption gains were chosen as $K_a = 1.5$ and $\epsilon = 0.1$ in both systems. The initial frequencies for both systems are 21.9911 rad/s (3.5 Hz). Both filters are Butter-worth filters. For these initial values, the tuning function $G(s)$ of the second-order low-pass filter system and first-order low-pass filter system were

$$\begin{aligned} G_{1^{st}}(s) &= \frac{125.6637}{s + 143.2566} \\ G_{2^{nd}}(s) &= \frac{15791}{s + 195.3082} \end{aligned} \tag{4.1}$$

The values of K_{ij} for this frequency in each internal model of the first-order low-pass filter system and second-order low-pass filter system are shown in Table. 4.1.

i	j	$K_{ij}(1^{st})$	$K_{ij}(2^{nd})$
1	1	-212.7031	-2.8143
1	2	-37.2230	-0.7036
1	3	-53.1758	-5.6286
1	4	-9.3058	-0.3518
2	1	-425.4061	9.2480
2	2	-74.4461	2.3120
2	3	-26.5879	18.4961
1	4	-4.6529	1.1560

Table 4.1: Values of K_{ij} in each internal model

4.2.2 Frequency Identification

With these parameters, the first-order low-pass filter system took 3.65 s to run a 50 s Simulink simulation, while the second-order low-pass filter system took 4.01 s to finish the simulation. Fig. 4.2 indicates the frequency identification of two different methods. It can be seen that both identified frequencies tracked the true frequency as we expected, and they are approximate and had the same trend. The convergence time for both systems to rise from $3.5Hz$ to about $4Hz$ is 1.9 s and 2.1 s. The second-order low-pass filter performed better in frequency convergence time. Moreover, in the zoom-in figure from 27 s to 28 s, it is apparent that the second-order low-pass filter system is nosier and less able to track the frequency changes than the first-order low-pass filter system in frequency identification.

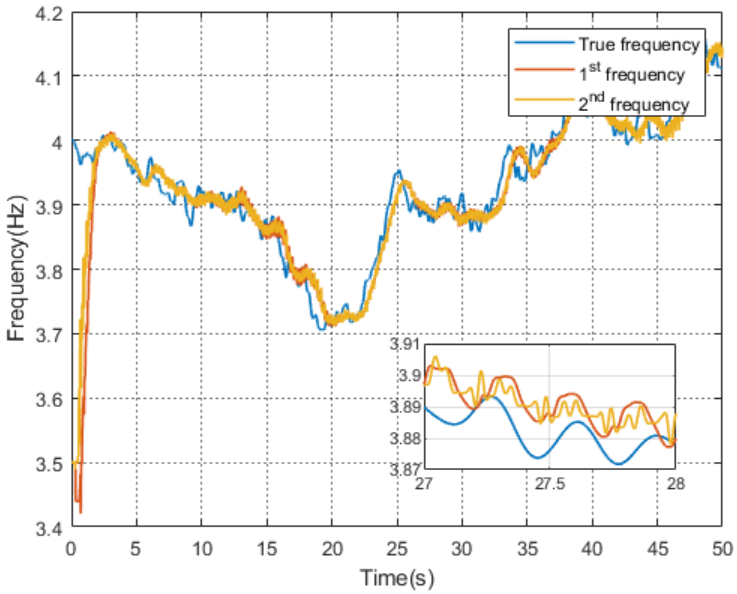

Figure 4.2: Frequency identification result of first-order low-pass filter system (1^{st}) and second-order low-pass filter system (2^{nd})

To get an overview of the accuracy of different identified models, the FFT of the input signal and the error after applying systems with different kinds of filters are shown in Fig. 4.3. Although both filters showed expected results in frequency identification, the second-order low-pass filter performed better than the first-order low-pass filter in FFT. Especially in the fundamental frequency, the second-order low-pass filter has a smaller error than the first-order low-pass filter.

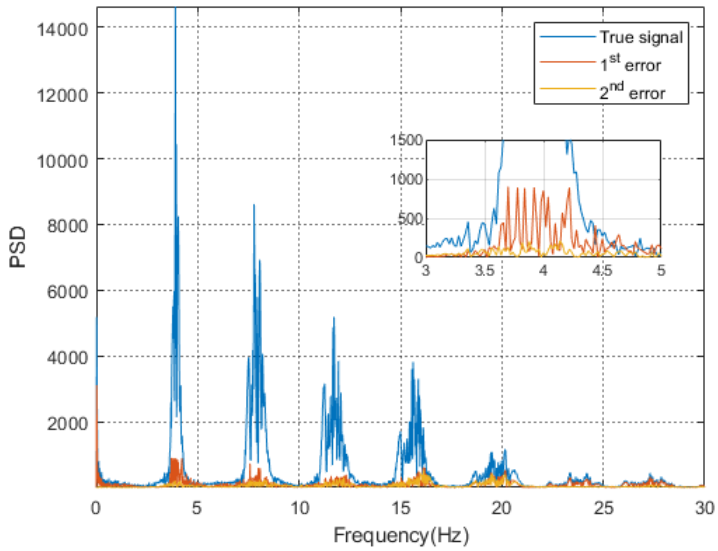

Figure 4.3: FFT of the input signal and the error of first-order low-pass filter system (1^{st}) and second-order low-pass filter system (2^{nd})

4.2.3 Signal Identification and Conclusion

Other than the comparison of frequency identification, a comparison of signal tracking is shown in Fig. 4.4. It can be seen that the second-order low-pass filter system captures the minor DC component and is closer to the true signal in those high peaks. Again both systems showed expected amplitude and relative phases matching.

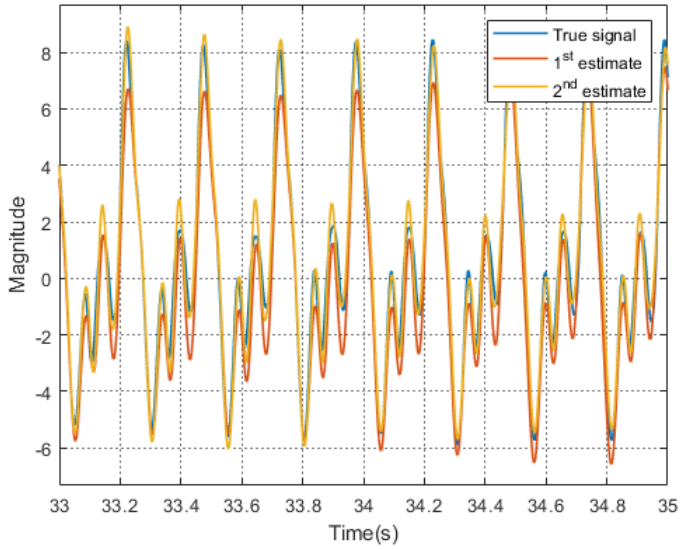

Figure 4.4: Signal identification result of first-order low-pass filter system (1^{st}) and second-order low-pass filter system (2^{nd})

In conclusion, both the first-order low-pass filter system and second-order low-pass filter system showed expected frequency and signal identification performance. By eliminating the integrator for the DC component, the first-order low-pass filter gets a faster simulation speed than the second-order low-pass filter system. However, considering that there will be a significant low-frequency component, approximating a slowly changing DC component in the signal when a patient is making a voluntary motion, the integrator for the DC component can not be removed. Hence, we decided to apply the second-order low-pass filter system in the Parkinsonian tremor identifier. Nevertheless, the first-order low-pass filter system is worthy of being put in the flexible unknown periodic signal identifier because of the lower calculation cost and higher processing speed.

4.3 Simulation Results and Comparison on Synthesized Parkinsonian Tremor Signal

A total of 18 sets of real signals are collected from patients with Parkinson's disease. Each set of data contains six groups of 3-D signals from different tasks. All data processing and analysis were performed offline using Matlab (R2020a) and Simulink. The model configuration parameters used with the MATLAB environment are as follows: Solver ode5 (Dormand-prince) selection with fundamental sample time 0.01s.

4.3.1 Preparation

Prior to applying our tremor identifier on real patient data, it was used to identify artificially synthesized Parkinsonian tremor signals. In order to imitate the real Parkinsonian tremor signal in one joint, our synthesized signal was produced by summing the outputs of three copies of the model shown in Fig. 4.1 and named as pitch, roll and yaw signal. The initial condition for all three fundamental frequencies ω is chosen to be 26.3894 rad/s (4.2 Hz). Furthermore, the signal only contains pure random noise from 0s to 5s and 35s to 43s because to simulate the scenario of the appearance and disappearance of Parkinsonian tremor. Three sets of signals are created in the same process and treated as index finger signal, thumb signal and wrist signal, respectively, to simulate the real patient data. Moreover, the DC component in the signal is deducted to a minimal number since the Parkinsonian tremor signal did not contain any DC component. Fig. 4.5 shows the synthesized index finger signal data and its corresponding frequency.

In order to get an overview of the identification performance, the frequency and signal estimation is evaluated by using RMS accuracy λ. For a 1-D signal, λ is defined as:

$$\begin{aligned} \lambda(s) &= \frac{RMS(s) - RMS(e)}{RMS(s)} \times 100 \\ RMS(s) &= \sqrt{\sum_{k=1}^{k=m} (s_k^2/m)} \end{aligned} \tag{4.2}$$

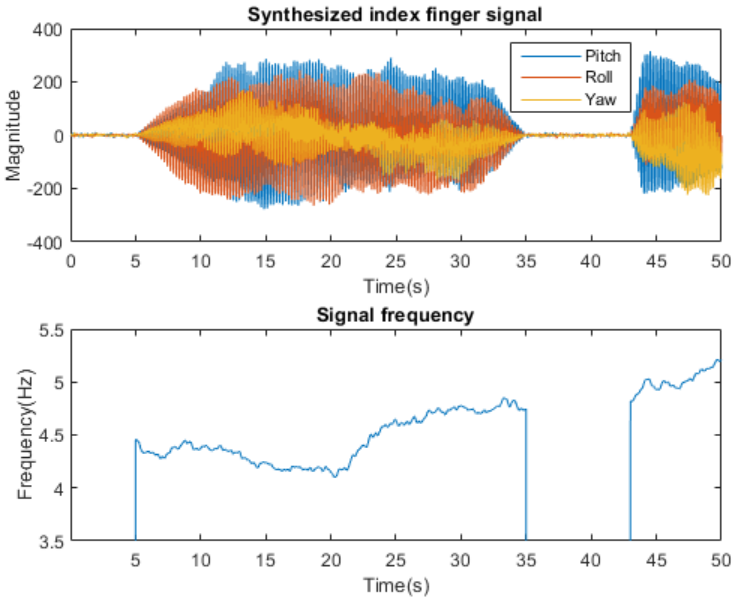

Figure 4.5: Synthesized index finger signal data and its frequency

where k is the number of samples, s is the signal, and e is the obtained estimation error. Since the tremor signal is treated as a 3-D signal, the final RMS accuracy λ is the average value of the RMS accuracies of all three directions. It can be described as

$$\lambda = \frac{\lambda(X) + \lambda(Y) + \lambda(Z)}{3} \tag{4.3}$$

Additionally, the tremor power estimation accuracy is defined by the difference between the power of the original tremor and the power of the estimated tremor. The tremor power is calculated as the total power of signal contained in the frequency band between 3 Hz and 18 Hz [54].

4.3.2 Frequency Identification

For the controller parameters, the frequency adaption gains were chosen as $K_a = 1.5$ and $\epsilon = 0.15$. System initialization time $T_i = 0.25$ s. The threshold A_{max} for judging whether it is a tremor signal or a non-tremor signal is 100. A second-order Butter-worth low-pass filter was designed and had a cut-off frequency ω_n of 157.0796 rad/s (25 Hz). The initial frequency I_0 of the system is 25.1327 rad/s (4 Hz). Finally, since the synthesized frequency does not have a measurement artifact, the measurement artifact suppression part is disabled for better results.

Under these conditions, a 50s MATLAB simulation could be performed in under 3s. The identified frequency of synthesized index finger signal is shown in Fig. 4.6. We can see an expected identification and tracking performance of the true frequency. Additionally, the system is able to recognize tremor and non-tremor periods, stop frequency estimation in a short time when

tremor disappeared and start frequency estimation when tremor reappeared. Besides, the estimated frequency converged and followed the actual frequency 1.2s after the system began to recognize and identify the tremor signal. That is a reasonable frequency convergence time from the initial frequency $4Hz$ to the actual frequency around $4.3Hz$.

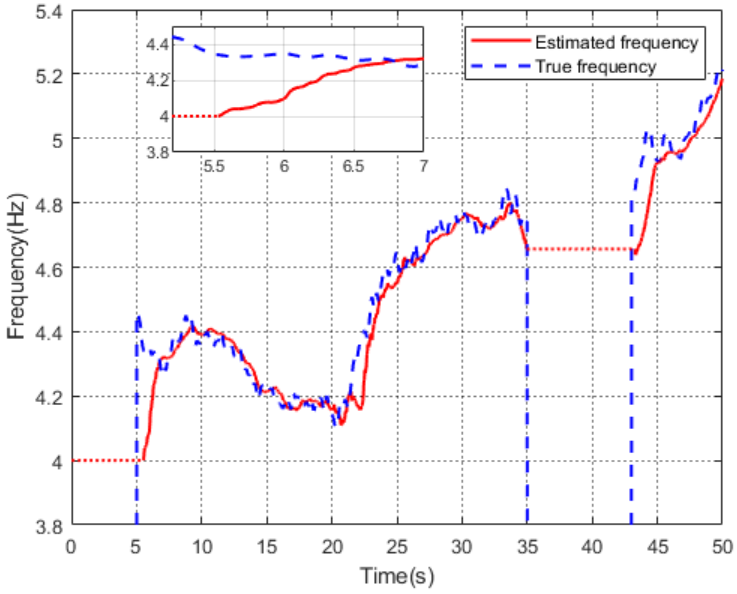

Figure 4.6: Frequency identification result of the synthesized index finger signal

Although the characteristics of the internal model principle guaranteed a minimal delay on signal tracking, the frequency identification, however, still had a delay because of the low-pass filter. To evaluate the delay of our proposed system on the frequency identification, the signal was inputted into the system reversed and compared. Fig. 4.7 gives the result of identifying the original signal and the reversed signal. It can be seen that the time shift between these two signals is around 1.5s. Thus the time delay of signal identification is about 0.75s. Fortunately, we can calculate the delay introduced by the low-pass filter $K_a/(s + K_a)$ and shift its estimated frequency by this amount of time to get the delay-free result. Note that this value may change with changes in tuning parameters and signals.

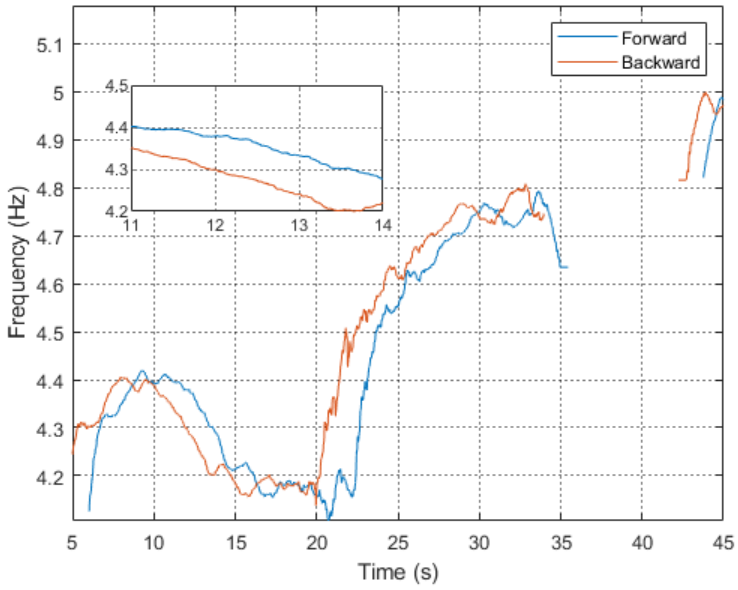

Figure 4.7: Frequency identification result of original signal (forward) and reversed signal (backward)

Among all the tuning parameters, the adaptation gain K_a is the one that has the biggest impact on frequency identification since it can directly change the speed of frequency updating. Theoretically, higher K_a will lead to higher frequency estimation accuracy and less convergence time. The frequency estimation accuracies of signals of three joints λ_{IF}, λ_T and λ_W with different K_a are shown in Table. 4.2. The average of frequency estimation accuracies is 97%. In Fig. 4.8, it can be seen that the system has a lower frequency estimation error when K_a gets higher. Furthermore, the error reduces faster when the system starts to identify the signal (5 s to 8 s), and when the frequency of the signal itself changes rapidly (20 s to 25 s). However, higher K_a will also cause the system to be more sensitive to some abnormal data or measurement artifacts. Therefore, the system needs a proper K_a to prevent instability while maintaining the accuracy and convergence speed of frequency estimation.

	Index finger (λ_{IF})	Thumb (λ_T)	Wrist (λ_W)
$K_a = 0.5$	97.1814%	96.7263%	96.5444%
$K_a = 1$	98.1139%	97.3911%	97.7758%
$K_a = 1.5$	98.4193%	97.5565%	98.2246%

Table 4.2: Frequency identification accuracy of signal of three joints with different K_a

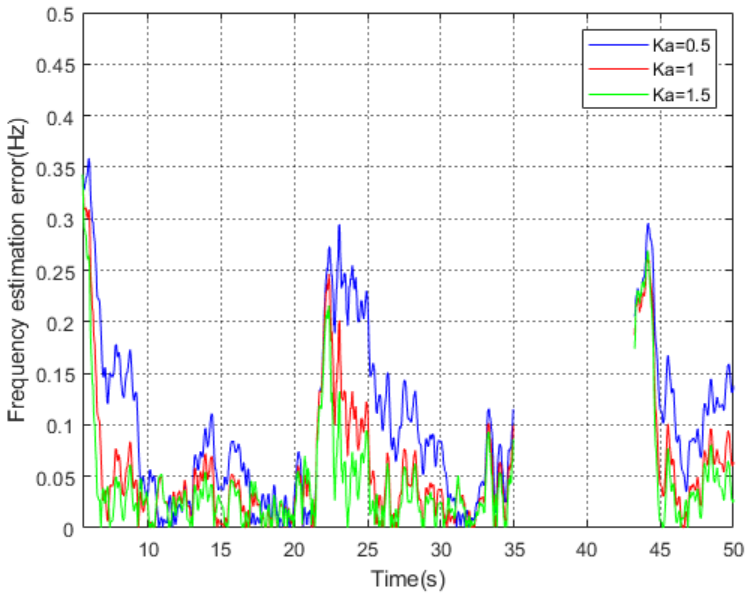

Figure 4.8: Frequency estimation error of the synthesized index finger signal with different K_a

4.3.3 Signal Identification

In this section, the signal identification of the synthesized index finger signal is given. Moreover, the instantaneous magnitude estimations for harmonics in the synthesized index finger signal are presented. The signal RMS accuracies of all nine 1-D signals with $K_a = 1.5$ are shown in Table. 4.3. The average signal RMS accuracy is 93%. Similar to frequency estimation, our system also has great performance in signal identification. Note that with appropriate adjustment of the tuning parameters, higher accuracy can always be obtained. In Fig. 4.9, it can be seen that the tracking performance is good in all three directions. However, having excessive accuracy in signal identification may not be a good thing. Since the synthesized signal contains random noise, the high accuracy may be due to the system identifying the tremor signal and the noise at the same time. Thus, as long as the accuracy is higher than an acceptable value, the system's performance is considered feasible. Additionally, there is no delay between the estimated signal and the actual signal, and that is the characteristic of any low-pass filtered signal. To take a close look at the difference between actual signal and estimated signal, Fig. 4.10 displays the actual signal, estimated signal and their difference (error). Compared to the true signal, the error is relatively small. Thus, good tracking of the synthesized signal is achieved in our proposed system.

	Index finger (λ_{IF})	Thumb (λ_T)	Wrist (λ_W)
Pitch	95.0971%	92.2088%	92.5131%
Roll	95.3846%	93.0857%	92.1235%
Yaw	93.0344%	94.7675%	92.0505%

Table 4.3: Signal RMS accuracies of signals of three joints

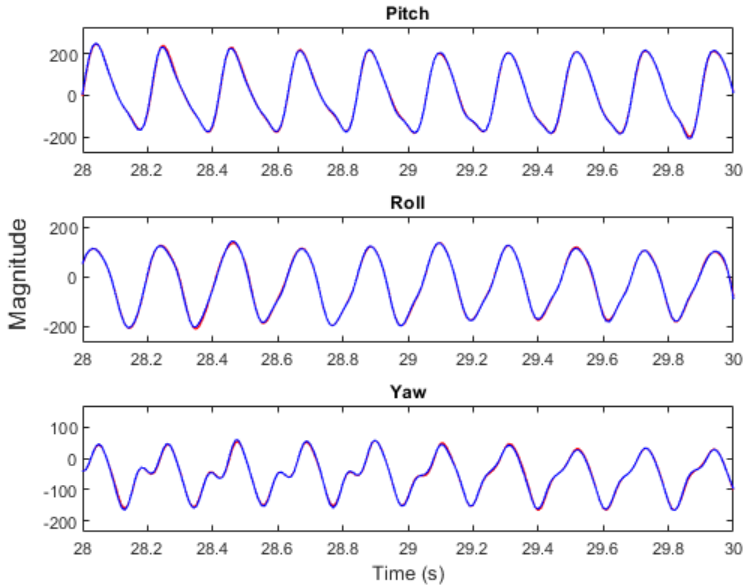

Figure 4.9: Signal identification result of the synthesized index finger signal in three directions. True signal (blue) and estimated signal (red) are shown in a 2s data segment.

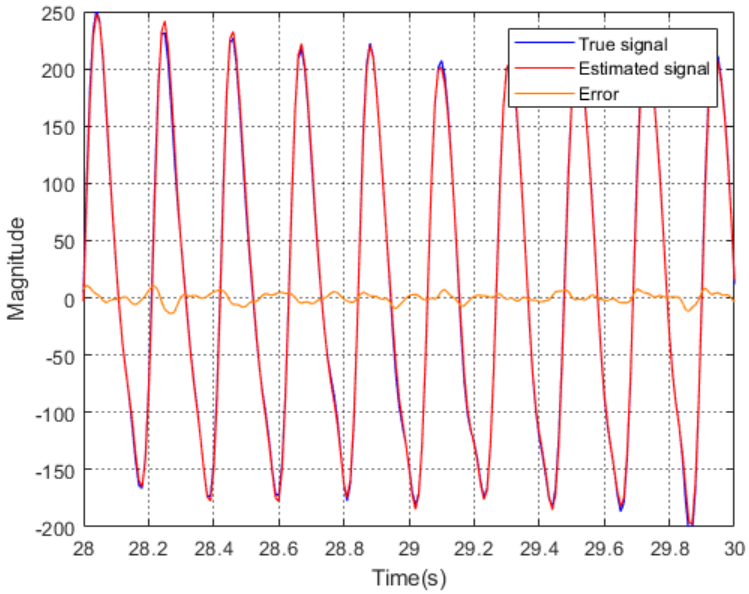

Figure 4.10: Comparison of pitch signal identification of true signal, estimated signal and their difference (error)

The harmonics are components of signals with a frequency that is positive integer multiplied by the fundamental frequency (1^{st} harmonic). Since our synthesized signal is not purely sinusoidal, the energy is included in some harmonics besides the fundamental frequency. In chapter 3, it is mentioned that the number of harmonics is set as four since the result of STFT and FFT shows that the power of the 5^{th} harmonic is almost invisible. The instantaneous magnitude of each harmonic in the pitch signal of the synthesized index finger signal can be seen in Fig. 4.11. Although it is evident that the fundamental frequency occupies most of the energy, in the meantime, the 2^{nd} and 3^{rd} harmonics also contain some of the energy. However, the magnitude of 4^{th} harmonic is extremely small and can be ignored. Hence, to reduce the calculation cost and improve the system performance, it is feasible to reduce the number of harmonics estimations from 4 to 3 in some cases.

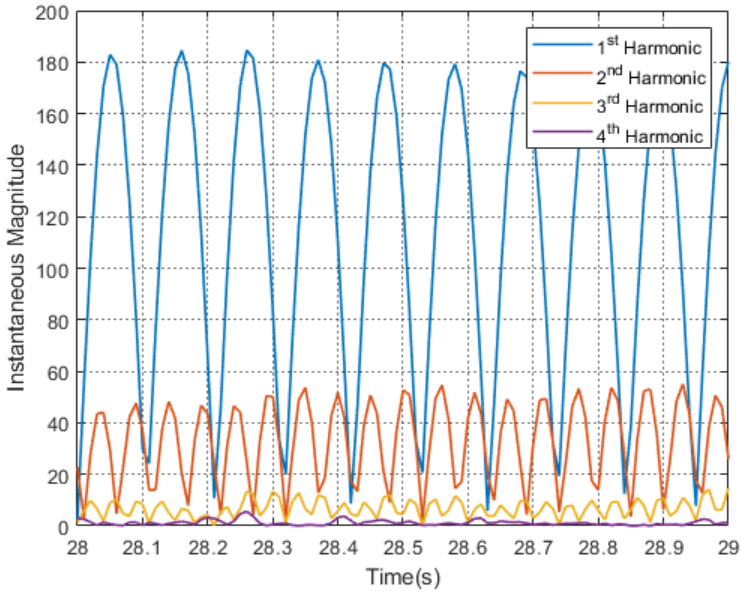

Figure 4.11: Instantaneous Magnitude of each harmonic in the pitch signal of the synthesized index finger signal

4.4 Simulation Results and Comparison on Real Patient Data

4.4.1 Resting Tremor

The initial parameters set in this section are the same as the synthesized signal identification except the K_a increased to 2 to get a faster frequency convergence speed. The measurement artifact suppression part is enabled to improve the stability of the system to the abnormal data. Moreover, the estimated signals in followed sections are chosen from the same patient to increase the confidence in results. The identified frequency of the index finger signal in Task 1B is shown in Fig. 4.12. The red, blue, and yellow lines represent the pitch, roll and yaw

signals in index finger signal data. The estimated frequency range is from 3.5 Hz to 4.5 Hz and mainly fluctuates around 4 Hz. The estimated frequency does not change drastically in general. However, it dropped rapidly by about 0.7 Hz in 1.5 seconds at around 28 seconds. In Fig. 4.13, the actual signal, frequency estimation and the square of fundamental amplitude $(A_1)^2$ during that time period is presented. It can be seen that the index finger signal from 27.5 s to 28.5 s had a smaller magnitude and showed less pattern of tremor than the signal in other periods. At the same time, A_i dropped quickly after 27.7s and start increasing again at 28.4s, which was consistent with the changing trend of frequency estimation.

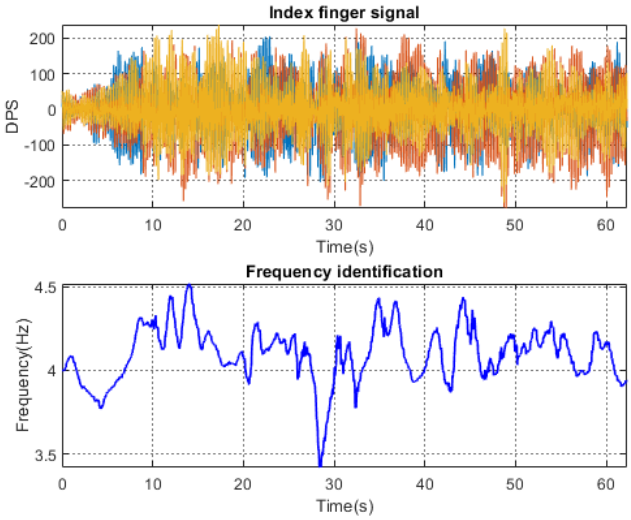

Figure 4.12: Top: Index finger signal in Task 1B. The red, blue and yellow lines represent the pith, roll and yaw signal. Bottom: Frequency identification result.

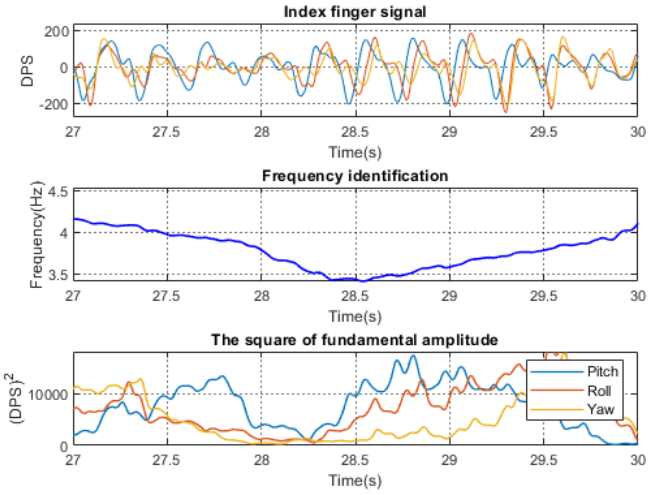

Figure 4.13: Top: Index finger signal from 27 s to 30 s. Middle: Frequency identification result. Bottom: The square of estimated fundamental amplitude.

As shown in Fig. 4.14, the frequency identification result of signals of all three joints are similar but have regions where they differ substantially. For example, from 26 s to 28 s, the frequency estimation of the wrist signal has a significant difference from other signals. As mentioned in Chapter 3, we can set proper weights for signals of three joints to reduce the effect of errors or exceptional values from each joint. However, the frequency estimation between different joints still has significant differences at some time. Hence, we conclude that tremor frequencies of different joints may be different. This can be physiologically justified on the basis that the mapping between signals from the brain to physical motion is certainly non-linear and may be different for different joints. Thus, the brain signal with the same frequency may generate tremor motions with different frequencies.

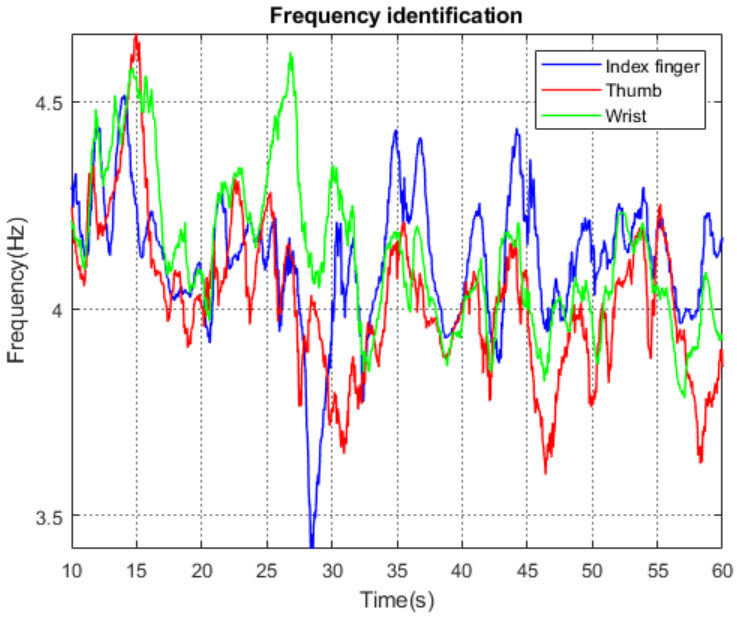

Figure 4.14: Frequency identification of index finger signal, thumb signal and wrist signal in task 1B

Unlike the synthesized signal, we do not have a precise frequency for real patient data. Here we compared our system to STFT and wavelet analysis to get a rough idea of the performance of our system in frequency identification. The frequency identification result of the pitch signal of index finger signal using our proposed system, STFT and wavelet analysis was shown in Fig. 4.15. The window size and overlapped window size of STFT are 256 and 128. The mother wavelet of wavelet analysis is the Morse wavelet. The outcome shows that the three methods have similar frequency estimation results. In most previous studies, Parkinsonian tremor was considered and reported as a signal with constant frequency. However, the frequency of this signal fluctuates in a range of 4.2 Hz to 5.8 Hz. The discovery of this pattern indicates that the frequency of Parkinsonian tremors may not be constant. Again a time delay of about 0.8s can be seen in the result of our proposed system compared to the other two approaches. The delay-free results of STFT and wavelet analysis are achieved by using the center of the window

as the time of the estimated frequency.

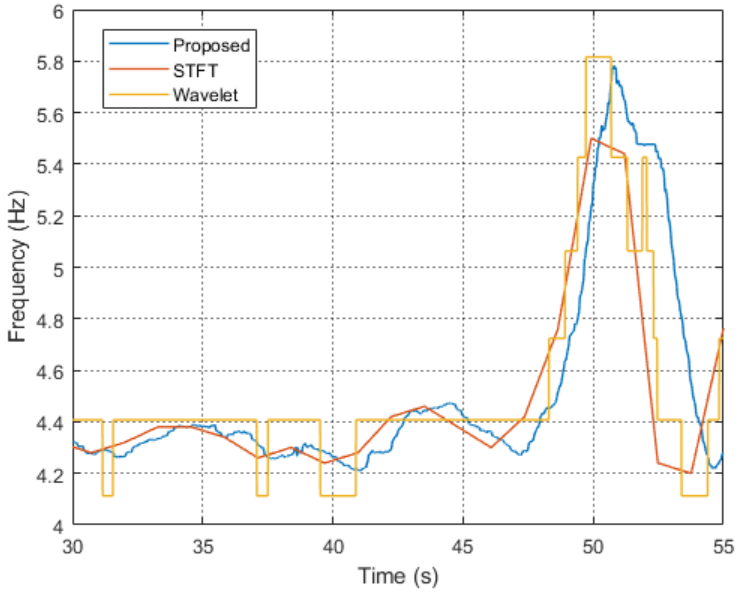

Figure 4.15: Frequency identification of the pitch signal of the index finger signal with our proposed system, STFT and wavelet analysis

Since the performance of frequency identification can not be seen from the frequency estimation results. Here we used the tremor power estimation accuracy mentioned before to represent the accuracy of frequency estimation. Fig. 4.16 shows that there are two obvious harmonics in the index finger's signal. This supports the tremor model assumed early in this thesis that the Parkinsonian tremor can be treated as the sum of a fundamental frequency and its harmonics. Moreover, the result shows good power estimation accuracy in all three directions with an average of 92%. In extension, the complete power estimation accuracies of all nine 1-D signals are shown in Table. 4.4.

	Index finger (λ_{IF})	Thumb (λ_T)	Wrist (λ_W)
Pitch	92.5682%	93.6916%	91.5210%
Roll	92.3998%	92.9420%	88.6358%
Yaw	92.5151%	93.9139%	88.9525%

Table 4.4: Tremor power estimation accuracy of signals of three joints

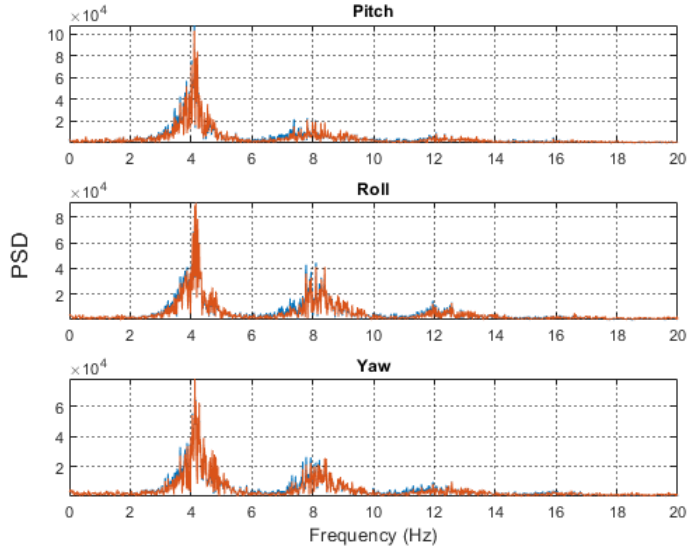

Figure 4.16: Tremor power estimation of the index finger signal in three directions. FFT of true signal (blue) and FFT of estimated signal (red).

The accuracy of signal identification is obtained by equations (4.2) and (4.3). Fig. 4.17 indicates the actual signal and identified signal of index finger signal in three directions. For all nine 1-D signals, the accuracies are shown in Table. 4.5. Again the result shows our proposed system has expected signal tracking performance as the average of the signal RMS accuracy is 85%.

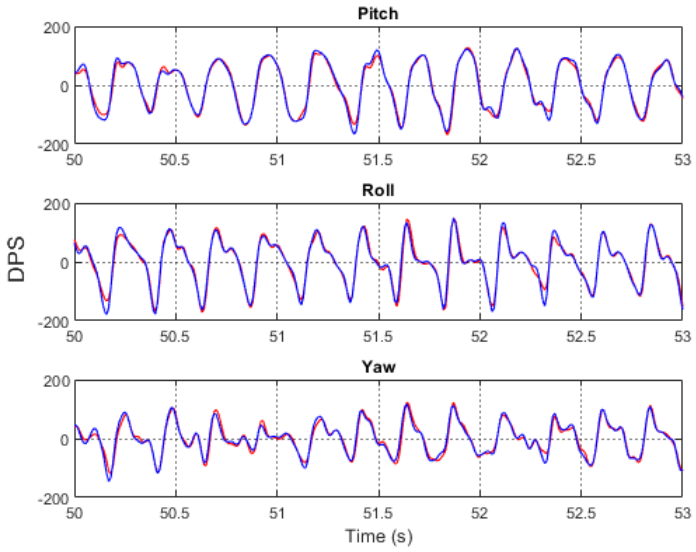

Figure 4.17: Signal identification of the index finger signal in three directions. True signal (blue) and estimated signal (red) are shown in a 3s data segment.

	Index finger (λ_{IF})	Thumb (λ_T)	Wrist (λ_W)
Pitch	88.8536%	89.7719%	81.7798%
Roll	87.7558%	82.4987%	79.0775%
Yaw	87.1621%	85.4692%	76.1312%

Table 4.5: Signal RMS accuracies of signals of three joints

However, every patient with Parkinson's disease has a unique Parkinsonian tremor with different amplitude and frequency in real life. In order to observe the general performance of our proposed system, it is applied to all 30 sets of valid data collected from 16 patients. Fig. 4.18 shows the over signal RMS accuracy and power estimation accuracy and these accuracies in the index finger, thumb, and wrist signal. The mean of signal RMS accuracy and tremor power estimation accuracy are 83.4% and 93.0%. The difference between the three joints is very small, within 0.5%.

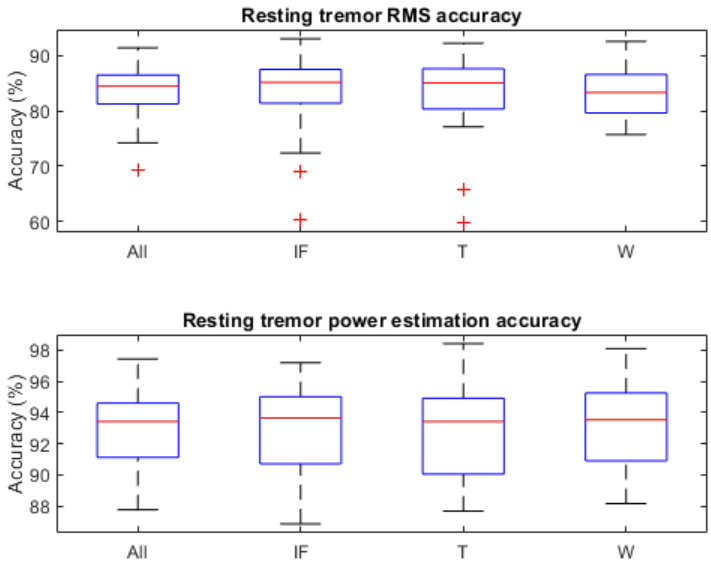

Figure 4.18: The overall signal estimation and power estimation accuracy and accuracies of the index finger, thumb and wrist signals in 30 resting tremor signals

Furthermore, our proposed identifier is compared with the HWFLC-KF and the enhanced HWFLC-KF in [54]. The test was done on 18 pitch signals of index finger index in Task 1A. Note that our proposed system was modified to identify a 1-D signal in this comparison, and the tuning parameters K_a and ϵ are increased to 4 and 0.2, respectively. The average signal RMS accuracy and its standard deviation are shown in Table. 4.6. It can be seen that the average accuracy of the enhanced HWFLC-KF and our proposed identifier is 22.4% and 21.17% higher than the HWFLC-KF. Although the accuracy of our proposed identifier is slightly lower than the enhanced HWFLC-KF, the standard deviation of our proposed system is 1.47% lower

than the enhanced HWFLC-KF.

	Mean	Standard Deviation
HWFLC-KF	67.83%	4.70%
Enhanced HWFLC-KF	90.07%	5.55%
Proposed identifier	89.00%	4.08%

Table 4.6: Signal RMS accuracy comparison of three tremor estimators

4.4.2 Postural Tremor

In this section, our proposed tremor signal identifier is applied to the postural tremor signal. The state transition time is set as $t_1 = 0.5s$ and $t_2 = 0.5s$ *i.e.* the tremor and non-tremor signals need to continue to appear for more than 0.5 seconds to be recognized by the system. The frequency identification of THE wrist signal in Task 2 is presented in Fig. 4.19. The blue line is the part that the system considers as the tremor period, and the red line is the part that the system recognizes as the non-tremor period. At 0 to 3, 15 to 17, 29 to 30, 36 to 39, and 44 to 47 seconds, the system considers the signal to be a non-tremor signal and stops updating the estimated frequency. Compare with signals in other periods, signals in these periods have a lower magnitude. To take a close look, the frequency identification and the square of estimated fundamental amplitude from 14 s to 18 s are shown in Fig. 4.20. It can be seen that the signal became chaotic and loses periodicity from 15 s to 16 s, and the tremor reappeared slowly at about 16.5 s. Moreover, $(A_1)^2$ was always lower than A_{max} in that period of time. Thus, when $(A_1)^2$ was lower than A_{max} at around 15.3 s, frequency identification stops updating the value. Note, the system only considered the signal after 15.8 s as a non-tremor signal since $(A_1)^2$ was lower than A_{max} for more than 0.5s. Same in 17.5 s, the system treated the signal as a tremor signal and started updating the frequency after $(A_1)^2$ were continuous higher than A_{max} for 0.5s.

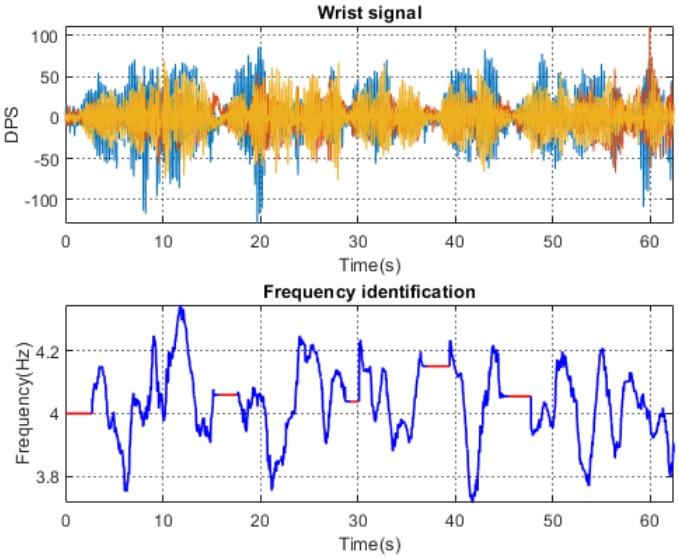

Figure 4.19: Top: Wrist signal in Task 2. The red, blue and yellow lines represent the pith, roll and yaw signal. Bottom: Frequency identification result.

In Fig. 4.21, the frequency identification of signals from all three joints is presented. The identified frequencies are approximate and matched when the values change rapidly. However, compared to the index finger signal and thumb signal, the result in the wrist signal is more fractional, and its value does not fluctuate a lot. Moreover, it can be seen that the frequency estimations of the three joints are not always similar. For example, the estimated frequencies of three joints shared the same trend from 50 s to 55 s, while the estimated frequency of the thumb signal was diverging from the other two joints from 40 s to 45 s.

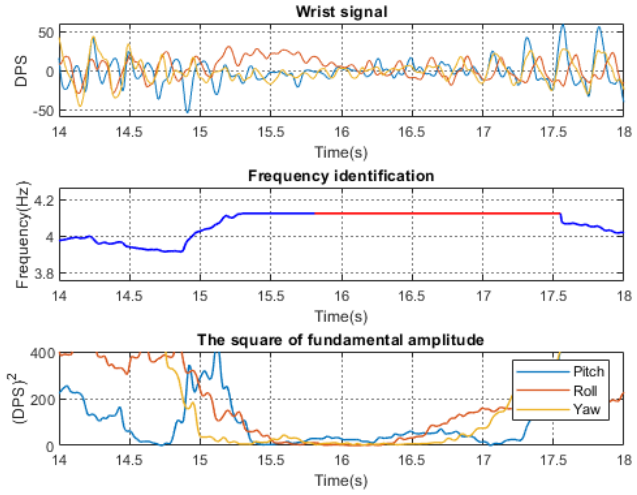

Figure 4.20: Top: Wrist signal from 14 s to 18 s. Middle: Frequency identification result. The blue line is the tremor part, and the red line is non-tremor part. Bottom: The square of estimated fundamental amplitude.

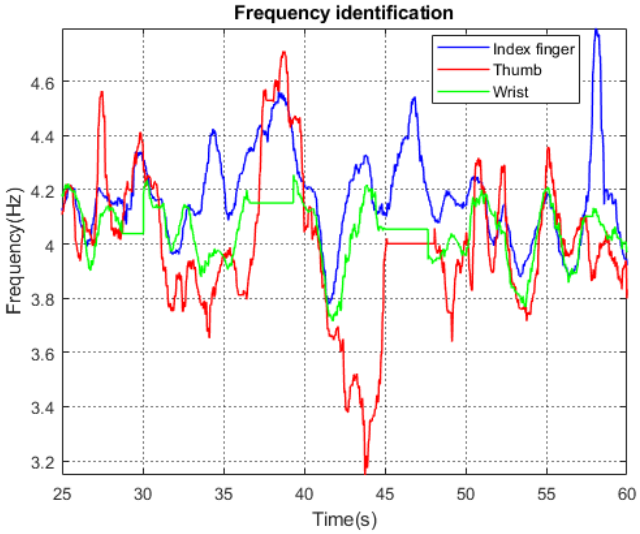

Figure 4.21: Frequency identification of index finger, thumb and wrist signal in Task 2

Fig 4.22 presents the tremor power estimation of signals of three directions in the wrist signal. The results indicate that our system achieved a reasonable tremor power estimation performance in postural tremor. The difference from the resting tremor is that the third harmonic is weaker and can barely be seen. Moreover, the complete power estimation accuracies of all nine 1-D signals are shown in Table. 4.7. The average power estimation accuracy is 92%.

Fig. 4.23 shows the signal identification result of the wrist signal in three directions from 14 s to 18 s. As mentioned before, the frequency identification in this time period is not as consistent

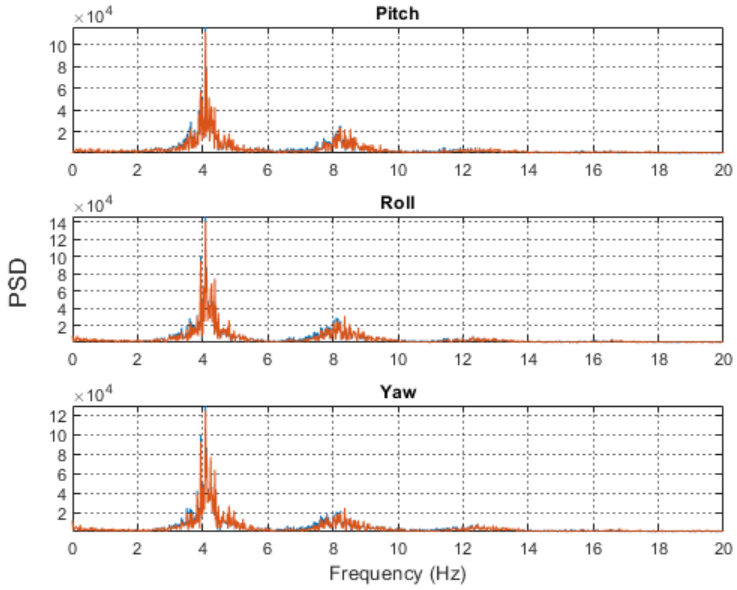

Figure 4.22: Tremor power estimation ratios of the wrist signal in three directions. FFT of true signal (blue) and FFT of estimated signal (red).

	Index finger (λ_{IF})	Thumb (λ_T)	Wrist (λ_W)
Pitch	93.5702%	91.9138%	92.7885%
Roll	93.5035%	90.8751%	91.0423%
Yaw	93.0128%	92.2715%	92.2294%

Table 4.7: Tremor power estimation accuracies of signals of three joints

as the resting tremor signal. Even so, our proposed system can still track the signal and show reasonable matching performance. In Table. 4.8, the signal RMS accuracies of all nine 1-D signals in Task 2 are presented. Note that only tremor periods are considered in the accuracy calculation. The system performance is good in signals from the index finger and thumb as the average accuracy is 88%. However, the accuracy of the wrist signal is much lower than the signals from the other two joints. Combined with the previous frequency identification result of this wrist signal, it can be seen that the wrist signal is less reliable than the other two joints. Thus, in the real-time test, we can set a low weight for wrist signal in frequency identification to improve our system performance.

	Index finger (λ_{IF})	Thumb (λ_T)	Wrist (λ_W)
Pitch	92.2746%	85.2256%	75.2817%
Roll	92.3909%	79.3792%	65.7598%
Yaw	91.7539%	78.1850%	73.8484%

Table 4.8: Signal RMS accuracies of signals of three joints

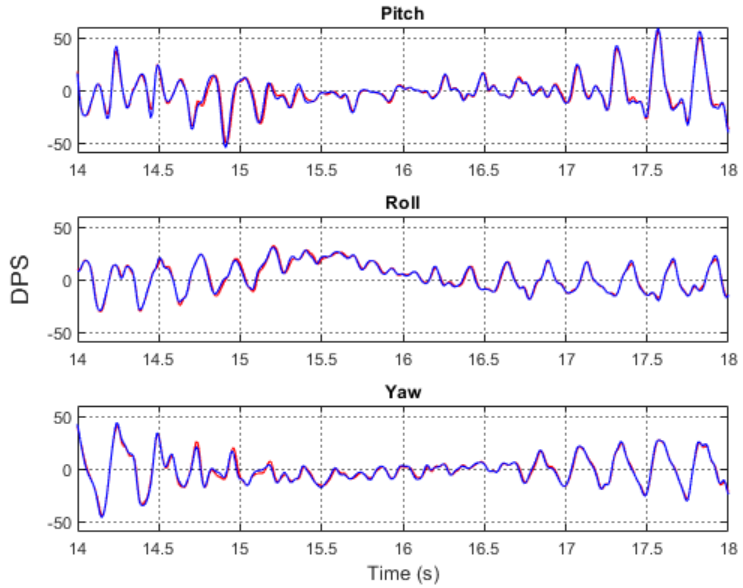

Figure 4.23: Signal identification of the index finger signal in three directions. True signal (blue) and estimated signal (red) are shown in a 4s data segment.

Again, to get an overview of our system's performance on the postural tremor, the simulation has been done in 13 sets of valid data recorded from 13 patients. The overall signal RMS accuracy and tremor power estimation accuracy are given in Fig. 4.24. Although the postural tremor signal is more complicated and harder to predict, our identifier still has expected performance on both signal identification and tremor power estimation. The mean of signal RMS accuracy and tremor power estimation accuracy are 80.7% and 91.3%.

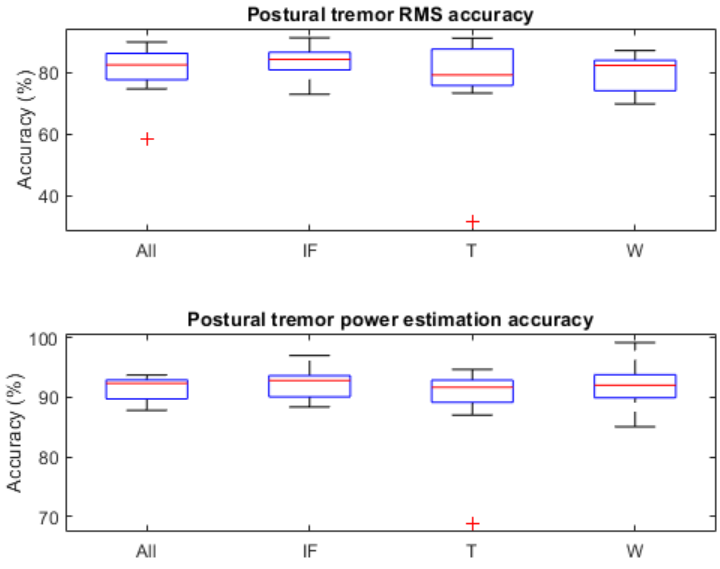

Figure 4.24: The overall signal RMS accuracy and power estimation accuracy, and the accuracies of the index finger, thumb and wrist signals in 13 postural tremor signals

4.4.3 Kinetic Tremor and Voluntary Motion (Task 3)

In this particular section, our proposed tremor signal identifier is applied to the experimental data from Task 3, 4 and 5 to identify the kinetic tremor. The patient moves the wrist and finger joints to interact with a pencil in Task 3 and 4, and they use a pen to draw spiral circles in Task 5. Note that during the experiment, any kinds of tremors can appear. Unfortunately, the tremor is not very likely to appear or be obvious when patients are making voluntary motions. However, having Parkinsonian tremors when doing voluntary can cause massive trouble even the tremor is not apparent. Hence, we aim to suppress the kinetic tremor as patients making voluntary movements *i.e.* separate tremor from voluntary motion and only suppress the tremor. Same as previous simulations, the data are chosen from the same patient in resting tremor and postural tremor parts. The analysis of Task 3 is shown in this section, and the analysis of Task 4 and 5 are in appendices A and B.

In Task 3, the patient was asked to lift the palm to a specific position, hold a pencil for a few seconds with index finger and thumb, then release the pencil and put down the palm back to the initial position naturally. This process was repeated five times. Here we divide this process into three steps: lifting the palm (A), holding the pencil (B), putting down the palm (C). To get an overview of the whole process, the signals of three joints divided into five cycles are shown in Fig. 4.25. A segment from 12 s to 17 s from Fig. 4.25 is divided into those three steps and shown in Fig. 4.26. There are resting tremor signals in the first few seconds and the last few seconds because the patient's palm just stayed still. From 2 s to 30 s, the patients were repeating the same movements five times. While an obvious pattern of tremor can be seen in the roll and yaw signal of index finger signal, the roll and yaw signal of wrist signal does not show an apparent pattern of tremor, but a slow voluntary motion causing by steps A and C.

Additionally, the pitch signal of thumb signal shows a trace of voluntary motion. In all signals from three joints, no pronounced tremor was appearing when the patient was trying to hold the pencil in step B in all five cycles.

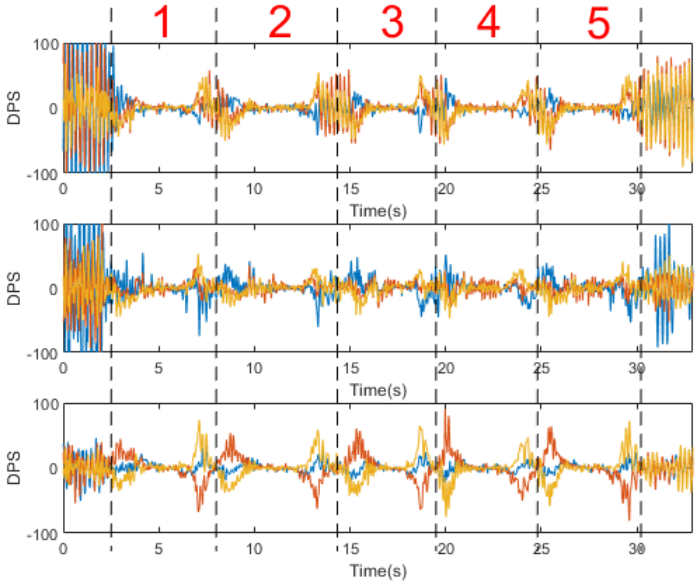

Figure 4.25: Overall signal in Task 3 with cycles division. Top: Index finger signal. Middle: Thumb signal. Bottom: Wrist signal. Blue line is pitch signal, red line is roll signal, yellow line is yaw signal.

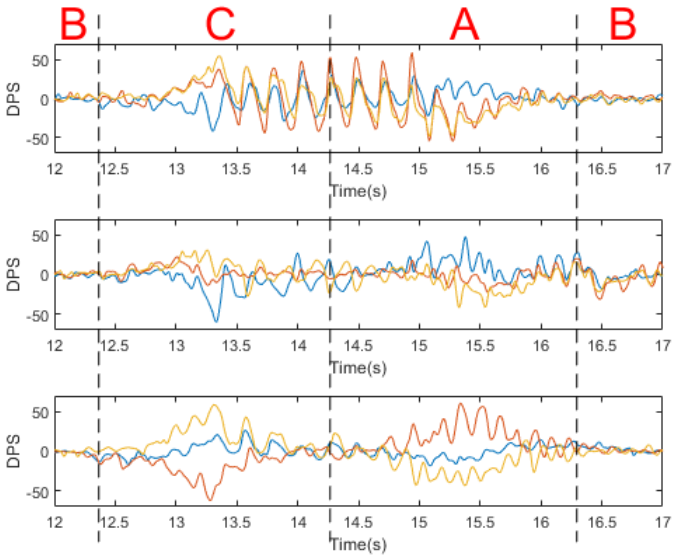

Figure 4.26: Segment from 12 s to 17 s with steps division. Top: Index finger signal. Middle: Thumb signal. Bottom: Wrist signal. Blue line is pitch signal, red line is roll signal, yellow line is yaw signal.

Considering that the tremor does not frequently appear continuously in the signal, the frequency adaptation gains K_a was increased to 2 to shorten the convergence time, and the t_1 and t_2 for confirming the state switch are reduced from 0.5s to 0.2s to let the system switching states more quickly. Fig. 4.27 shows the frequency identification and fundamental amplitude estimation after applying our proposed signal identifier to the index finger signal in Fig. 4.25. In frequency identification, the blue line represents the tremor frequency, and the red line maintains straight because the system recognizes this period as a non-tremor signal and stops frequency updating. It can be seen that our system detected the kinetic tremor in steps A and C and estimated the frequency of tremor. Unfortunately, the tremor period is too short for us to know if the system keeps up with the actual frequency. Besides, $(A_1)^2$ of the roll and yaw signal in the tremor period is significantly higher than in the non-tremor period. This result supports our previous hypothesis for this signal. To evaluate the performance of our system in frequency identification, the power estimation accuracies of signals of three directions in the index finger signal are given in Fig. 4.28. A huge low-frequency component is identified because of the voluntary motion. The tremor frequency ranges from 4 to 4.5 Hz, and we can see a weak second harmonic. The tremor power estimation accuracies are 93.3%, 93.1% and 94.1% in three directions. Here we did not calculate the tremor power estimation accuracies of the thumb and wrist signal since the tremor in those joints is too weak to be identified. Although the tremor is not strong and consistent in this signal, our proposed identifier still achieved an expected performance on tremor power estimation.

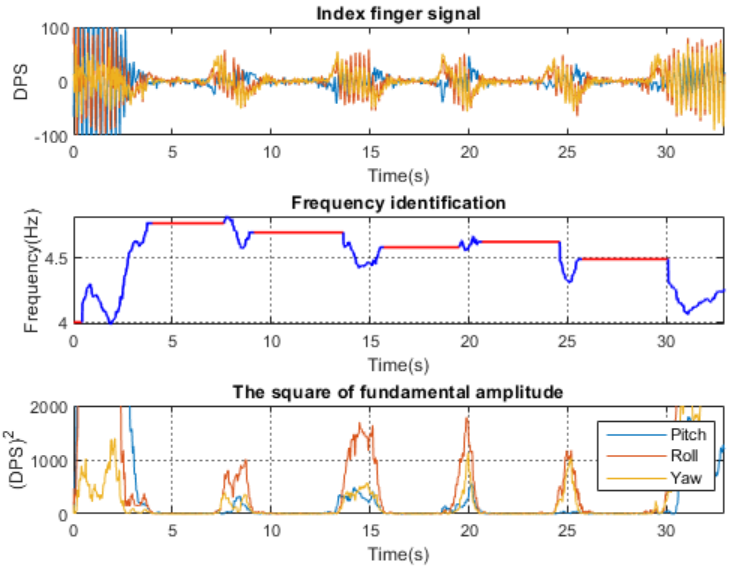

Figure 4.27: Top: Index finger signal in Task 3. Middle: Frequency identification result. The blue line is the tremor part, and the red line is non-tremor part. Bottom: The square of estimated fundamental amplitude.

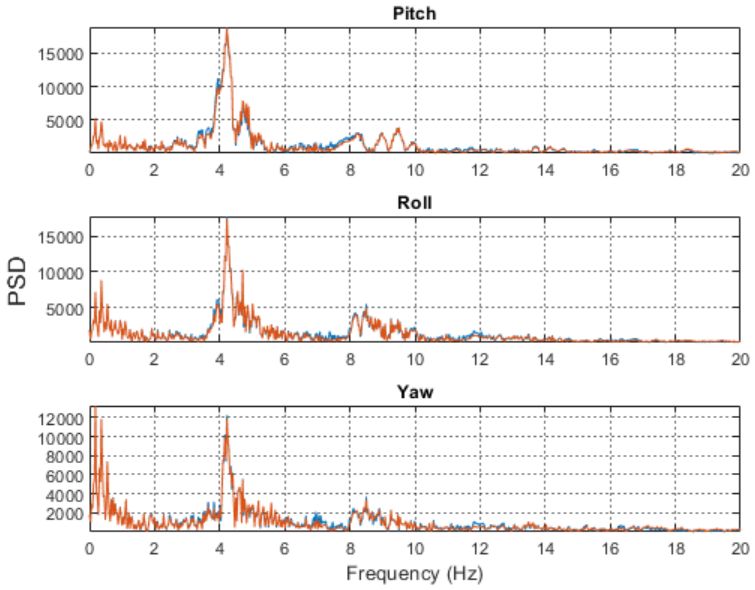

Figure 4.28: Tremor power estimation ratios of the index finger signal in three directions. FFT of the true signal (blue) and FFT of estimated signal (red).

The signal identification result of the index finger signal is given in Fig. 4.29. Similar to the previous two tasks, the signal tracking performance of our proposed system is also reasonable in this task. Again we did not compute the signal RMS accuracy since only a small part of the signal contained tremor. Because this signal contains both tremor and voluntary motion, in order to achieve effective power suppression, it is necessary to separate the tremor from the signal and only suppress the tremor. Otherwise, the voluntary motion will also be suppressed if we treat the whole signal as a tremor signal. As mentioned in Chapter 3, the estimated signal of our proposed system is the sum of the outputs of internal models and an integrator that represents the DC and low-frequency components. Thus, the estimated tremor is represented as the sum of the outputs of internal models, and the estimated voluntary motion is represented as the output of the integrator, and the noise is assumed to be the difference between the tremor signal and the sum of these two estimated signal.

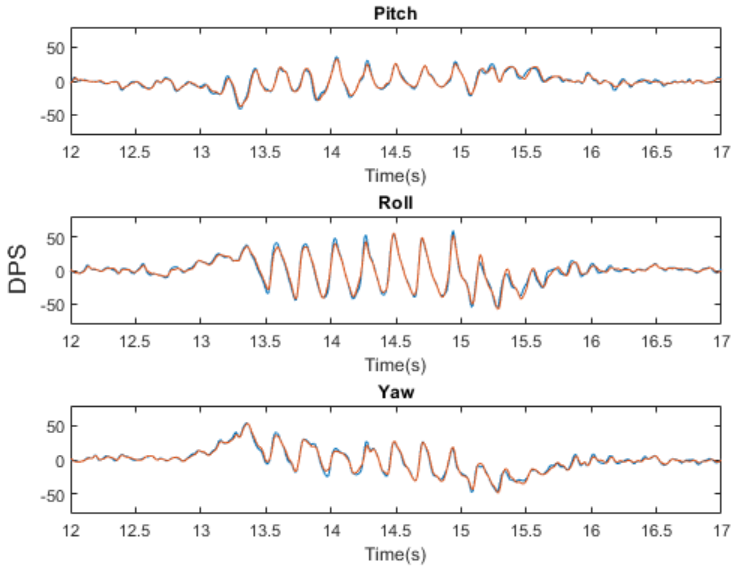

Figure 4.29: Signal identification of the index finger signal in three directions. True signal (blue) and estimated signal (red) are shown in a 5s data segment.

Fig. 4.30 gives the estimated signal in Fig. 4.29 after separating the tremor signal and the voluntary motion signal. The blue line represents the tremor signal, and the red line represents voluntary motion and noise. It can be seen that the estimated tremor is a quasi-sinusoidal signal with zero means, and the estimated low-frequency component is showing a pattern of voluntary motion. After applying this approach to the whole signal, the result is given in Fig. 4.33. The tremor and voluntary motion are separated in each period which contains step A and C. Unfortunately, no data or indicators can prove the effectiveness of this approach or the accuracy of the estimated tremor. However, just by eyeballing it, the outcome already showed a reasonable result in separating tremor and voluntary motion signal.

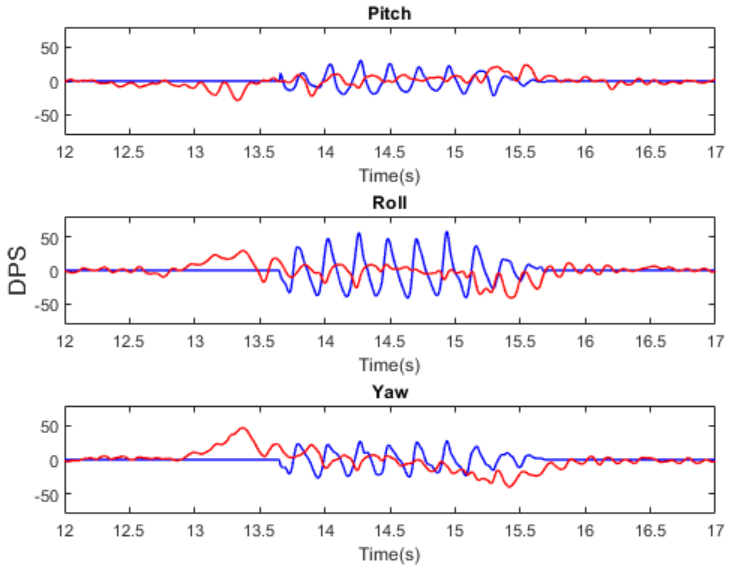

Figure 4.30: Estimated tremor (blue) and estimated voluntary motion (red) of Fig. 4.29

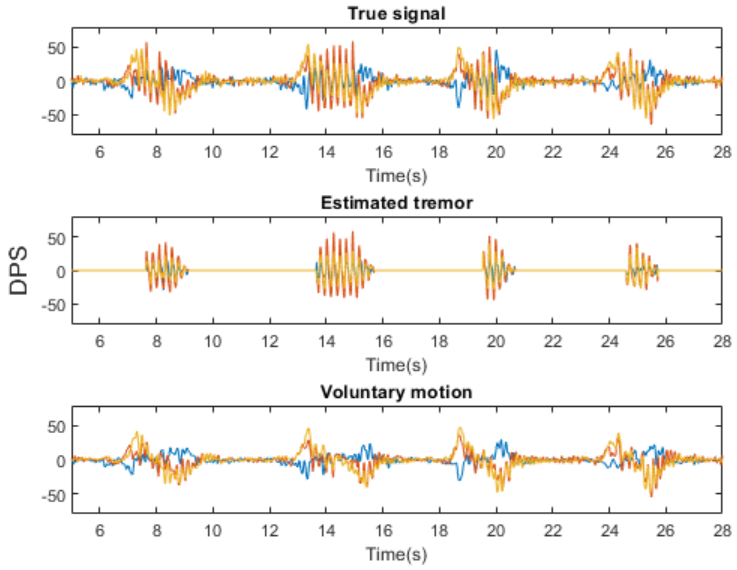

Figure 4.31: Top: Original index finger signal. Middle: Estimated tremor. Bottom: estimated voluntary motion. Blue line is pitch signal, red line is roll signal, yellow line is yaw signal.

To explore the connections between different joints and answer the final question in Chapter 3, Fig. 4.32 plots the comparison of $(A_1)^2$ between the index finger and wrist finger. Note that the threshold A_{max} in the wrist signal identification was reduced to 50 because of the lower

magnitude. $(A_1)^2$ in all three directions of the index finger signal are much higher than the wrist signal. Moreover, the $(A_1)^2$ in steps A and C are still higher than in step B, whether in the index finger or wrist signal. In other words, the tremor exists in the wrist signal, but it is too weak to be recognized by our proposed system under these tuning parameters. The comparison of the FFT between the index finger and wrist finger is given in Fig. 4.33. Again the power around 4 Hz in the index finger signal is greater than in the wrist signal, which is probably the frequency of tremor. Furthermore, the power in the low-frequency range in the wrist signal is stronger than the index finger signal, which indicates that the voluntary motion on the wrist may be stronger than on the index finger.

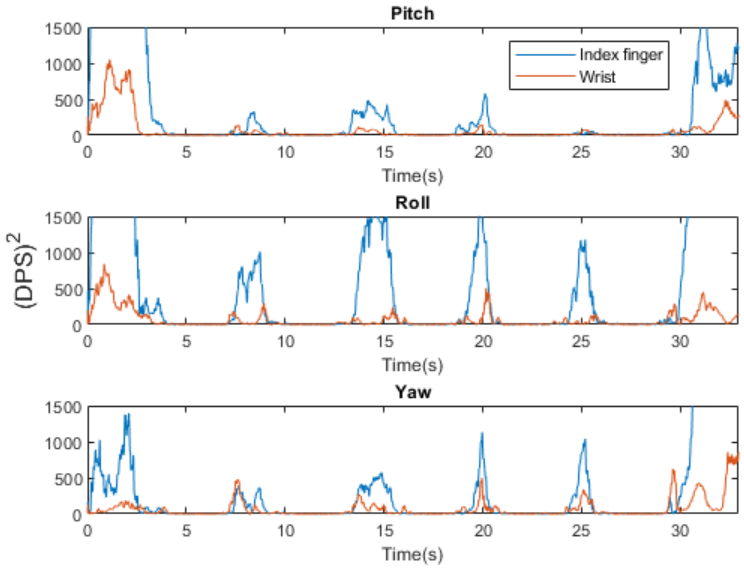

Figure 4.32: Comparison of the square of estimated fundamental amplitudes of three directions between the index finger and wrist signal

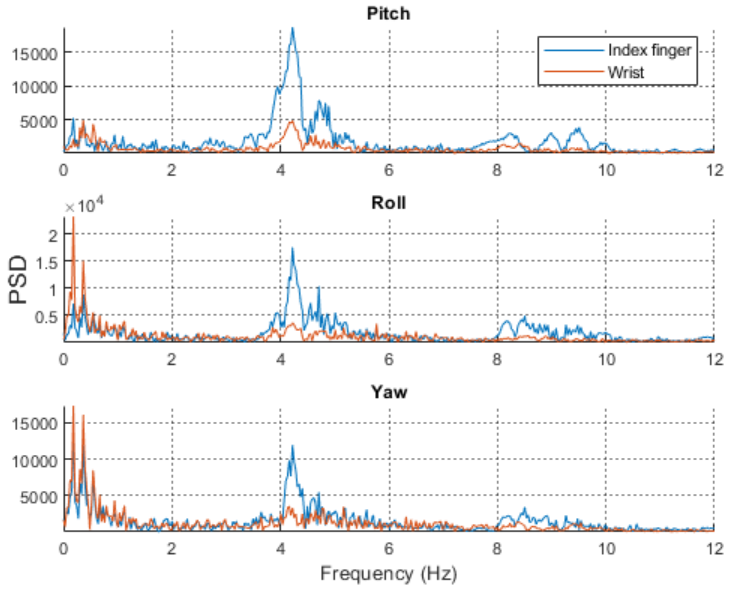

Figure 4.33: Comparison of the FFT of three directions between the index finger and wrist signal

In conclusion, the tremor was appeared in steps A and C in this task but did not appear in step B. Moreover, the tremor in the index finger signal is stronger than the wrist signal, but the voluntary motion is quite the opposite. This result may be caused by the different degrees of freedom of the index finger and wrist. When the patient raises or lowers the palm, it is mainly the wrist exerting force to control voluntary movement. Also, the patient's arm is placed on the table, so the freedom of movement is less than that of the index finger. Furthermore, the patient does not deliberately control the index finger during this process, which also causes the tremor to be more obvious in the index finger signal. Again our proposed system showed expected signal tracking and tremor power estimation performance. Additionally, our proposed system can separate the tremor and voluntary motion in a complicated signal, which we have not seen in previous Parkinsonian tremor estimators.

Chapter 5

Real-time Test

5.1 Experiment Setup

The simulation results in Chapter 4 already showed that our proposed Parkinsonian tremor identifier has an excellent performance in tracking and identifying tremor signals. Moreover, the system is capable of distinguishing the tremor signal, voluntary movement signal and noise. This is a function that the previous estimators have never had before. To assess the performance of our proposed Parkinsonian tremor identifier in real-time, a bench-top tremor simulator that Zhou developed was used as the test object in this experiment [54]. The recorded signals from the index finger joint and wrist joint of 15 patients in chapter 4 were reproduced on this artificial finger. This simulator consists of a 3D printed hand model, a brushless DC motor and a motor controller. A velocity PID controller was constructed and tuned to reproduce the recorded motion with the motor using LabVIEW software. The angular velocity measured from the IMU on the artificial finger was recorded directly by the PC through serial communication CH 340 port with a sampling frequency of 100 Hz.

Our proposed Parkinsonian tremor identifier in MATLAB and Simulink was transferred to Python 3.7 code using Pycharm. The ordinary differential equation solver in Python is the adaptive Runge-Kutta method. Since this simulator only moves in a single axis direction, our system is modified to only process one-dimensional signal *i.e.* reduce the number of fundamentals from three to one. When receiving the recorded angular velocity from the IMU, the identifier will identify and track the signal simultaneously. All tuning parameters are set as the same as in chapter 4.

5.2 Result

Fig. 5.2 shows the difference between the signal in simulation and the signal in the real-time test. It can be seen that the amplitude of the real-time test signal is slightly lower than the simulation signal. Moreover, a small DC component always exists in the real-time test signal. A zoom-in figure from 38s to 38.6s shows that the real-time signal is noisier than the simulation signal. Most of it comes from high-frequency components caused by the mechanical error of the simulator.

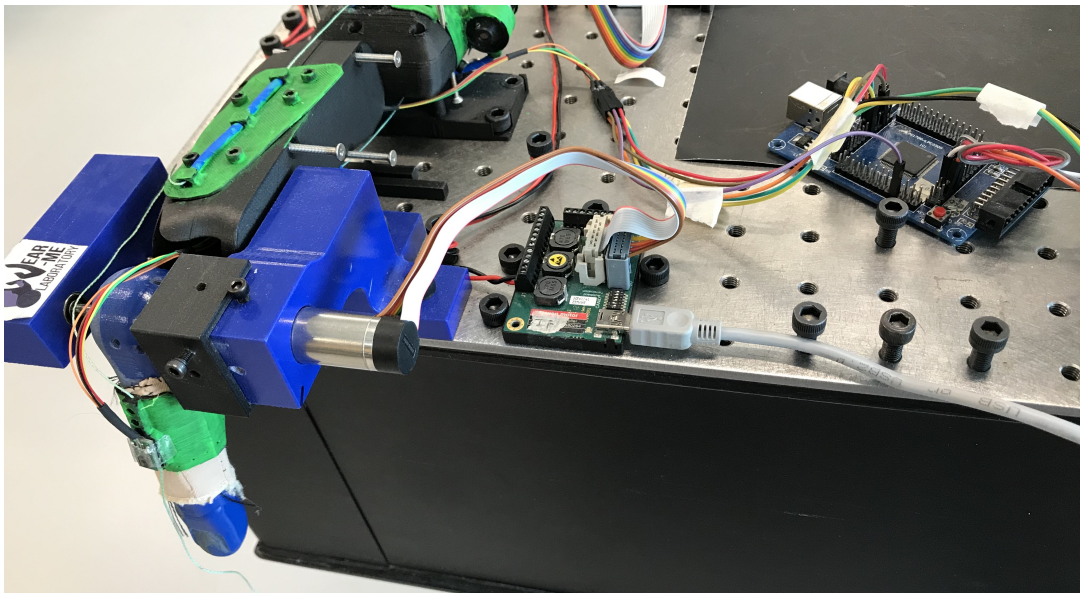

Figure 5.1: Top view of the bench-top experimental setup for real-time test

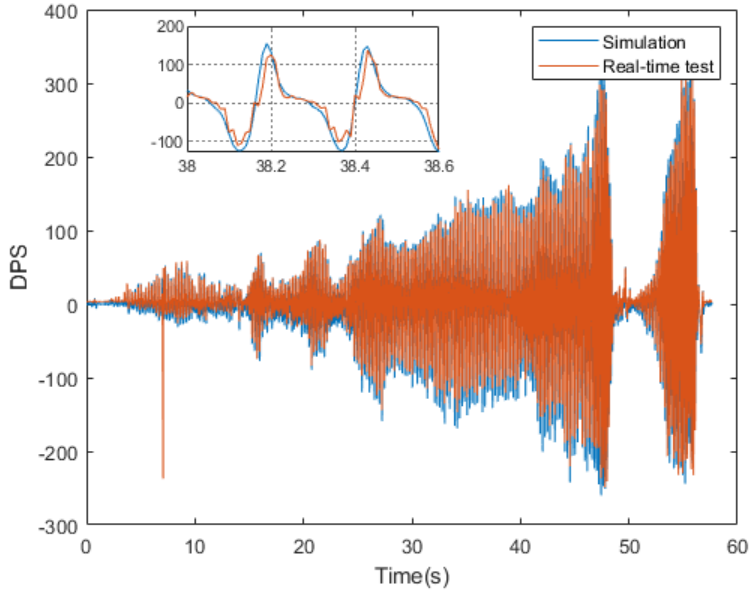

Figure 5.2: Signal in simulation and signal in real-time test

The estimated frequencies of the simulation signal and real-time test signal are shown in Fig. 5.3. Their results are very similar, and the frequency trends are also the same. However, since the real-time test signal is noisier, the frequency identification in real-test time is less sensitive than in simulation *i.e.* the estimated frequency is reacting more slowly to the change. However, the power estimation of the real-time test signal is still showing good results in Fig. 5.4. The power estimation ratio is 96.7% in this signal. Note that the power range from 4.2 Hz to 5.7 Hz

in the estimated signal is higher than in the true signal, but the power range from 5.7 Hz to 8.5 Hz is lower than in the true signal. In chapter 4, the estimated frequency range of this signal in simulation is 4.2 Hz to 5.8 Hz. This result indicates that the power in the estimated signal is more concentrated in the tremor range. In other words, our proposed system is capable of rejecting noise that is not in the tremor frequency range.

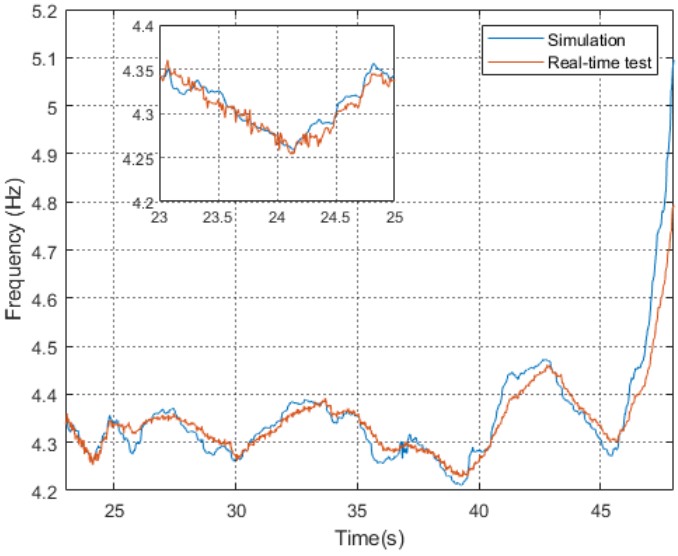

Figure 5.3: Frequency identification of simulation and real-time test signal

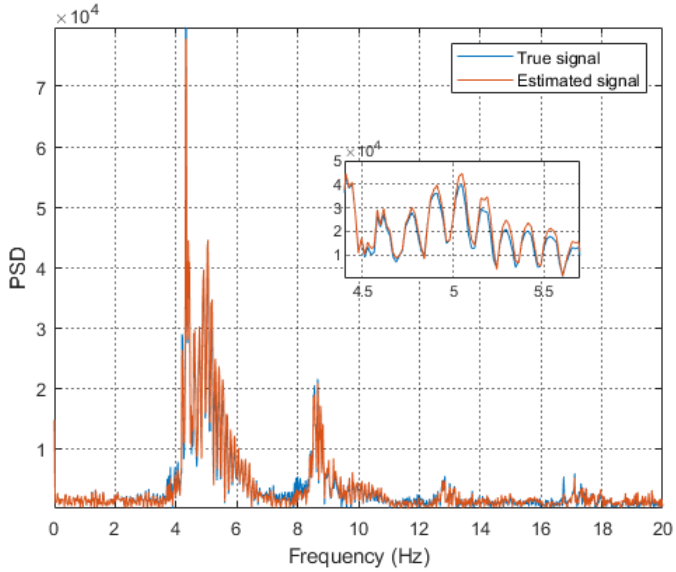

Figure 5.4: FFT of the true signal and estimated signal in real-time test

The signal identification in real-time rest is given in Fig. 5.5. It can be seen that the noise in the signal affects the tracking performance of our proposed system. The siignal RMS accuracy of this signal in the real-time test is 69.4%, which is lower than the signal RMS accuracy in simulation. However, considering the fact that this signal contains much more mechanical noise genrated by the motor and artifical finger, the decrease in signal RMS accuracy is mainly because our system did not try to track the noise. The overall signal RMS accuracy and tremor power estimation accuracy in 60 signals are given in Fig. 5.6. The mean of RMS accuracy and tremor power estimation accuracy are 68.1% and 96.0%, respectively. Although the signal RMS accuracy is dropped because of the additional noise, the tremor power estimation accuracy is better comapred to the simulation result. This result shows that our proposed Parkinsonian signal identifier maintains high accuracy and stability in the presence of much noise.

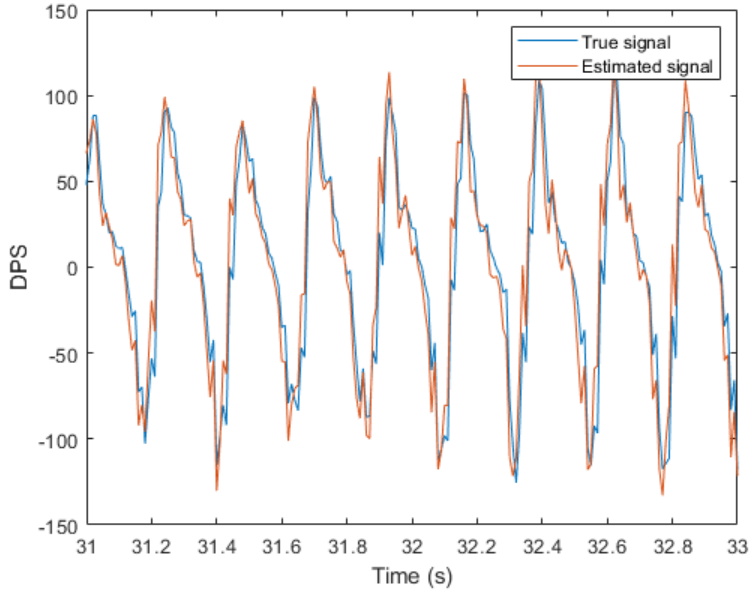

Figure 5.5: Signal identification in real-time test

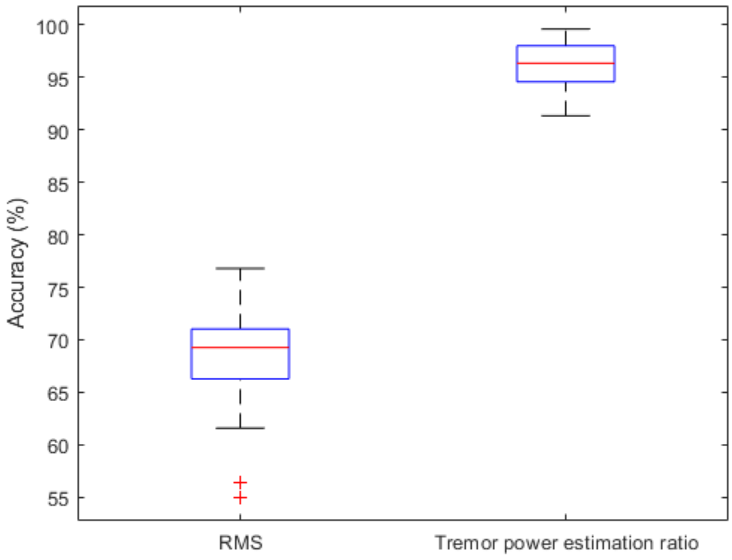

Figure 5.6: The overall signal RMS accuracy and tremor power estimation accuracy in 60 real-time test signals

Lastly, the mean ± standard deviation of computation time of each sample point is 3.5 ms ± 0.35ms. Since the sampling frequency is 100 Hz, the theoretical maximum computation time for each sample point is 10ms. Apparently, our proposed Parkinsonian tremor estimator achieved real-time estimation in this experiment. Furthermore, this time can be improved if we used other software or a computer with better performance.

Chapter 6

Conclusion and Future Work

6.1 Contributions

This thesis proposed a real-time high-accuracy parkinsonian tremor signal identifier that can identify 3-D angular velocity signals collected from a specific glove device. It was tested in experimental data recorded from 18 patients in 5 groups of different tasks. The codes were transferred to Python and achieved real-time tremor estimation in a bench-top tremor simulator. The specific contributions of this work are given below.

1. Extended the function and enhanced the flexibility of the previous internal model principle-based unknown periodic signal identifier [36]. Proposed a new system that can identify signals with any number of fundamentals and harmonics. Improved the structure of the system, which can let users control tuning parameters easily.

2. Developed a new adaptive algorithm to identify parkinsonian tremor signal based on internal model principle and instantaneous Fourier decomposition. The new algorithm accepted input signals from three axes simultaneously and used the average of estimated frequencies of three axes to identify the signal. This approach increased the stability of the algorithm and decreased the influence of noise.

3. Proposed a new idea that the parkinsonian tremor signal should be divided into tremor, voluntary motion and noise instead of a complete tremor signal. The proposed tremor signal identifier can distinguish tremor, voluntary motion and noise by setting proper tuning parameters. Furthermore, the substitute frequency allowed the system to switch between tremor and non-tremor signals and achieved intermittent control. Hence, our system can achieve real-time identification and track the tremor signal simultaneously.

4. Tested the proposed system in simulation with experimental data collected from 18 patients in 5 different tasks. The results showed that our proposed system achieved 80%+ signal estimation accuracy and 90%+ power estimation accuracy in both resting tremor and postural tremor signals. Moreover, our system showed the ability to recognize the non-tremor signal and stop identifying it. The results also showed that parkinsonian tremor is a multi-harmonic signal, and its frequency is not consistent.

5. Tested the proposed system in simulation kinetic tremor signal. The result presented that our proposed system can separate voluntary motion from tremor signal and estimate tremor and voluntary motion, respectively. Therefore, our system can only suppress the tremor while

the patient is doing voluntary movements.

6. Finally, the real-time test on the bench-top tremor simulator with Python proved that our system could achieve real-time tremor estimation. Moreover, our proposed system maintained a good performance on signal tracking and power estimation in a noisier situation.

6.2 Future Work

Although our proposed tremor identifier showed excellent stability and accuracy in both simulation and the real-time test, a significant amount of work can be foreseen. The future work is shown as follows:

1. All tests were conducted using simple tuning parameters. However, the performance of our proposed system can be improved significantly by selecting proper tuning parameters. For better identification results, it is necessary to develop an adaptive auto-tuning algorithm that can adjust tuning parameters in different situations automatically.

2. The current experimental data from five tasks only studied a few situations that the patient may experience in real life. Nevertheless, the patient may do other actions in daily life. The tremor signal collected when the patient fetches a glass of water with his hand is likely to be very different from the tremor signal collected when the patient draws a spiral circle with a pencil. Thus, our proposed system needs to be tested in a wider variety of tremor signals to ensure performance.

3. Our proposed tremor identifier has satisfactory performance in estimating the tremor signal. However, there is still a long way to go from estimation to suppression. Although the system is not computationally expensive and can achieve real-time estimation, the real-time suppression may require more computation time. Hence, the algorithm still needs further optimization to reduce unnecessary calculations.

Bibliography

[1] Kabita Adhikari et al. “A quaternion weighted Fourier linear combiner for modeling physiological tremor”. In: *IEEE Transactions on Biomedical Engineering* 63.11 (2016), pp. 2336–2346.

[2] Eduard Bakstein et al. “Parkinsonian tremor identification with multiple local field potential feature classification”. In: *Journal of neuroscience methods* 209.2 (2012), pp. 320–330.

[3] Antônio Padilha Lanari Bó, Philippe Poignet, and Christian Geny. “Pathological tremor and voluntary motion modeling and online estimation for active compensation”. In: *IEEE Transactions on Neural Systems and Rehabilitation Engineering* 19.2 (2010), pp. 177–185.

[4] Antônio Padilha Lanari Bó, Philippe Poignet, and Christian Geny. “Pathological tremor and voluntary motion modeling and online estimation for active compensation”. In: *IEEE Transactions on Neural Systems and Rehabilitation Engineering* 19.2 (2010), pp. 177–185.

[5] Antônio Padilha Lanari Bó, Philippe Poignet, and Christian Geny. “Pathological tremor and voluntary motion modeling and online estimation for active compensation”. In: *IEEE Transactions on Neural Systems and Rehabilitation Engineering* 19.2 (2010), pp. 177–185.

[6] Antônio PL Bó et al. “Online pathological tremor characterization using extended Kalman filtering”. In: *2008 30th Annual International Conference of the IEEE Engineering in Medicine and Biology Society*. IEEE. 2008, pp. 1753–1756.

[7] M. Bodson, A. Sacks, and P. Khosla. “Harmonic generation in adaptive feedforward cancellation schemes”. In: *IEEE Transactions on Automatic Control* 39.9 (1994), pp. 1939–1944. DOI: 10.1109/9.317130.

[8] P. Bremaud. “Mathematical principles of signal processing: Fourier and wavelet analysis”. In: *Springer* (2013).

[9] L. J. Brown and Qing Zhang. “Control for canceling periodic disturbances with uncertain frequency”. In: *Proceedings of the 40th IEEE Conference on Decision and Control (Cat. No.01CH37228)*. Vol. 5. 2001, 4909–4914 vol.5. DOI: 10.1109/CDC.2001.980986.

[10] L. J. Brown and Qing Zhang. “Identification of periodic signals with uncertain frequency”. In: *IEEE Transactions on Signal Processing* 51.6 (2003), pp. 1538–1545. DOI: 10.1109/TSP.2003.811242.

[11] L.J. Brown and Qing Zhang. "Periodic disturbance cancellation with uncertain frequency". In: *Automatica* 40.4 (2004), pp. 631–637. ISSN: 0005-1098. DOI: https://doi.org/10.1016/j.automatica.2003.10.024. URL: https://www.sciencedirect.com/science/article/pii/S0005109803003820.

[12] Lyndon J Brown and JS Schwaber. "Intermittent cancellation control: a control paradigm inspired by mammalian blood pressure control". In: *Proceedings of the 1999 American Control Conference (Cat. No. 99CH36251)*. Vol. 1. IEEE. 1999, pp. 139–143.

[13] J. O. Chapa and R. M. Rao. "Algorithms for designing wavelets to match a specified signal". In: *IEEE Transactions on Signal Processing* 48.12 (2000), pp. 3395–3406. DOI: 10.1109/78.887001.

[14] Jie Chen, Lyndon J Brown, and Edris Mohsen. "Signal identification based on internal model in discrete time". In: *2018 IEEE International Symposium on Signal Processing and Information Technology (ISSPIT)*. IEEE. 2018, pp. 685–689.

[15] Qiuhui Chen et al. "A B-spline approach for empirical mode decompositions". In: *Advances in computational mathematics* 24.1-4 (2006), pp. 171–195.

[16] Bryan T. Cole et al. "Dynamic neural network detection of tremor and dyskinesia from wearable sensor data". In: *2010 Annual International Conference of the IEEE Engineering in Medicine and Biology*. 2010, pp. 6062–6065. DOI: 10.1109/IEMBS.2010.5627618.

[17] ROGER C. CONANT and W. ROSS ASHBY. "Every good regulator of a system must be a model of that system". In: *International Journal of Systems Science* 1.2 (1970), pp. 89–97. DOI: 10.1080/00207727008920220. eprint: https://doi.org/10.1080/00207727008920220. URL: https://doi.org/10.1080/00207727008920220.

[18] Günther Deuschl, Frank Papengut, and Helge Hellriegel. "The phenomenology of parkinsonian tremor". In: *Parkinsonism & related disorders* 18 (2012), S87–S89.

[19] Günther Deuschl et al. "Consensus statement of the movement disorder society on tremor". In: *Movement disorders* 13.S3 (1998), pp. 2–23.

[20] D. Donnelly. "The Fast Fourier and Hilbert-Huang Transforms: A Comparison". In: *The Proceedings of the Multiconference on "Computational Engineering in Systems Applications"*. Vol. 1. 2006, pp. 84–88. DOI: 10.1109/CESA.2006.4281628.

[21] B.A. Francis and W.M. Wonham. "The internal model principle of control theory". In: *Automatica* 12.5 (1976), pp. 457–465. ISSN: 0005-1098. DOI: https://doi.org/10.1016/0005-1098(76)90006-6. URL: https://www.sciencedirect.com/science/article/pii/0005109876900066.

[22] Peter Gawthrop et al. "Intermittent control: a computational theory of human control". In: *Biological cybernetics* 104.1 (2011), pp. 31–51.

[23] Peter J Gawthrop and Liuping Wang. "Event-driven intermittent control". In: *International Journal of Control* 82.12 (2009), pp. 2235–2248.

[24] D. N. Gerasimov, V. O. Nikiforov, and A. V. Paramonov. "Adaptive disturbance compensation in delayed linear systems: Internal model approach". In: *2015 IEEE Conference on Control Applications (CCA)*. 2015, pp. 1692–1696. DOI: 10.1109/CCA.2015.7320853.

[25] S. Hara et al. "Repetitive control system: a new type servo system for periodic exogenous signals". In: *IEEE Transactions on Automatic Control* 33.7 (1988), pp. 659–668. DOI: 10.1109/9.1274.

[26] Rick C Helmich. "The cerebral basis of Parkinsonian tremor: a network perspective". In: *Movement Disorders* 33.2 (2018), pp. 219–231.

[27] Norden Eh Huang. "Hilbert-Huang Transform and Its Applications". In: *World Scientific* (2014).

[28] Joseph Jankovic. "Parkinson's disease: clinical features and diagnosis". In: *Journal of neurology, neurosurgery & psychiatry* 79.4 (2008), pp. 368–376.

[29] S Kazi et al. "Experimental implementation of smart glove incorporating piezoelectric actuator for hand tremor control". In: *WSEAS transactions on Systems and Control* 5.6 (2010), pp. 443–453.

[30] Sunghan Kim and James McNames. "Tracking tremor frequency in spike trains using the extended Kalman filter". In: *2005 IEEE Engineering in Medicine and Biology 27th Annual Conference*. IEEE. 2006, pp. 7576–7579.

[31] Chun-lin Ma et al. "The prevalence and incidence of Parkinson's disease in China: a systematic review and meta-analysis". In: *Journal of neural transmission* 121.2 (2014), pp. 123–134.

[32] N. Malhotra. "Online tip voltage and dynamic resistance measurement in RSW process". In: (2005).

[33] Riccardo Marino and Patrizio Tomei. "Disturbance cancellation for linear systems by adaptive internal models". In: *Automatica* 49.5 (2013), pp. 1494–1500. ISSN: 0005-1098. DOI: https://doi.org/10.1016/j.automatica.2013.02.011. URL: https://www.sciencedirect.com/science/article/pii/S0005109813000757.

[34] C Marras et al. "Prevalence of Parkinson's disease across North America". In: *NPJ Parkinson's disease* 4.1 (2018), pp. 1–7.

[35] E Mohsen, LJ Brown, and J Chen. "A Real time Alternative to the Hilbert Huang Transform Based on Internal Model Principle". In: *J Electr Electron Syst* 6.233 (2017), pp. 2332–0796.

[36] E. Mohsen and L. J. Brown. "Realtime implementation of an internal-model-principle signal identifier". In: *2017 IEEE 30th Canadian Conference on Electrical and Computer Engineering (CCECE)*. 2017, pp. 1–5. DOI: 10.1109/CCECE.2017.7946672.

[37] M. Mojiri and A. R. Bakhshai. "An adaptive notch filter for frequency estimation of a periodic signal". In: *IEEE Transactions on Automatic Control* 49.2 (2004), pp. 314–318. DOI: 10.1109/TAC.2003.821414.

[38] M. Mojiri, M. Karimi-Ghartemani, and A. Bakhshai. “Time-Domain Signal Analysis Using Adaptive Notch Filter”. In: *IEEE Transactions on Signal Processing* 55.1 (2007), pp. 85–93. DOI: 10.1109/TSP.2006.885686.

[39] Wonchul Nho. “DEVELOPMENT AND EVALUATION OF AN ENHANCED WEIGHTED FREQUENCY FOURIER LINEAR COMBINER ALGORITHM USING BANDWIDTH INFORMATION IN JOYSTICK OPERATION”. PhD thesis. University of Pittsburgh, 2006.

[40] Tamara Pringsheim et al. “The prevalence of Parkinson’s disease: a systematic review and meta-analysis”. In: *Movement disorders* 29.13 (2014), pp. 1583–1590.

[41] Qing Zhang and L. J. Brown. “Designing of adaptive bandpass filter with adjustable notch for frequency demodulation”. In: *Proceedings of the 2003 American Control Conference, 2003.* Vol. 4. 2003, 2931–2936 vol.4. DOI: 10.1109/ACC.2003.1243770.

[42] Cameron N Riviere, R Scott Rader, and Nitish V Thakor. “Adaptive cancelling of physiological tremor for improved precision in microsurgery”. In: *IEEE Transactions on Biomedical Engineering* 45.7 (1998), pp. 839–846.

[43] Eduardo Rocon et al. “Design and validation of a rehabilitation robotic exoskeleton for tremor assessment and suppression”. In: *IEEE Transactions on neural systems and rehabilitation engineering* 15.3 (2007), pp. 367–378.

[44] Ervin Sejdić, Igor Djurović, and Jin Jiang. “Time–frequency feature representation using energy concentration: An overview of recent advances”. In: *Digital Signal Processing* 19.1 (2009), pp. 153–183. ISSN: 1051-2004. DOI: https://doi.org/10.1016/j.dsp.2007.12.004. URL: https://www.sciencedirect.com/science/article/pii/S105120040800002X.

[45] Soroosh Shahtalebi et al. “Wake: Wavelet decomposition coupled with adaptive kalman filtering for pathological tremor extraction”. In: *Biomedical Signal Processing and Control* 48 (2019), pp. 179–188.

[46] Y. Sun. “Instantaneous fourier series estimation”. In: (2006).

[47] Behzad Taheri. “Real-time pathological tremor identification and suppression in human arm via active orthotic devices”. PhD thesis. Southern Methodist University, 2013.

[48] Behzad Taheri, David Case, and Edmond Richer. “Theoretical development and experimental validation of an adaptive controller for tremor suppression at musculoskeletal level”. In: *ASME 2013 Dynamic Systems and Control Conference*. American Society of Mechanical Engineers Digital Collection. 2013.

[49] Ole-Bjørn Tysnes and Anette Storstein. “Epidemiology of Parkinson’s disease”. In: *Journal of Neural Transmission* 124.8 (2017), pp. 901–905.

[50] Christopher Vaz, Xuan Kong, and Nitish Thakor. “An adaptive estimation of periodic signals using a Fourier linear combiner”. In: *IEEE Transactions on Signal Processing* 42.1 (1994), pp. 1–10.

[51] Kalyana C Veluvolu, Win Tun Latt, and Wei Tech Ang. “Double adaptive bandlimited multiple Fourier linear combiner for real-time estimation/filtering of physiological tremor”. In: *Biomedical Signal Processing and Control* 5.1 (2010), pp. 37–44.

[52] Kalyana C Veluvolu et al. “Bandlimited multiple fourier linear combiner for real-time tremor compensation”. In: *2007 29th Annual International Conference of the IEEE Engineering in Medicine and Biology Society*. IEEE. 2007, pp. 2847–2850.

[53] Ferdinan Widjaja et al. “Kalman filtering of accelerometer and electromyography (EMG) data in pathological tremor sensing system”. In: *2008 IEEE International Conference on Robotics and Automation*. IEEE. 2008, pp. 3250–3255.

[54] Y Zhou et al. “Characterization of parkinsonian hand tremor and validation of a high-order tremor estimator”. In: *IEEE Transactions on Neural Systems and Rehabilitation Engineering* 26.9 (2018), pp. 1823–1834.

[55] Y. Zhou et al. “Design and validation of a high-order weighted-frequency fourier linear combiner-based Kalman filter for parkinsonian tremor estimation”. In: *2016 38th Annual International Conference of the IEEE Engineering in Medicine and Biology Society (EMBC)*. 2016, pp. 5893–5896. DOI: 10.1109/EMBC.2016.7592069.

[56] Y. Zhou et al. “The measurement and analysis of Parkinsonian hand tremor”. In: *2016 IEEE-EMBS International Conference on Biomedical and Health Informatics (BHI)*. 2016, pp. 414–417. DOI: 10.1109/BHI.2016.7455922.

[57] Yue Zhou et al. “Design and validation of a novel mechatronic transmission system for a wearable tremor suppression device”. In: *Robotics and autonomous systems* 91 (2017), pp. 38–48.

[58] Yue Zhou et al. “Development of a wearable tremor suppression glove”. In: *2018 7th IEEE International Conference on Biomedical Robotics and Biomechatronics (Biorob)*. IEEE. 2018, pp. 640–645.

Appendix A

Kinetic Tremor and Voluntary Motion (Task 4)

In Task 4, the patient was asked to lift the palm and take the pencil, put down the palm and lift it back with the pencil, then release the pencil and put down the palm to the original position. This process was repeated five times. Except that the patient is asked to hold the pencil and move up and down, the other steps are the same as Task 3. Fig. A.1 shows the figure below shows the comparison between the index finger signal of Task 3 and the index finger signal of Task 4. Compared to Task 3, the index finger signal recorded in Task 4 did not show an obvious pattern of tremor. Moreover, the square of estimated fundamental amplitude in Fig. A.2 indicates that the tremor intensity in Task 4 is much weaker than in Task 3, and it is more difficult to be identified. Although we can still observe peaks at 11 seconds and 18 seconds, its $(A_1)^2$ is not high enough to be accurately separated from signals in other periods. Thus, the threshold A_{max} needs to be chosen carefully to recognize the tremor in the signal successfully.

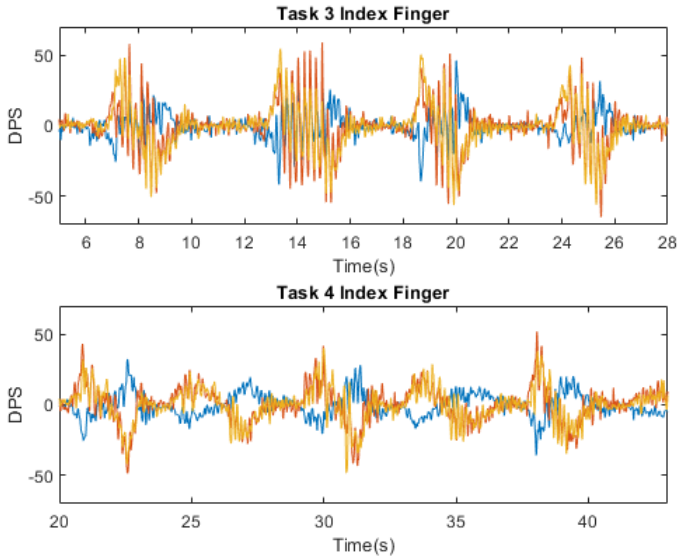

Figure A.1: Index finger signals of the same patient in Task 3 and 4. The red, blue and yellow lines represent the pith, roll and yaw signal.

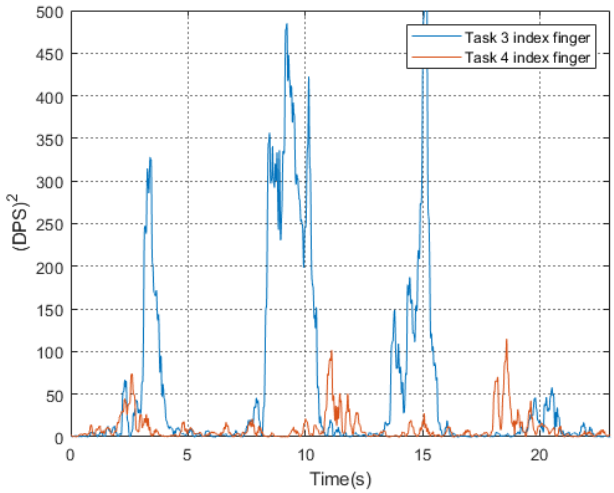

Figure A.2: The square of estimated fundamental amplitude of pitch signal of index finger signals in Task 3 and 4

Fig A.3 gives the frequency estimation results of the index finger signal in Task 4 under different A_{max}. The dotted line represents the period of no tremor, and the solid line represents the period of tremor. It can be seen that our proposed system identified many periods of tremor when $A_{max} = 20$. However, this may not be an ideal threshold since we can not calculate the exact threshold for identifying tremors. Moreover, it is also difficult to tell from the experimental video when the tremor occurred because the patient's hands were moving. Fortunately, we can calculate the fundamental amplitude of a noiseless periodic signal with a certain frequency and magnitude and use this value to set a proper threshold. However, the value of magnitude is also needed to be determined, and we need more experiments and tests to analyze the influence of noise and voluntary motion on fundamental amplitude.

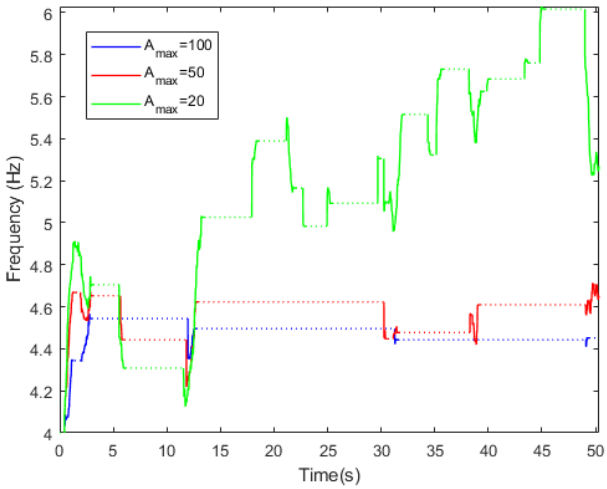

Figure A.3: Frequency identification results under different A_{max}

Appendix B

Kinetic Tremor and Voluntary Motion (Task 5)

In Task 5, the patient was asked to draw spiral circles clockwise with a pencil. The recorded signals of three joints are shown in Fig. B.1. It can be seen that the angular velocities in three directions, especially in roll and yaw, gradually grow over time as the patient needs to draw a bigger circle. Similar to Task 4, the kinetic tremor in these signals is weak and hard to be identified because of the short period and inconsistency. Unlike other tasks, the roll signal is stronger than the pitch and yaw signals in this task. Fig. B.2 gives the fundamental amplitude estimation result of the index finger signal in three directions. It is obvious that the fundamental amplitude of the roll signal is much higher than the other two directions. Note that the signal may have a second fundamental frequency since the fundamental amplitude estimation result shows periodicity.

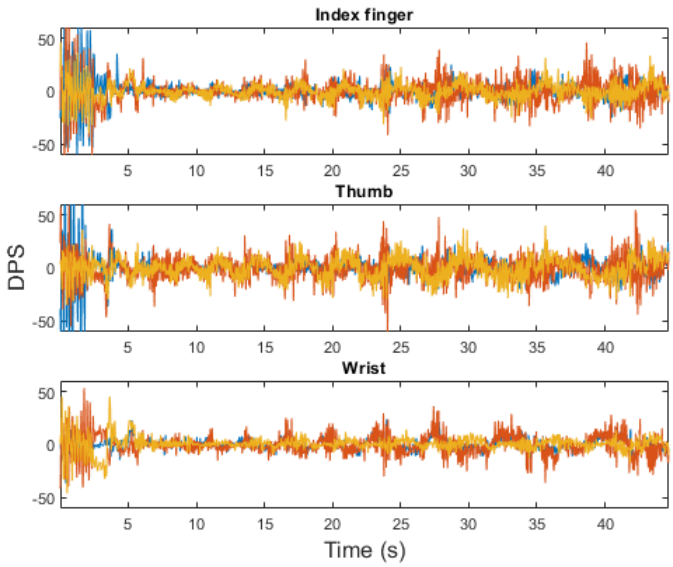

Figure B.1: Overall signal in Task 5. Top: Index finger signal. Middle: Thumb signal. Bottom: Wrist signal. Blue line is pitch signal, red line is roll signal, yellow line is yaw signal.

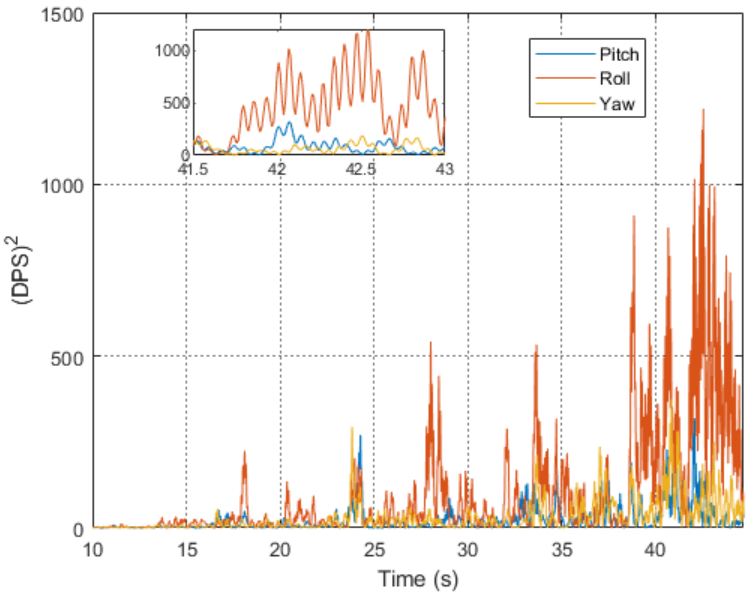

Figure B.2: The square of estimated fundamental amplitude in pitch, roll and yaw signal of index finger signal

In chapter 3, we mentioned that the tremor would be considered if the fundamental amplitudes in two directions are higher than the threshold. However, this signal only shows an obvious pattern of tremor in the roll direction. Continuing to use the previous setting may result in ignorance of the kinetic tremor. Thus we modified the system so that it only needed the fundamental amplitude in one direction above the threshold to confirm the presence of tremor. Fig. B.3 shows the frequency estimation result before and after the change of setting. Our proposed system recognizes more tremor periods in the last 20 seconds after the modification. It is common to encounter a voluntary motion which only moves in one direction. Therefore, the standard for identifying tremors in our system needs to be improved to deal with any possible real-life scenarios.

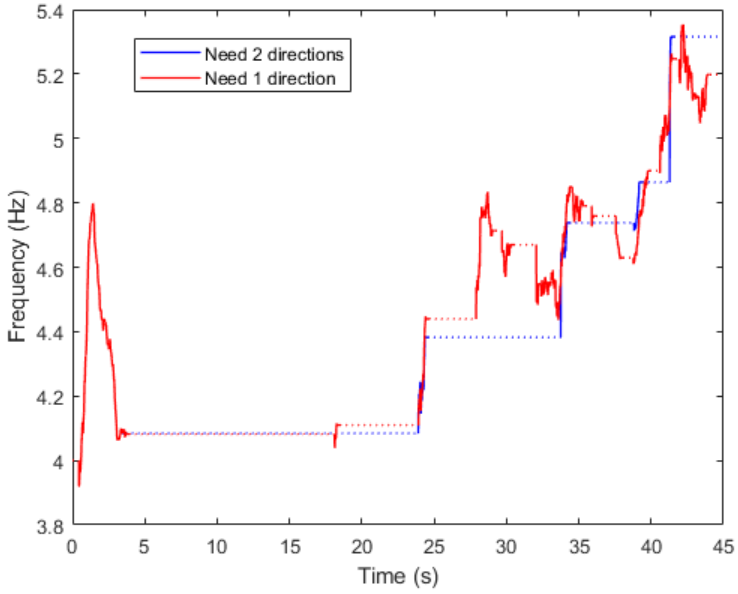

Figure B.3: Frequency identification results under different system settings

Western Research

Date: 1 October 2020

To: Mary Jenkins

Project ID: 106172

Study Title: Assessment of Hand Tremor

Application Type: HSREB Amendment Form

Review Type: Delegated

Full Board Reporting Date: 20October2020

Date Approval Issued: 01/Oct/2020 14:14

REB Approval Expiry Date: 20/Feb/2021

Dear Mary Jenkins ,

The Western University Health Sciences Research Ethics Board (HSREB) has reviewed and approved the WREM application form for the amendment, as of the date noted above.

Documents Approved:

Document Name	Document Type	Document Date	Document Version
ethics application-Amendment clean	Summary of Changes	01/Oct/2020	1

Documents Acknowledged:

Document Name	Document Type	Document Date	Document Version
Summary of changes	Summary of Changes	24/Aug/2020	1
ethics application-Amendment tracked	Summary of Changes	01/Oct/2020	1

REB members involved in the research project do not participate in the review, discussion or decision.

The Western University HSREB operates in compliance with, and is constituted in accordance with, the requirements of the TriCouncil Policy Statement: Ethical Conduct for Research Involving Humans (TCPS 2); the International Conference on Harmonisation Good Clinical Practice Consolidated Guideline (ICH GCP); Part C, Division 5 of the Food and Drug Regulations; Part 4 of the Natural Health Products Regulations; Part 3 of the Medical Devices Regulations and the provisions of the Ontario Personal Health Information Protection Act (PHIPA 2004) and its applicable regulations. The HSREB is registered with the U.S. Department of Health & Human Services under the IRB registration number IRB 00000940.

Please do not hesitate to contact us if you have any questions.

Sincerely,

Nicola Geoghegan-Morphet, Ethics Officer on behalf of Dr. Joseph Gilbert, HSREB Chair

Note: This correspondence includes an electronic signature (validation and approval via an online system that is compliant with all regulations).

Curriculum Vitae

Name:	Jian Dong
Post-Secondary Education and Degrees:	Beijing Institute of Technology Beijing, China 2015 - 2019 B.Eng. in Electrical and Computer Engineering The University of Western Ontario London, Ontario, Canada 2019 - 2021 M.E.Sc. in Electrical and Computer Engineering
Related Work Experience:	Graduate Teaching Assistant The University of Western Ontario 2020 - 2021